



for geotechnics & structures

BOREHOLE HEAT EXCHANGERS

Report 220430

(revised 30.04.2022)

A. Truty

GeoDev.

PO Box CH-1001 Lausanne
Switzerland
<https://zsoil.com>

Contents

1	List of symbols	7
2	Introduction	9
3	Theory	11
3.1	Balance equations for 1U exchanger	11
3.2	Balance equations for the 2U exchanger	14
3.3	Balance equations for CXA exchanger	17
3.4	Balance equations for CXC exchanger	19
3.5	Balance equations for a single pipe with explicit grout discretization	21
3.6	Weakly coupled hydro-thermal formulation	21
4	Finite elements for borehole heat exchangers (BHE elements)	23
4.1	Pipe type heat exchanger	23
4.2	CXA heat exchanger	23
4.3	CXC heat exchanger	24
4.4	1U heat exchanger	24
4.5	2U heat exchanger	25
5	User interface	27
5.1	Preprocessing	27
5.1.1	Generating heat exchangers	27
5.1.1.1	Generating heat exchangers with explicit grout	27
5.1.1.2	Generating heat exchangers with implicit grout	28
5.1.2	Meshing soil volume in the vicinity of the BHE elements	29
5.2	Material data	29

CONTENTS

5.3	Initial and boundary conditions	30
5.4	Postprocessing	30
6	Benchmarks for different classes of heat exchnagers	33
6.1	Benchmarks for the pipe type exchanger	33
6.1.1	Heat exchange between pipe and ground assuming constant ground temperature and steady state conditions	33
6.1.2	Heat exchange between pipe and ground assuming constant ground temperature and transient state conditions	37
6.1.3	Heat exchange between pipe and ground assuming constant ground temperature and steady state conditions using local form of constraints to connect nonconforming soil and exchanger meshes	39
6.1.4	Heat exchange between pipe and ground assuming constant ground temperature and steady state conditions using non-local form of constraints to connect nonconforming soil and exchanger meshes	40
6.1.5	Heat exchange between pipe and ground assuming variable ground temperature	41
6.2	Heat exchange problem under steady state conditions and constant borehole wall temperature	49
6.2.1	CXA exchanger	50
6.2.2	CXC heat exchanger	53
6.2.3	1U heat exchanger	56
6.2.4	2U heat exchanger	59
6.3	Heat exchange between single pipe and soil under transient conditions and constant soil temperature	63
6.3.1	Pipe type heat exchanger	63
6.3.2	1U type heat exchanger	66
6.4	Mesh sensitivity study	68
6.4.1	Transient BHE solution for the CXA system	68
6.4.1.1	Results for the case of laminar flow with exchanger located at the center of the mesh	72
6.4.1.2	Results for the case of laminar flow with exchanger shifted from the center of the mesh	78
6.4.1.3	Results for the case of turbulent flow and exchanger located at the center of the mesh	84
6.4.1.4	Results for the case of turbulent flow with exchanger shifted from the center of the mesh	90
6.4.2	Conclusions concerning meshing	96
7	Benchmarks for soil-structure interaction problems	97

7.1	Energy pile problem using 1U exchanger with the explicit grout zone	97
7.1.1	Thermal problem	98
7.1.2	Thermo-mechanical problem	101
7.2	Energy pile problem using 1U exchanger with the implicit grout zone	103
7.2.1	Thermal problem	103
7.2.2	Thermo-mechanical problem	105
A	Thermal resistances for heat exchangers with the implicit grout zones	109
A.1	Thermal resistances for the 1U heat exchanger	109
A.1.1	Thermal resistances caused by the advective flow of refrigerant in inlet/outlet pipes . .	109
A.1.2	Thermal resistances resulting from pipes material and grout transition	110
A.1.3	Thermal resistances between grout zones	110
A.1.4	Thermal resistance due to grout-soil exchange	111
A.2	Thermal resistances for the 2U heat exchanger	112
A.2.1	Thermal resistances caused by the advective flow of refrigerant in inlet/outlet pipes . .	112
A.2.2	Thermal resistances resulting from pipes material and grout transition	113
A.2.3	Thermal resistances between grout zones	113
A.2.4	Thermal resistance due to grout-soil exchange	114
A.3	Thermal resistances for the CXA heat exchanger	115
A.3.1	Thermal resistances caused by the advective flow of refrigerant in inlet/outlet pipes . .	115
A.3.2	Thermal resistances resulting from pipes material and grout transition	116
A.3.3	Thermal resistance due to grout-soil exchange	117
A.4	Thermal resistances for the CXC heat exchanger	118
A.4.1	Thermal resistances caused by the advective flow of refrigerant in inlet/outlet pipes . .	118
A.4.2	Thermal resistances resulting from pipes material and grout transition	119
A.4.3	Thermal resistance due to grout-soil exchange	120

CONTENTS

Chapter 1

List of symbols

Symbol	Unit	Meaning
1U		Borehole heat exchanger of 1U type
2U		Borehole heat exchanger of 2U type
CXA		Borehole heat exchanger with annular inlet
CXC		Borehole heat exchanger with centered inlet
\bar{L}	[m]	Borehole echanager length
d_i^{ext}	[m]	inflow pipe external diameter
d_i^{int}	[m]	inflow pipe internal diameter
h_i	[m]	inflow pipe wall thickness
d_o^{ext}	[m]	outflow pipe external diameter
d_o^{int}	[m]	outflow pipe internal diameter
h_o	[m]	outflow pipe wall thickness
w	[m]	distance between inflow and outflow pipes for the 1U and 2U exchangers
D	[m]	borehole diameter
$\rho^r c^r$	[J / m ³ /K]	refrigerant volumetric heat capacity
ρ^r	[kg / m ³]	refrigerant density
λ^r	[W /m /K]	refrigerant heat conductivity
μ^r	[Pa s]	refrigerant dynamic viscosity
$\rho^g c^g$	[J / m ³ /K]	grout volumetric heat capacity
λ^g	[W /m /K]	grout heat conductivity
$\rho^g c^g$	[J / m ³ /K]	grout volumetric heat capacity
λ_i^p	[W /m /K]	inflow pipe heat conductivity
λ_o^p	[W /m /K]	outflow pipe heat conductivity
v_i^r	[m/s]	refrigerant velocity in the inflow pipe
v_o^r	[m/s]	refrigerant velocity in the outflow pipe
Q^r	[m ³ /s]	volumetric flow discharge
R_{fig}	[m K /W]	thermal resistance between inflow pipe and grout
R_{fog}	[m K /W]	thermal resistance between outflow pipe and grout
R_{gs}	[m K /W]	thermal resistance due to grout-soil exchange
R_{gg}	[m K /W]	thermal resistance due to inter-grout exchange (inflow-outflow grout zones) (1U only)

CHAPTER 1. LIST OF SYMBOLS

R_{gg1}	[m K /W]	thermal resistance due to inter-grout exchange (inflow-outflow grout zones) (2U only)
R_{gg2}	[m K /W]	thermal resistance due to inter-grout exchange (inflow-inflow or outflow-outflow grout zones)(2U only)
R_{ff}	[m K /W]	thermal resistance due to fluid-fluid exchange (CXA and CXC only)
Φ_{fig}	[W / m /K]	thermal heat transfer coefficient related to the R_{fig} resistance
Φ_{fog}	[W / m /K]	thermal heat transfer coefficient related to the R_{fog} resistance
Φ_{gs}	[W / m /K]	thermal heat transfer coefficient related to the R_{gs} resistance
Φ_{gg}	[W / m /K]	thermal heat transfer coefficient related to the R_{gg} resistance
Φ_{gg1}	[W / m /K]	thermal heat transfer coefficient related to the R_{gg1} resistance
Φ_{gg2}	[W / m /K]	thermal heat transfer coefficient related to the R_{gg2} resistance
Φ_{ff}	[W / m /K]	thermal heat transfer coefficient related to the R_{ff} resistance
Nu	[-]	Nusselt number
Re	[-]	Reynolds number
Pr	[-]	Prandtl number

Chapter 2

Introduction

This report contains the theory, implementation details and benchmark sections for different classes of borehole heat exchangers. The theory is fully based on the paper 'Finite element modeling of borehole heat exchanger system. Part 1. Fundamentals'. published by H.J.G. Diersch et al.[1] and the FEFLOW white papers vol. V.[3].

Chapter 3

Theory

3.1 Balance equations for 1U exchanger

The cross section of 1U heat exchanger and relations between heat resistances in all transition zones are shown in fig.3.1.

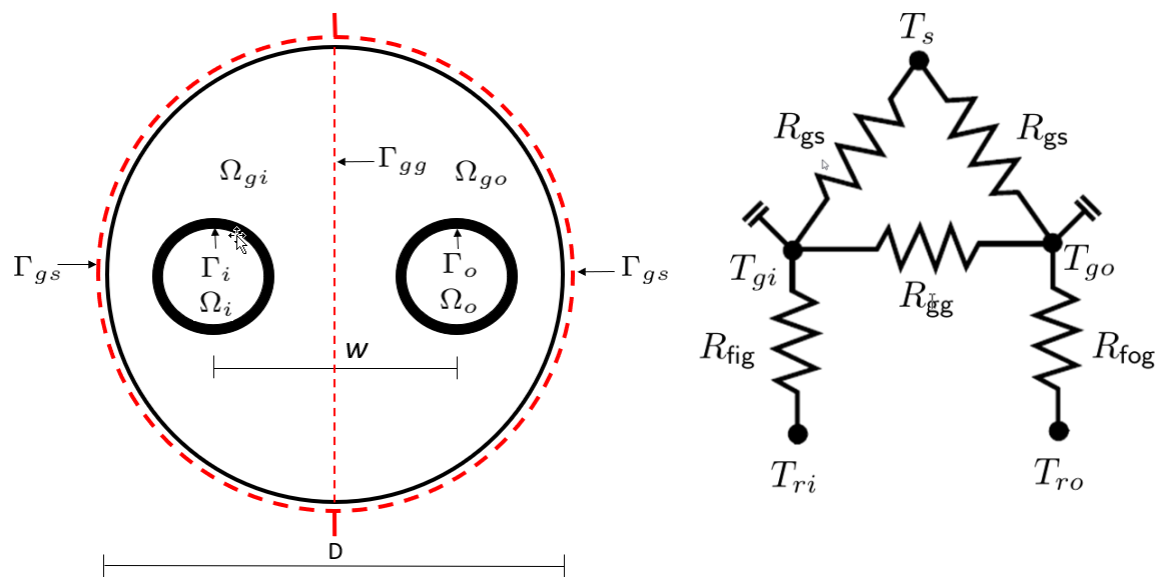


Figure 3.1: General scheme and heat resistance relations for 1U system

The set of heat balance equations is expressed as follows

$$\int_{\Omega_i} \left(w \rho^r c^r \left(\dot{T}_{ri} + \mathbf{v}_i^r \nabla T_{ri} \right) + \nabla w \tilde{\lambda}_i^r \nabla T_{ri} \right) d\Omega + \int_{\Gamma_i} w \Phi_{fig} T_{ri} d\Gamma = \int_{\Gamma_i} w \Phi_{fig} T_{gi} d\Gamma \quad (3.1)$$

$$\int_{\Omega_o} \left(w \rho^r c^r \left(\dot{T}_{ro} + \mathbf{v}_o^r \nabla T_{ro} \right) + \nabla w \tilde{\lambda}_o^r \nabla T_{ro} \right) d\Omega + \int_{\Gamma_o} w \Phi_{fog} T_{ro} d\Gamma = \int_{\Gamma_o} w \Phi_{fog} T_{go} d\Gamma \quad (3.2)$$

$$\begin{aligned} \int_{\Omega_{gi}} \left(w \rho^g c^g \dot{T}_{gi} + \nabla w \lambda^g \nabla T_{gi} \right) d\Omega + \int_{\Gamma_{gs}} w \Phi_{gs} T_{gi} d\Gamma + \int_{\Gamma_{gi}} w \Phi_{fig} T_{gi} d\Gamma + \int_{\Gamma_{gg}} w \Phi_{gg} T_{gi} d\Gamma = \\ \int_{\Gamma_{gs}} w \Phi_{gs} T_s d\Gamma + \int_{\Gamma_{gi}} w \Phi_{fig} T_{gi} d\Gamma + \int_{\Gamma_{gg}} w \Phi_{gg} T_{go} d\Gamma \end{aligned} \quad (3.3)$$

$$\begin{aligned} \int_{\Omega_{go}} \left(w \rho^g c^g \dot{T}_{go} + \nabla w \lambda^g \nabla T_{go} \right) d\Omega + \int_{\Gamma_{gs}} w \Phi_{gs} T_{go} d\Gamma + \int_{\Gamma_{go}} w \Phi_{fog} T_{go} d\Gamma + \int_{\Gamma_{gg}} w \Phi_{gg} T_{go} d\Gamma = \\ \int_{\Gamma_{gs}} w \Phi_{gs} T_s d\Gamma + \int_{\Gamma_{go}} w \Phi_{fog} T_{go} d\Gamma + \int_{\Gamma_{gg}} w \Phi_{gg} T_{gi} d\Gamma \end{aligned} \quad (3.4)$$

where thermal heat transfer coefficients Φ for all transition zones (refrigerant-grout, grout-grout, grout-soil) are computed using the following formulas

$$\Phi_{fig} = \frac{1}{R_{fig}} \frac{1}{S_i} \quad (3.5)$$

$$\Phi_{fog} = \frac{1}{R_{fog}} \frac{1}{S_o} \quad (3.6)$$

$$\Phi_{gg} = \frac{1}{R_{gg}} \frac{1}{S_{gg}} \quad (3.7)$$

$$\Phi_{gs} = \frac{1}{R_{gs}} \frac{1}{S_{gs}} \quad (3.8)$$

$$S_i = \pi (d_i^{\text{int}}) \quad (3.9)$$

$$S_o = \pi (d_o^{\text{int}}) \quad (3.10)$$

$$S_{gg} = D \quad (3.11)$$

$$S_{gs} = \frac{\pi D}{2} \quad (3.12)$$

For detailed information on how to compute resistances and heat transfer coefficients please refer to the paper [1] and FEFLOW white paper[3]. It is worth to mention that certain misprints appear in both references.

It has to be mentioned, following the FEFLOW white paper [3], that for some geometries certain resulting resistances may be negative and a correcting procedure is needed. In fact the following constraint must be satisfied

$$\left(\frac{1}{R_{gg}} + \frac{1}{2R_{gs}} \right)^{-1} > 0 \quad (3.13)$$

In case of violation of the above condition a special correction procedure (see [3]) has to be used (see appendix A.1).

3.2 Balance equations for the 2U exchanger

The cross section of 2U heat exchanger is shown in fig.3.2.

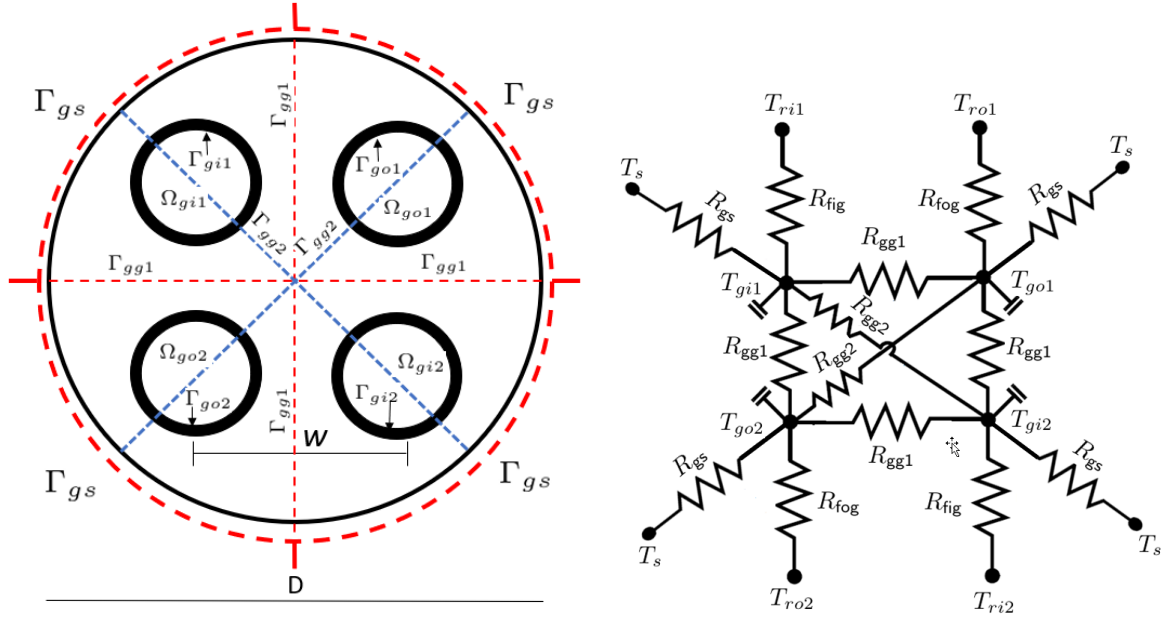


Figure 3.2: General scheme and heat resistance relations for 2U system

The set of heat balance equations is expressed as follows

$$\int_{\Omega_{i1}} \left(w \rho^r c^r \left(\dot{T}_{ri1} + \mathbf{v}_i^r \nabla T_{ri1} \right) + \nabla w \tilde{\lambda}_i^r \nabla T_{ri1} \right) d\Omega + \int_{\Gamma_{i1}} w \Phi_{fig} T_{ri1} d\Gamma = \int_{\Gamma_{i1}} w \Phi_{fig} T_{gi1} d\Gamma \quad (3.14)$$

$$\int_{\Omega_{i2}} \left(w \rho^r c^r \left(\dot{T}_{ri2} + \mathbf{v}_i^r \nabla T_{ri2} \right) + \nabla w \tilde{\lambda}_i^r \nabla T_{ri2} \right) d\Omega + \int_{\Gamma_{i2}} w \Phi_{fig} T_{ri2} d\Gamma = \int_{\Gamma_{i2}} w \Phi_{fig} T_{gi2} d\Gamma \quad (3.15)$$

$$\int_{\Omega_{o1}} \left(w \rho^r c^r \left(\dot{T}_{ro1} + \mathbf{v}_o^r \nabla T_{ro1} \right) + \nabla w \tilde{\lambda}_o^r \nabla T_{ro1} \right) d\Omega + \int_{\Gamma_{o1}} w \Phi_{fog} T_{ro1} d\Gamma = \int_{\Gamma_{o1}} w \Phi_{fog} T_{go1} d\Gamma \quad (3.16)$$

$$\int_{\Omega_{o2}} \left(w \rho^r c^r \left(\dot{T}_{ro2} + \mathbf{v}_o^r \nabla T_{ro2} \right) + \nabla w \tilde{\lambda}_o^r \nabla T_{ro2} \right) d\Omega + \int_{\Gamma_{o2}} w \Phi_{fog} T_{ro2} d\Gamma = \int_{\Gamma_{o2}} w \Phi_{fog} T_{go2} d\Gamma \quad (3.17)$$

$$\begin{aligned}
 & \int_{\Omega_{gi1}} \left(w\rho^g c^g \dot{T}_{gi1} + \nabla w \lambda^g \nabla T_{gi1} \right) d\Omega + \\
 & \int_{\Gamma_{gs}} w\Phi_{gs} T_{gi1} d\Gamma + \int_{\Gamma_{gi1}} w\Phi_{fig} T_{gi1} d\Gamma + \int_{\Gamma_{gg2}} w\Phi_{gg2} T_{gi1} d\Gamma + 2 \int_{\Gamma_{gg1}} w\Phi_{gg1} T_{gi1} d\Gamma = \\
 & \int_{\Gamma_{gs}} w\Phi_{gs} T_s d\Gamma + \int_{\Gamma_{gi1}} w\Phi_{fig} T_{ri1} d\Gamma + \int_{\Gamma_{gg2}} w\Phi_{gg2} T_{gi2} d\Gamma + \int_{\Gamma_{gg1}} w\Phi_{gg1} T_{go1} d\Gamma + \int_{\Gamma_{gg1}} w\Phi_{gg1} T_{go2} d\Gamma \quad (3.18)
 \end{aligned}$$

$$\begin{aligned}
 & \int_{\Omega_{gi2}} \left(w\rho^g c^g \dot{T}_{gi2} + \nabla w \lambda^g \nabla T_{gi2} \right) d\Omega + \\
 & \int_{\Gamma_{gs}} w\Phi_{gs} T_{gi2} d\Gamma + \int_{\Gamma_{gi2}} w\Phi_{fig} T_{gi2} d\Gamma + \int_{\Gamma_{gg2}} w\Phi_{gg2} T_{gi2} d\Gamma + 2 \int_{\Gamma_{gg1}} w\Phi_{gg1} T_{gi2} d\Gamma = \\
 & \int_{\Gamma_{gs}} w\Phi_{gs} T_s d\Gamma + \int_{\Gamma_{gi2}} w\Phi_{fig} T_{ri2} d\Gamma + \int_{\Gamma_{gg2}} w\Phi_{gg2} T_{gi1} d\Gamma + \int_{\Gamma_{gg1}} w\Phi_{gg1} T_{go1} d\Gamma + \int_{\Gamma_{gg1}} w\Phi_{gg1} T_{go2} d\Gamma \quad (3.19)
 \end{aligned}$$

$$\begin{aligned}
 & \int_{\Omega_{go1}} \left(w\rho^g c^g \dot{T}_{go1} + \nabla w \lambda^g \nabla T_{go1} \right) d\Omega + \\
 & \int_{\Gamma_{gs}} w\Phi_{gs} T_{go1} d\Gamma + \int_{\Gamma_{go1}} w\Phi_{fog} T_{go1} d\Gamma + \int_{\Gamma_{gg2}} w\Phi_{gg2} T_{go1} d\Gamma + 2 \int_{\Gamma_{gg1}} w\Phi_{gg1} T_{go1} d\Gamma = \\
 & \int_{\Gamma_{gs}} w\Phi_{gs} T_s d\Gamma + \int_{\Gamma_{go1}} w\Phi_{fog} T_{ro1} d\Gamma + \int_{\Gamma_{gg2}} w\Phi_{gg2} T_{go2} d\Gamma + \int_{\Gamma_{gg1}} w\Phi_{gg1} T_{gi1} d\Gamma + \int_{\Gamma_{gg1}} w\Phi_{gg1} T_{gi2} d\Gamma \quad (3.20)
 \end{aligned}$$

$$\begin{aligned}
 & \int_{\Omega_{go2}} \left(w\rho^g c^g \dot{T}_{go2} + \nabla w \lambda^g \nabla T_{go2} \right) d\Omega + \\
 & \int_{\Gamma_{gs}} w\Phi_{gs} T_{go2} d\Gamma + \int_{\Gamma_{go2}} w\Phi_{fog} T_{go2} d\Gamma + \int_{\Gamma_{gg2}} w\Phi_{gg2} T_{go2} d\Gamma + 2 \int_{\Gamma_{gg1}} w\Phi_{gg1} T_{go2} d\Gamma = \\
 & \int_{\Gamma_{gs}} w\Phi_{gs} T_s d\Gamma + \int_{\Gamma_{go2}} w\Phi_{fog} T_{ro2} d\Gamma + \int_{\Gamma_{gg2}} w\Phi_{gg2} T_{go1} d\Gamma + \int_{\Gamma_{gg1}} w\Phi_{gg1} T_{gi1} d\Gamma + \int_{\Gamma_{gg1}} w\Phi_{gg1} T_{gi2} d\Gamma \quad (3.21)
 \end{aligned}$$

where thermal heat transfer coefficients Φ for all transition zones (refrigerant-grout, grout-grout, grout-soil) are computed using the following formulas

$$\Phi_{\text{fig}} = \frac{1}{R_{\text{fig}}} \frac{1}{S_i} \quad (3.22)$$

$$\Phi_{\text{fog}} = \frac{1}{R_{\text{fog}}} \frac{1}{S_o} \quad (3.23)$$

$$\Phi_{\text{gg1}} = \frac{1}{R_{\text{gg1}}} \frac{1}{S_{\text{gg1}}} \quad (3.24)$$

$$\Phi_{\text{gg2}} = \frac{1}{R_{\text{gg2}}} \frac{1}{S_{\text{gg2}}} \quad (3.25)$$

$$\Phi_{\text{gs}} = \frac{1}{R_{\text{gs}}} \frac{1}{S_{\text{gs}}} \quad (3.26)$$

$$S_i = \pi (d_i^{\text{int}}) \quad (3.27)$$

$$S_o = \pi (d_o^{\text{int}}) \quad (3.28)$$

$$S_{\text{gg1}} = \frac{D}{2} \quad (3.29)$$

$$S_{\text{gg2}} = D \quad (3.30)$$

$$S_{\text{gs}} = \frac{\pi D}{4} \quad (3.31)$$

Detailed information on how to compute resistances ([1], [3]) is given in the appendix A.2. In fact the following constraints must be satisfied

$$\left(\frac{1}{R_{\text{gg1}}} + \frac{1}{2R_{\text{gs}}} \right)^{-1} > 0 \quad (3.32)$$

$$\left(\frac{1}{R_{\text{gg2}}} + \frac{1}{2R_{\text{gs}}} \right)^{-1} > 0 \quad (3.33)$$

In case of violation of the above conditions a special correction procedure (see [3]) has to be used (see appendix A.2).

3.3 Balance equations for CXA exchanger

The cross section of CXA heat exchanger and relations between heat resistances in all transition zones are shown in fig.3.3.

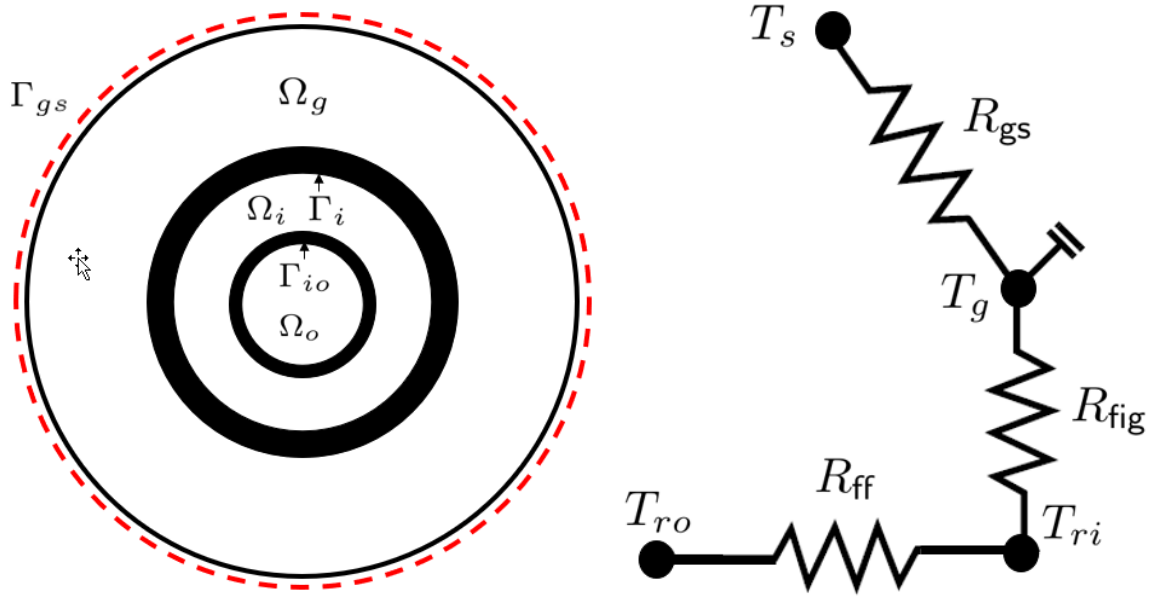


Figure 3.3: General scheme and heat resistance relations for CXA system

The set of heat balance equations is expressed as follows

$$\begin{aligned} \int_{\Omega_i} \left(w \rho^r c^r \left(\dot{T}_{ri} + \mathbf{v}_i^r \nabla T_{ri} \right) + \nabla w \tilde{\lambda}_i^r \nabla T_{ri} \right) d\Omega + \int_{\Gamma_i} w \Phi_{fig} T_{ri} d\Gamma + \int_{\Gamma_{io}} w \Phi_{ff} T_{ri} d\Gamma = \\ \int_{\Gamma_i} w \Phi_{fig} T_g d\Gamma + \int_{\Gamma_{io}} w \Phi_{ff} T_{ro} d\Gamma \end{aligned} \quad (3.34)$$

$$\begin{aligned} \int_{\Omega_o} \left(w \rho^r c^r \left(\dot{T}_{ro} + \mathbf{v}_o^r \nabla T_{ro} \right) + \nabla w \tilde{\lambda}_o^r \nabla T_{ro} \right) d\Omega + \int_{\Gamma_{io}} w \Phi_{ff} T_{ro} d\Gamma = \\ \int_{\Gamma_{io}} w \Phi_{ff} T_{ri} d\Gamma \end{aligned} \quad (3.35)$$

$$\begin{aligned} \int_{\Omega_g} \left(w \rho^g c^g \dot{T}_g + \nabla w \lambda^g \nabla T_g \right) d\Omega + \int_{\Gamma_{gs}} w \Phi_{gs} T_g d\Gamma + \int_{\Gamma_i} w \Phi_{fig} T_g d\Gamma = \\ \int_{\Gamma_{gs}} w \Phi_{gs} T_s d\Gamma + \int_{\Gamma_i} w \Phi_{fig} T_i d\Gamma \end{aligned} \quad (3.36)$$

where thermal heat transfer coefficients Φ for all transition zones (refrigerant-grout, grout-grout, grout-soil) are computed using the following formulas

$$\Phi_{\text{fig}} = \frac{1}{R_{\text{fig}}} \frac{1}{S_i} \quad (3.37)$$

$$\Phi_{\text{ff}} = \frac{1}{R_{\text{ff}}} \frac{1}{S_{io}} \quad (3.38)$$

$$\Phi_{\text{gs}} = \frac{1}{R_{\text{gs}}} \frac{1}{S_{gs}} \quad (3.39)$$

$$S_i = \pi (d_i^{\text{int}}) \quad (3.40)$$

$$S_{io} = \pi (d_o^{\text{int}}) \quad (3.41)$$

$$S_{gs} = \pi D \quad (3.42)$$

For detailed information on how to compute resistances and heat transfer coefficients please refer to the paper [1] and FEFLOW white paper[3].

3.4 Balance equations for CXC exchanger

The cross section of CXC heat exchanger and relations between heat resistances in all transition zones are shown in fig.3.4.

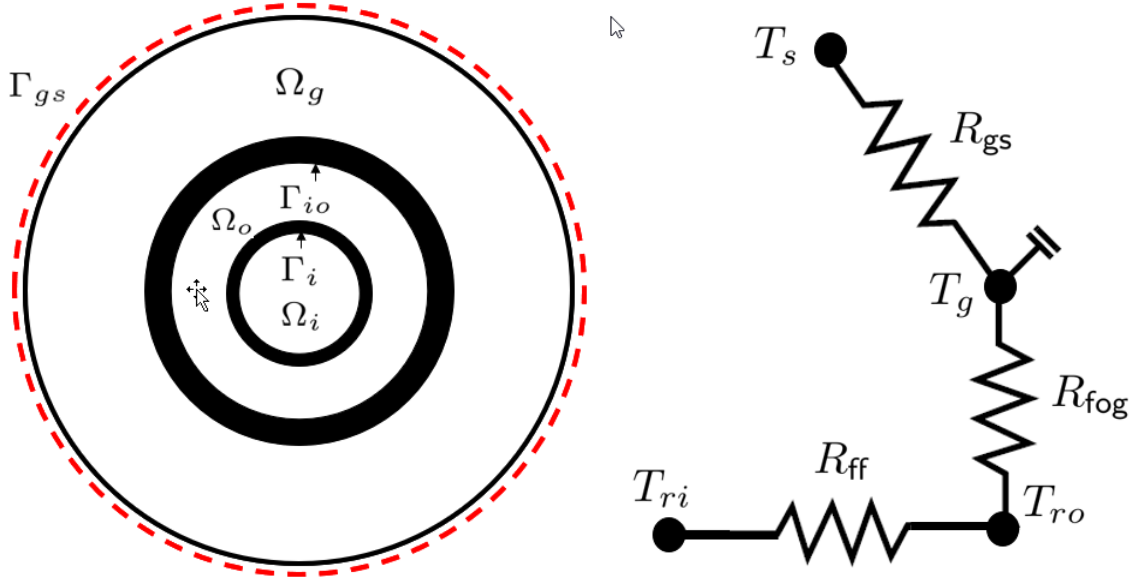


Figure 3.4: General scheme and heat resistance relations for CXC system

The set of heat balance equations is expressed as follows

$$\int_{\Omega_i} \left(w \rho^r c^r \left(\dot{T}_{ri} + \mathbf{v}_i^r \nabla T_{ri} \right) + \nabla w \tilde{\lambda}_i^r \nabla T_{ri} \right) d\Omega + \int_{\Gamma_{io}} w \Phi_{ff} T_{ri} d\Gamma = \int_{\Gamma_{io}} w \Phi_{ff} T_{ro} d\Gamma \quad (3.43)$$

$$\int_{\Omega_o} \left(w \rho^r c^r \left(\dot{T}_{ro} + \mathbf{v}_o^r \nabla T_{ro} \right) + \nabla w \tilde{\lambda}_o^r \nabla T_{ro} \right) d\Omega + \int_{\Gamma_o} w \Phi_{ff} T_{ro} d\Gamma + \int_{\Gamma_{io}} w \Phi_{ff} T_{ro} d\Gamma = \int_{\Gamma_o} w \Phi_{fog} T_g d\Gamma + \int_{\Gamma_{io}} w \Phi_{ff} T_{ri} d\Gamma \quad (3.44)$$

$$\int_{\Omega_g} \left(w \rho^g c^g \dot{T}_g + \nabla w \lambda^g \nabla T_g \right) d\Omega + \int_{\Gamma_{gs}} w \Phi_{gs} T_g d\Gamma + \int_{\Gamma_o} w \Phi_{fog} T_g d\Gamma = \int_{\Gamma_{gs}} w \Phi_{gs} T_s d\Gamma + \int_{\Gamma_o} w \Phi_{fog} T_o d\Gamma \quad (3.45)$$

where thermal heat transfer coefficients Φ for all transition zones (refrigerant-grout, grout-grout, grout-soil) are computed using the following formulas

$$\Phi_{\text{fog}} = \frac{1}{R_{\text{fog}}} \frac{1}{S_o} \quad (3.46)$$

$$\Phi_{\text{ff}} = \frac{1}{R_{\text{ff}}} \frac{1}{S_{io}} \quad (3.47)$$

$$\Phi_{\text{gs}} = \frac{1}{R_{\text{gs}}} \frac{1}{S_{gs}} \quad (3.48)$$

$$S_o = \pi (d_o^{\text{int}}) \quad (3.49)$$

$$S_{io} = \pi (d_i^{\text{int}}) \quad (3.50)$$

$$S_{gs} = \pi D \quad (3.51)$$

For detailed information on how to compute resistances and heat transfer coefficients please refer to the paper [1] and FEFLOW white paper[3].

3.5 Balance equations for a single pipe with explicit grout discretization

The cross section of 1U heat exchanger and relations between heat resistances in all transition zones are shown in fig.3.1.

The set of heat balance equations is expressed as follows

$$\int_{\Omega_r} \left(w \rho^r c^r \left(\dot{T}_r + \mathbf{v}_i^r \nabla T_r \right) + \nabla w \tilde{\lambda}_i^r \nabla T_r \right) d\Omega + \int_{\Gamma_r} w \Phi_{\text{fig}} T_r d\Gamma = \int_{\Gamma_r} w \Phi_{\text{fig}} T_s d\Gamma \quad (3.52)$$

where thermal heat transfer coefficient Φ_{fig} in the transition zone (refrigerant-grout) is computed using the following formulas

$$\Phi_{\text{fig}} = \frac{1}{R_{\text{fig}}} \frac{1}{S_i} \quad (3.53)$$

$$S_i = \pi d^{\text{int}} \quad (3.54)$$

$$(3.55)$$

Computation of the R_{fig} resistance is the same as for the 1U system.

3.6 Weakly coupled hydro-thermal formulation

In the current ZSoil v24 version weakly coupled hydro-thermal formulation has been implemented by adding advective term to the heat transfer balance equation. This term is expressed as follows

$$\int_{\Omega} \rho^f c^f \mathbf{v}^f \text{grad} T d\Omega \quad (3.56)$$

In order to take this term into account a seepage (steady/transient) problem has to be solved first and then associated with the heat transfer one. The Darcy velocity \mathbf{v}^f vector and saturation ratio are then mapped, at each time instance, on the heat transfer mesh, by means of the super-convergent patch recovery method. No extra stabilization term is added to the heat transfer equations for soil as we assume that Darcy velocities are rather small. Once the seepage project is associated with the heat transfer one soil is treated as the two-phase medium. Therefore, the heat conductivity as well as the heat capacity are computed using the following formulas

$$\lambda = (1 - n) \lambda^s + n S \lambda^f \quad (3.57)$$

$$c^* = \rho c = (1 - n) c^{s,*} + n S c^{f,*} \quad (3.58)$$

where porosity is denoted by n and saturation ratio by S . Once the seepage project is not associated with the heat transfer one thermal soil parameters are taken as for the solid $\lambda = \lambda^s$ and $c^* = c^{s,*}$. User may switch off the advection term locally at the material level in the FLOW group of parameters. Benchmarks for the advective heat transfer problem can be found in the Benchmarks ZSoil book.

Chapter 4

Finite elements for borehole heat exchangers (BHE elements)

4.1 Pipe type heat exchanger

The pipe type finite element consists of 4 nodes as shown in fig. 4.1. Two first nodes belong to the pipe while the remaining two nodes are attached to the soil mesh in a conforming manner or by using local/nonlocal form of constraints. This element requires an explicit grout discretization.

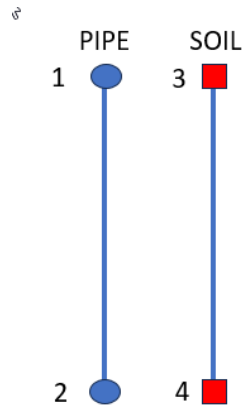


Figure 4.1: Pipe type finite element

4.2 CXA heat exchanger

The finite element for the CXA exchanger consists of 8 nodes as shown in fig. 4.2. Two first nodes belong to the inlet pipe next two to the outlet pipe, then the next two to the grout and the remaining two nodes are attached to the soil mesh in a conforming manner or by using local/nonlocal form of constraints. In this element a periodic boundary condition is enforced $T_{ri}(z = L) = T_{ro}(z = L)$ at the bottom of the macro-exchanger.

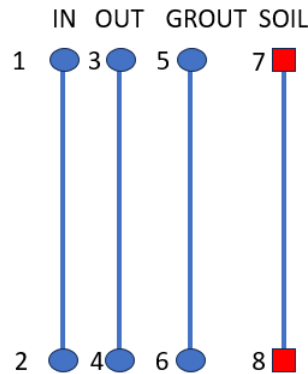


Figure 4.2: Finite element for modeling the CXA exchanger

4.3 CXC heat exchanger

The finite element for the CXC exchanger consists of 8 nodes as shown in fig. 4.3. Two first nodes belong to the inlet pipe next two to the outlet pipe, then the next two to the grout and the remaining two nodes are attached to the soil mesh in a conforming manner or by using local/nonlocal form of constraints. In this element a periodic boundary condition is enforced $T_{ri}(z = L) = T_{ro}(z = L)$ at the bottom of the macro-exchanger. In fact it is practically the same as the one for the CXA system.

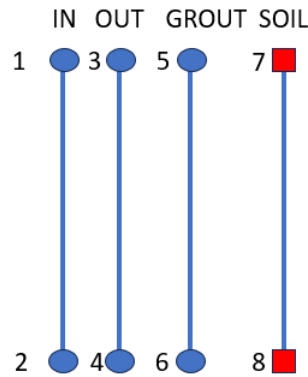


Figure 4.3: Finite element for modeling the CXC exchanger

4.4 1U heat exchanger

The finite element for the 1U exchanger consists of 10 nodes as shown in fig. 4.4. The first two nodes belong to the inlet pipe, the next two to the outlet pipe, then the next two to the grout in pipe-in zone, next two to the grout in the pipe-out zone and the remaining two nodes are attached to the soil mesh in a conforming manner, or by using local/nonlocal form of constraints. In this element a periodic boundary condition is enforced $T_{ri}(z = L) = T_{ro}(z = L)$ at the bottom of the macro-exchanger.

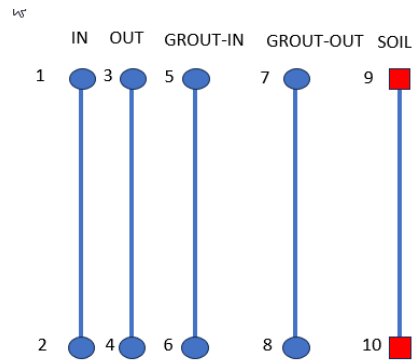


Figure 4.4: Finite element for modeling the 1U exchanger

4.5 2U heat exchanger

The finite element for the 2U exchanger consists of 18 nodes as shown in fig. 4.5. The first two pairs of nodes belong to the pipe-in 1 and pipe-in 2, the next two pairs of nodes belong to the pipe-out 1 and pipe-out 2, then the next two pairs of nodes to the grout zones of pipe-in 1 and pipe-in 2, next two pairs to the grout zone of the pipe-out 1 and 2, and the remaining two nodes are attached to the soil mesh in a conforming manner, or by using local/nonlocal form of constraints.

For the parallel discharge two periodic conditions are enforced $T_{ri,1}(z = L) = T_{ro,1}(z = L)$ and $T_{ri,2}(z = L) = T_{ro,2}(z = L)$, at the bottom of the macro-exchanger. For the serial discharge three periodic conditions are enforced $T_{ri,1}(z = L) = T_{ro,1}(z = L)$, $T_{ri,2}(z = 0) = T_{ro,1}(z = 0)$ and $T_{ri,2}(z = L) = T_{ro,2}(z = L)$.

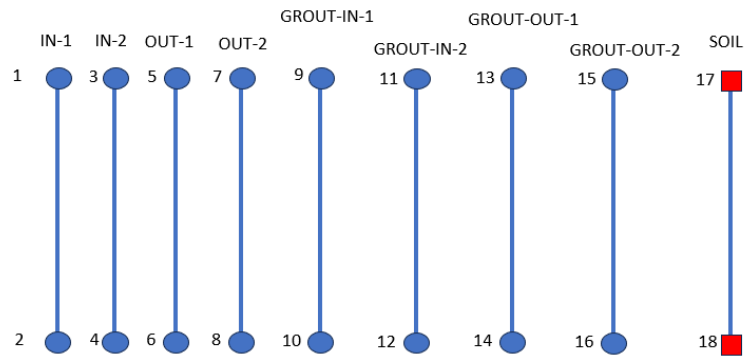


Figure 4.5: Finite element for modeling the 2U exchanger

Chapter 5

User interface

5.1 Preprocessing

5.1.1 Generating heat exchangers

In general the two types of heat exchangers can be modeled with the current ZSoil version, ones with the explicit grout (pipes with the refrigerant only) or ones with the implicit grout zone (pipe with refrigerant and grout zone). In the first group grout has to be discretized using standard continuum elements, therefore it may have any geometrical form, while the second group is limited to the circular form only. Heat exchangers with the implicit grout zone can be of 1U, 2U, CXA or CXC type. **Its worth to mention that heat exchangers can be analyzed exclusively in 3D models.**

5.1.1.1 Generating heat exchangers with explicit grout

Heat exchangers can be defined exclusively at the macro-model level. In order to create such an exchanger (or its segment) one has to select drawing primitives (lines, polylines) and use the option *Macro-model/Heat exchanger/Create/Pipes on objects* (see fig.5.1). In case the exchanger is created on a polyline all detected segments are listed in the following dialog box (see fig.5.2). In order to differentiate pipe properties (to model insulation for instance) exchangers must be defined separately on different line segments. On each segment different material can be set. In the configuration shown in fig.5.1 there is no need to add the short exchanger segment at the bottom but both pipe endpoints have to be connected using option *Macro-model/Heat exchanger/Link pipe nodes*. Using this option pipe nodes will be unified. Heat exchanger elements can flow through the continuum 3D mesh in an arbitrary manner. The exchanger macro-element has to be split using automatic split option or hand splitting by declaring approximate element length or number of elements per segment. Once the option *Link soil nodes with background mesh using nonlocal constraints* is ON, the heat exchanger mesh, no matter if it is conforming with the soil mesh or not, will be linked to the background continuum mesh using nonlocal constraints (soil temperature is taken as an average along the circle with radius equal to the radius of the pipe). Otherwise, in case of nonconforming meshes, exchanger soil nodes are linked to the background mesh using local form of the constraints.

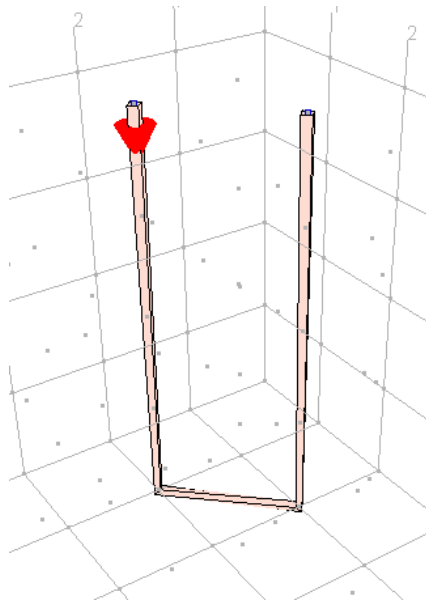


Figure 5.1: Creating heat exchanger with the explicit grout on selected line segments

Heat Exchanger

Parameters

	Material	Material zone begins at depth
1	Define	0 [m]
	Define	

Existence function: 0 <Edit...>

Split

☐ Automatic (adaptive split) Eliminate segments shorter than 0.25 [m]

Segment	Split type	Split Length
1-2 (4 m)	Number of segments	5
2-3 (1.41421 m)	Number of segments	1
3-4 (4 m)	Approximate segment length	1 [m]

☐ Link BHE soil nodes with background mesh using nonlocal constraints

OK Cancel

Figure 5.2: Creating heat exchanger with the explicit grout on objects

5.1.1.2 Generating heat exchangers with implicit grout

Borehole heat exchangers with implicit grout can be defined exclusively at the macro-model level. Type of the exchanger is declared at the material level. In order to create such an exchanger (or its segment) one has to select drawing primitives (lines, polylines) and use the option *Macro-model/Heat exchanger/Create/Pipes*

on objects (see fig.5.3). In case the exchanger is created on a polyline all detected segments are listed in the following dialog box (see fig.5.4). In order to differentiate pipe properties (to model insulation for instance) exchangers must be defined separately on different line segments. On each segment different material can be set. In the configuration shown in fig.5.1 there is no need to add the short exchanger segment at the bottom but both pipe endpoints have to be connected using option *Macro-model/Heat exchanger/Link pipe nodes*. Using this option pipe nodes will be unified.

The dialog box is titled "Heat Exchanger" and contains the following sections:

- Parameters:** A table with columns "Material" and "Material zone begins at depth". It has two rows, each with a "Define" button. Below the table is an "Existence function" field with the value "0" and an "<Edit...>" button.
- Split:** A section with a checked "Automatic (adaptive split)" checkbox and a text field "Eliminate segments shorter than" with the value "0.25" and a "[m]" unit. Below this is a table:

Segment	Split type	Split Length
1-2 (4 m)	Approximate segment length	1 [m]
2-3 (3 m)	Approximate segment length	1 [m]
- At the bottom, there is a checkbox "Link BHE soil nodes with background mesh using nonlocal constraints" and "OK" and "Cancel" buttons.

Figure 5.3: Creating borehole heat exchanger with the implicit grout on selected line segments

5.1.2 Meshing soil volume in the vicinity of the BHE elements

In the current implementation it is recommended to use non-local form of constraints to link exchanger soil nodes with the background mesh. This method preserves h -convergence property which is expected in finite element formulations. It is well known that standard formulation may yield severe mesh dependency once the mesh size is relatively small. Optimal continuum mesh size in the vicinity of heat exchangers is of order $5..6D$ in case of exchangers with the implicit grout.

5.2 Material data

Material properties for the exchanger are defined in the following dialog box invoked under material menu. Parameters that are unused for a given exchanger class are grayed. In this dialog box user may calculate resulting heat resistances for given set of material properties of all constituents but approximate exchanger length must explicitly be given (button **Compute** must be pressed to activate the option). To model insulation along the pipe thermal conductivity of the pipe has to be set to very low value.

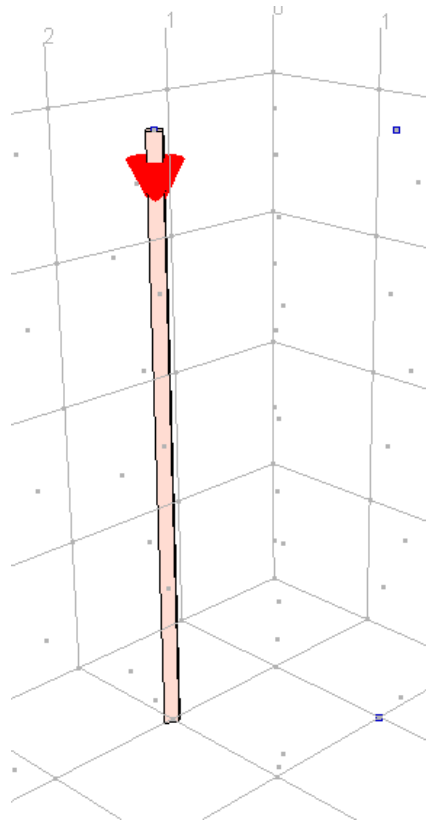



Figure 5.4: Creating borehole heat exchanger with the implicit grout on objects

5.3 Initial and boundary conditions

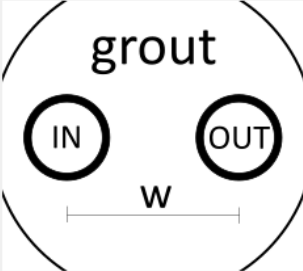
Boundary conditions in form of the nodal temperature on the inlet pipe can be set using option *Macro-model/Temperature BC/Create/On heat exchanger point*. Another possibility is to set the heat flux using option *Macro-model/Heat flux/Create/On heat exchanger point*. The optimal way to control the initial conditions is to add the *Initial state* driver which runs steady state analysis at time $t = 0$. The transient driver can be added and exchanger nodal temperature, or flux, are progressively applied.

5.4 Postprocessing

Results from heat exchanger are stored in the external file (*.csv format) with the extension *.bhe. Temperatures in any set of exchanger nodes (pipes IN, pipes OUT, grout pipe-IN zones, grout pipe-OUT zones and soil) are plot in the postprocessor.

 Borehole heat exchangers

Parameter	Value	Unit
BHE type	1U	
Borehole diameter	0.15	[m]
Pipe distance	0.06	[m]
Pipe IN outer diameter	0.032	[m]
Pipe IN wall thickness	0.0029	[m]
Pipe IN thermal conductivity	0.38	[W/m/C]
Pipe OUT outer diameter	0.032	[m]
Pipe OUT wall thickness	0.0029	[m]
Pipe OUT thermal conductivity	0.38	[W/m/C]
Refrigerant vol. flow discharge	19.9999584	[m ³ /day]
Refrigerant vol. flow discharge type	Parallel	
Refrigerant thermal conductivity	0.64	[W/m/C]
Refrigerant dyn. viscosity	0.000000000006	[kN/m ² *day]
Refrigerant vol. heat capacity	4130	[kJ/m ³ /C]
Refrigerant density	0.000000000132	[kN/m ⁴ *day ²]
Grout thermal conductivity	2.3	[W/m/C]
Grout vol. heat capacity	2190	[kJ/m ³ /C]



Compute

Heat transfer coeff.	Value	Unit
Use coefficients given below	<input type="checkbox"/>	
Approximate exchanger length	100	[m]
Heat transfer coeff. Phi_fig	0	[W/m ² /C]
Heat transfer coeff. Phi_fog	0	[W/m ² /C]
Heat transfer coeff. Phi_gg1	0	[W/m ² /C]
Heat transfer coeff. Phi_gg2	0	[W/m ² /C]
Heat transfer coeff. Phi_gs	0	[W/m ² /C]

OK Cancel

Figure 5.5: Material parameters for the exchanger

Chapter 6

Benchmarks for different classes of heat exchnagers

6.1 Benchmarks for the pipe type exchanger

6.1.1 Heat exchange between pipe and ground assuming constant ground temperature and steady state conditions

Files: BHE_PPE_steady_const_T.inp, BHE_PPE_transient_const_T.inp

In this benchmark heat exchange between the 50m long vertical pipe and soil is analyzed. Soil temperature is fixed at each node of the soil mesh at $T_s=10^\circ\text{C}$. Temperature at the top point of the heat exchanger varies in time with the following load time function

Table 6.1: Load time function for the temperature at the top point of the heat exchanger

Time [s]	$T_s(t)$ [$^\circ\text{C}$]
0	10
10	30
20	50

Here we run the multi-steady steady analysis which starts at time $t=0$ s, then two steps are executed at $t = 10\text{s}$ and $t = 20$ s. This problem has the following closed form analytical solution

$$T(z) = T_s - (T_s - T_r(z=0)) \exp\left(\frac{-\pi d_i^{\text{int}} z \Phi_{\text{fig}}}{Q^r \rho^r c^r}\right) \quad (6.1)$$

A uniform mesh generated for this benchmark is shown in the fig.6.1. The same split is used here for the soil and for the exchanger meshes. In case on the single pipe exchanger type its orientation is very important due to presence of the advective term.

Material properties for the heat exchanger are given in the following table

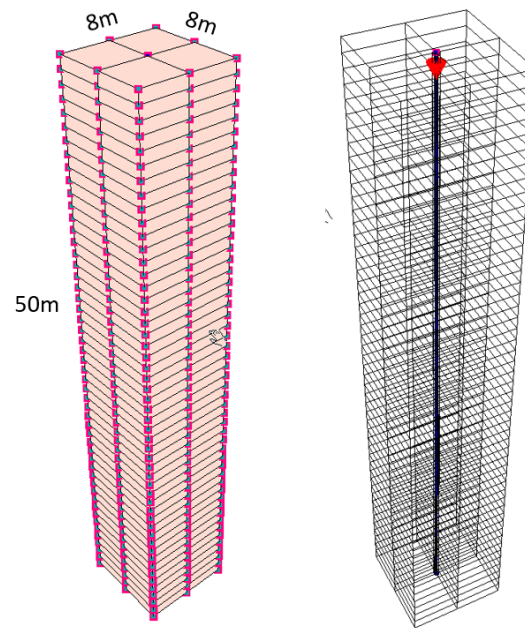


Figure 6.1: FE model

Comparizon of the analytical and numerical solutions for the steady state conditions is shown in fig.6.2. It is well visible that the numerical solution matches perfectly the analytical one.

Table 6.2: Material properties for the heat exchanger

Parameter	Symbol	Unit	Value
BHE type			Pipe (no grout)
Borehole diameter	D	[m]	unused
Pipe distance	w	[m]	unused
Pipe (IN) outer diameter	d_i^{ext}	[m]	0.036
Pipe (IN) wall thickness	h_i	[m]	0.003
Pipe (IN) thermal conductivity	λ_i^p	[W/m/K]	0.38
Pipe (OUT) outer diameter	d_o^{ext}	[m]	unused
Pipe (OUT) wall thickness	h_o	[m]	unused
Pipe (OUT) thermal conductivity	λ_o^p	[W/m/K]	unused
Refrigerant vol. flow discharge	Q^r	[m ³ /s]	2.120575E-04
Refrigerant vol. flow discharge type			unused
Refrigerant thermal conductivity	λ^r	[W/m/K]	0.64
Refrigerant dynamic viscosity	μ^r	[kPa s]	5.5e-7
Refrigerant vol. heat capacity	$\rho^r c^r$	[kJ/m ³ /K]	4130.0
Refrigerant density	ρ^r	[kg/m ³]	1000.0
Grout thermal conductivity	λ^g	[W/m/K]	2.30
Grout heat capacity	$\rho^g c^g$	[kJ/m ³ /K]	2190.0

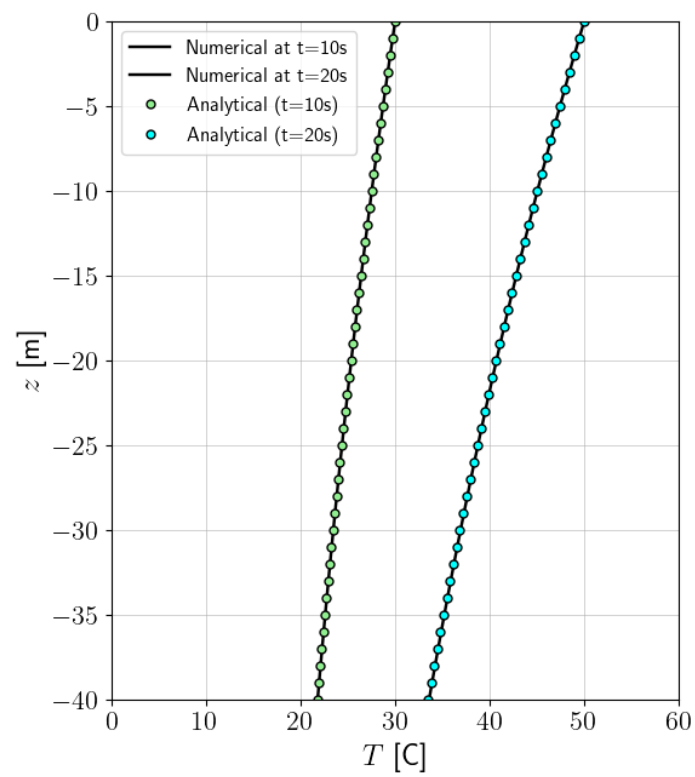


Figure 6.2: Comparizon of computed and analytical temperature profiles for steady state conditions at time instances $t = 1$ s and $t = 20$ s

6.1.2 Heat exchange between pipe and ground assuming constant ground temperature and transient state conditions

Files: BHE_PPE_transient_const_T.inp

In this benchmark a transient case of the problem described in section 6.1.1 is analyzed. The load time function for the temperature fixed at the top exchanger point is shown in the following table.

Table 6.3: Load time function for the temperature at the top point of the heat exchanger

Time [s]	$T_s(t)$ [°C]
0	10
1	30
300	30

Three drivers are set up to carry out this analysis ie. The initial state (equivalent to the steady state one at $t = 0$), then the transient one from $t = 0..1$ [s] with step 0.1s and the next transient one from $t = 1..100$ s with the initial step $\Delta t_0=0.1$ s and time increment multiplier $\Delta t_{FAC} = 1.02$. The remaining data is exactly the same as in the benchmark presented in the section 6.1.2.

The evolution of refrigerant temperature profiles for the four selected time instances is shown in fig.6.3. At time $t = 300$ [s] steady state conditions are achieved.

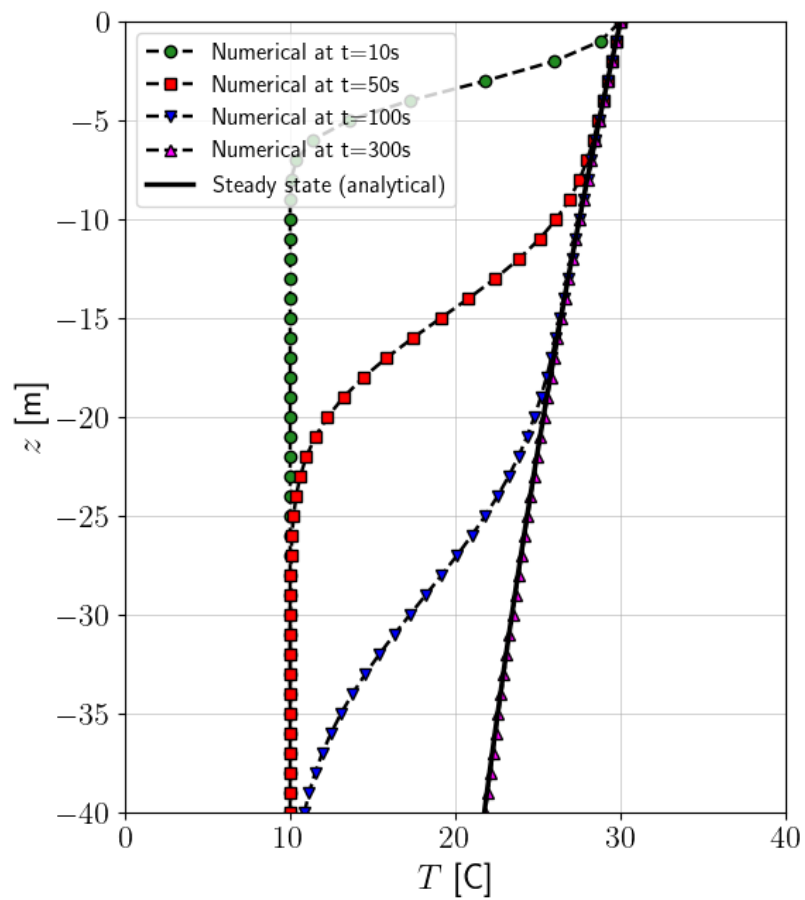


Figure 6.3: Computed temperature profiles for transient state conditions at time instances $t = 10, 50, 100$ and 300s

6.1.3 Heat exchange between pipe and ground assuming constant ground temperature and steady state conditions using local form of constraints to connect nonconforming soil and exchanger meshes

Files: BHE_PPE_steady_const_T-LocLink.inp

In this benchmark exactly the same problem as described in the section 6.1.1 is analyzed but exchanger mesh is not compatible with the soil mesh. Therefore soil nodes of the exchanger element are implicitly connected to the soil continuum mesh using local form of constraints (equivalent to the *Nodal link* option in which temperature is the active degree of freedom). The 50m long exchanger is split to 60 elements (in the continuum soil mesh 50 elements are used).

Comparizon of the analytical and numerical solutions for the steady state conditions is shown in fig.6.4. It is well visible that the numerical solution matches perfectly the analytical one.

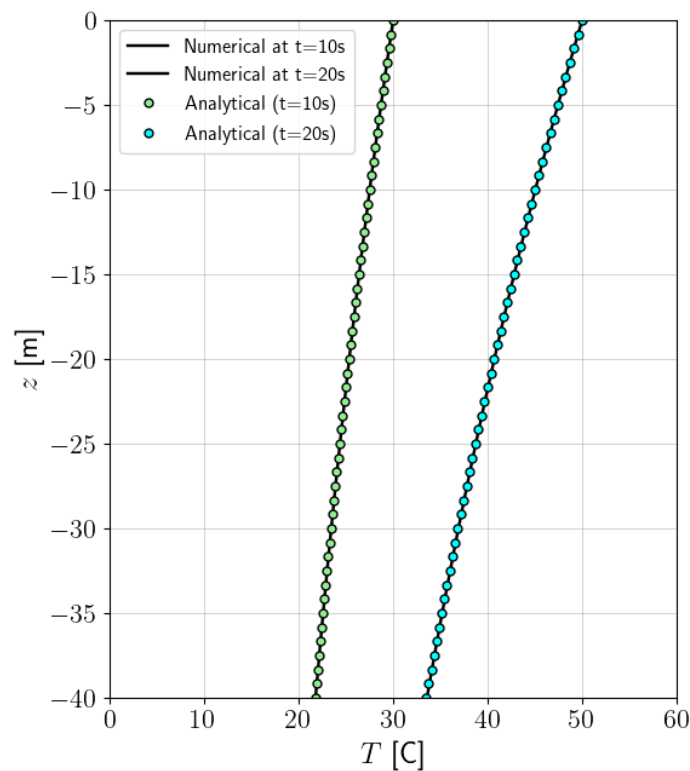


Figure 6.4: Comparizon of computed and analytical temperature profiles for steady state conditions at time instances $t = 10s$ and $t = 20s$

6.1.4 Heat exchange between pipe and ground assuming constant ground temperature and steady state conditions using non-local form of constraints to connect nonconforming soil and exchanger meshes

Files: BHE_PPE_steady_const_T-nnlink.inp

In this benchmark exactly the same problem as described in the section 6.1.1 is analyzed but exchanger mesh is not compatible with the soil mesh. Therefore soil nodes of the exchanger element are implicitly connected to the soil continuum mesh using non-local form of constraints. The 50m long exchanger is split to 60 elements (in the continuum soil mesh 50 elements are used).

Comparizon of the analytical and numerical solutions for the steady state conditions is shown in fig.6.5. It is well visible that the numerical solution matches perfectly the analytical one.

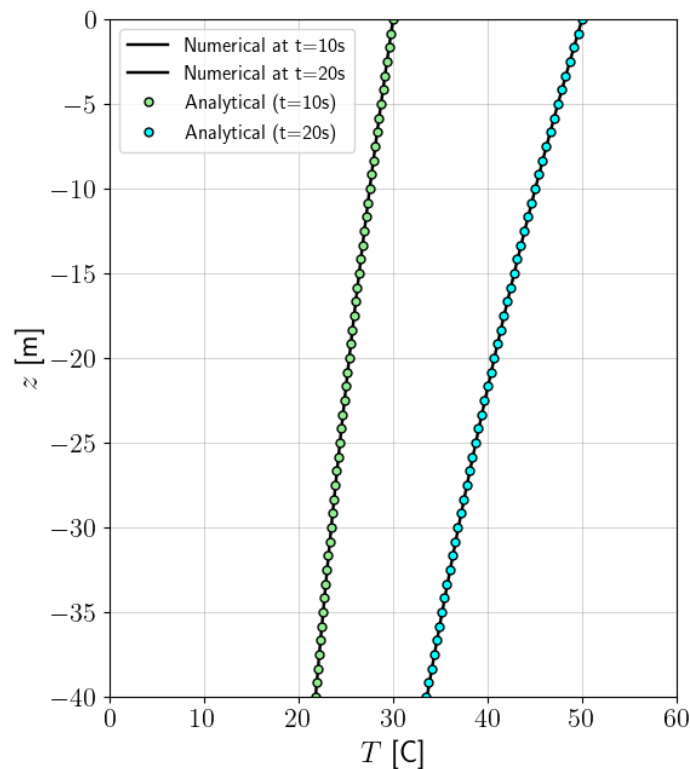


Figure 6.5: Comparizon of computed and analytical temperature profiles for steady state conditions at time instances $t = 10s$ and $t = 20s$

6.1.5 Heat exchange between pipe and ground assuming variable ground temperature

Files: BHEpipe_transient_var_T-1lay.inp, BHEpipe_transient_var_T-1lay-Qr.inp

In this benchmark the problem of a line heat source in the unbounded domain is analyzed. Geometry of the problem and discretization is shown in figure 6.6.

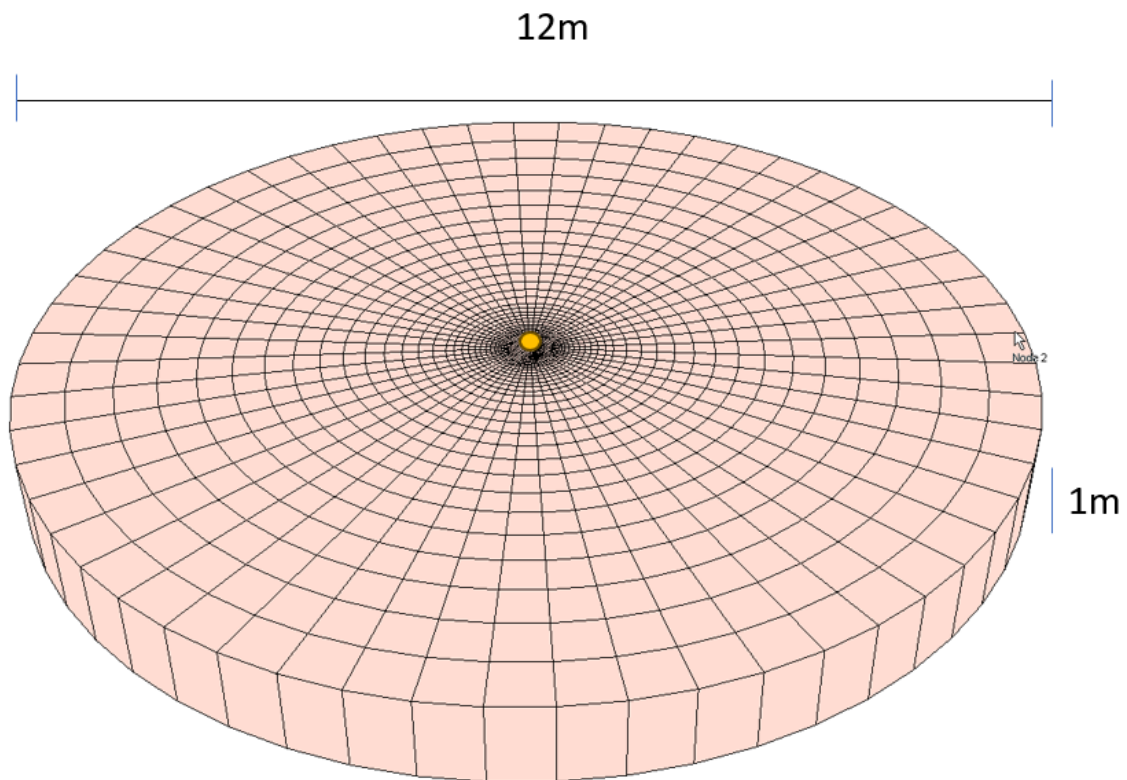


Figure 6.6: Finite element mesh

This problem is solved using the two data setups

1. the refrigerant volumetric discharge is very small ($Q_r = 10^{-12} \text{ m}^3/\text{s}$) while the heat conductivity coefficients for the pipe and for the refrigerant are very large and at the top exchanger point the nodal heat flux $Q = 50 \text{ W}$ is applied; this yields a linear heat source $q = 50 \text{ W/m}$
2. the refrigerant volumetric discharge is very large ($Q_r = 100 \text{ m}^3/\text{s}$) while the heat conductivity coefficients for the pipe and for the refrigerant are very large and at the top exchanger point the nodal heat flux $Q = 25 \text{ W}$ is applied

In both cases the resulting heat transfer coefficient Φ_{fig} becomes very large.

Material properties for the pipe type exchanger and soil are summarized in the two following tables.

Table 6.4: Material properties for the heat exchanger

Parameter	Symbol	Unit	Value
BHE type			Pipe (no grout)
Borehole diameter	D	[m]	unused
Pipe distance	w	[m]	unused
Pipe (IN) outer diameter	d_i^{ext}	[m]	0.036
Pipe (IN) wall thickness	h_i	[m]	0.003
Pipe (IN) thermal conductivity	λ_i^p	[W/m/K]	0.38×10^6
Pipe (OUT) outer diameter	d_o^{ext}	[m]	unused
Pipe (OUT) wall thickness	h_o	[m]	unused
Pipe (OUT) thermal conductivity	λ_o^p	[W/m/K]	unused
Refrigerant vol. flow discharge	Q^r	[m ³ /s]	$10^{-12}/100$
Refrigerant vol. flow discharge type			unused
Refrigerant thermal conductivity	λ^r	[W/m/K]	0.64×10^6
Refrigerant dynamic viscosity	μ^r	[kPa s]	$5.5e-7$
Refrigerant vol. heat capacity	$\rho^r c^r$	[kJ/m ³ /K]	4130.0
Refrigerant density	ρ^r	[kg/m ³]	1000.0
Grout thermal conductivity	λ^g	[W/m/K]	unused
Grout heat capacity	$\rho^g c^g$	[kJ/m ³ /K]	unused

Table 6.5: Material properties for soil

Parameter	Symbol	Unit	Value
Soil thermal conductivity	λ^s	[W/m/K]	0.294
Soil heat capacity	$\rho^s c^s$	[kJ/m ³ /K]	2300

The closed form solution for radial temperature profile strictly depends on the soil properties and is expressed by the formula

$$T = T_{g,0} + \frac{q}{2\pi k} \int_{\epsilon}^{\infty} \frac{\exp(-\xi^2)}{\xi} d\xi \quad (6.2)$$

$$\epsilon = \frac{r}{2\sqrt{\alpha t}} \quad (6.3)$$

$$\alpha = \frac{\lambda^s}{\rho^s c^s} \quad (6.4)$$

where q is the linear heat source value (power density in [W/m]), r is the radial distance from the source, α is the diffusivity coefficient and t is the current time value.

Comparizon of numerical and analytical temperature profiles drawn along radial direction for the first data setup, for time instances $t = 1\text{h}, 3\text{h}, 6\text{h}, 30\text{h}$ and 100h , are shown in fig. 6.7, 6.8, 6.9, 6.10, 6.11 while the corresponding results for the second data setup in fig. 6.12, 6.13, 6.14, 6.15, 6.16 respectively. All numerical results perfectly match the analytical solutions.

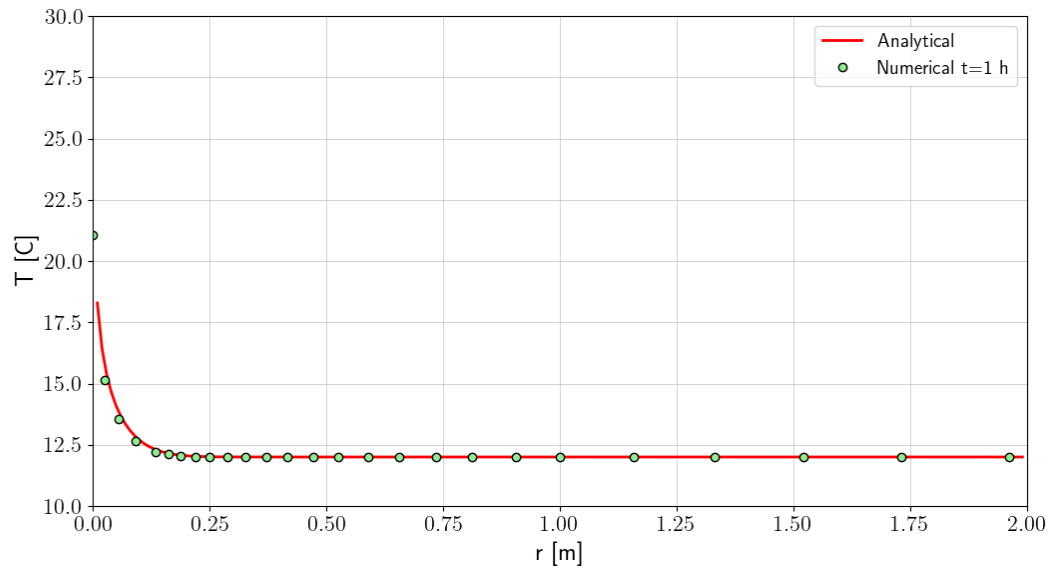


Figure 6.7: Comparison of computed and analytical temperature profiles at $t = 1$ h for the case of very small refrigerant volumetric discharge

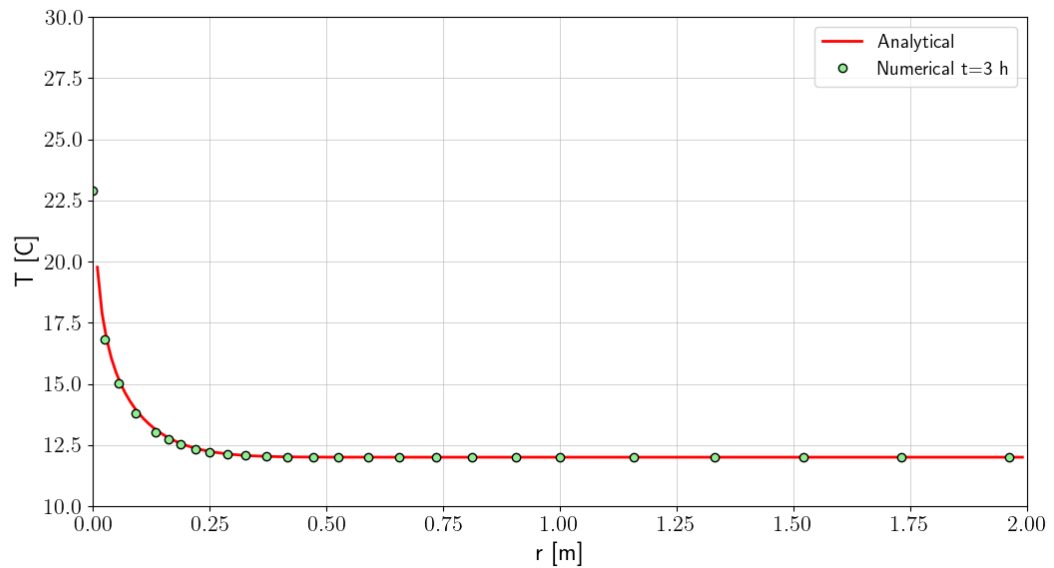


Figure 6.8: Comparison of computed and analytical temperature profiles at $t = 3$ h for the case of very small refrigerant volumetric discharge

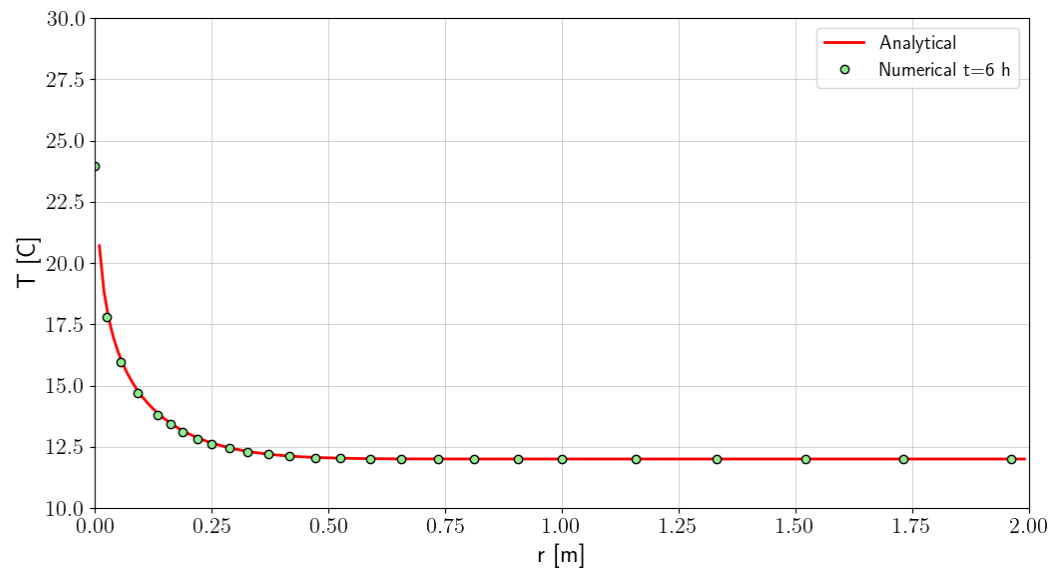


Figure 6.9: Comparizon of computed and analytical temperature profiles at $t = 6h$ for the case of very small refrigerant volumetric discharge

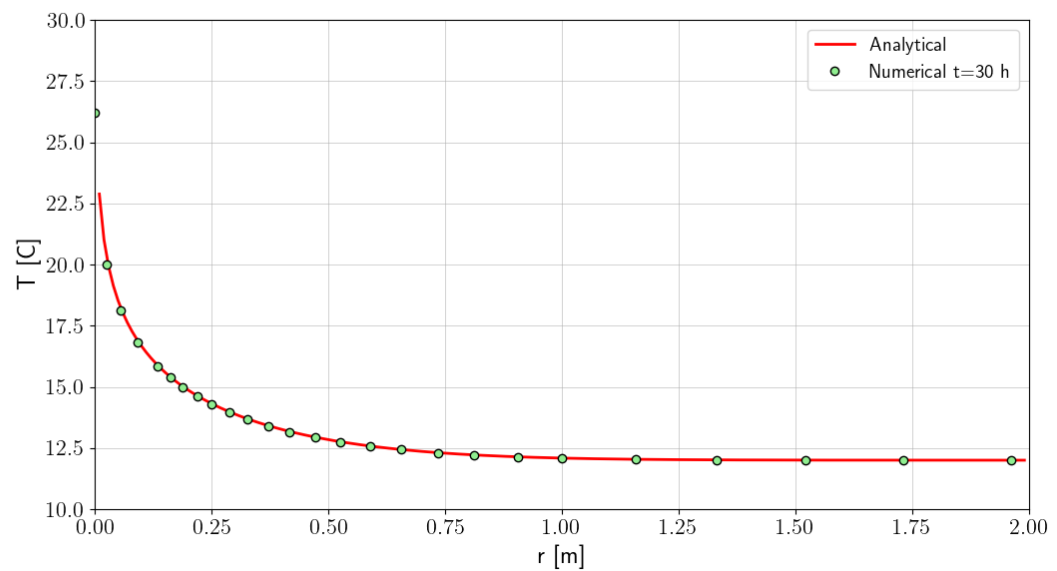


Figure 6.10: Comparizon of computed and analytical temperature profiles at $t = 30h$ for the case of very small refrigerant volumetric discharge

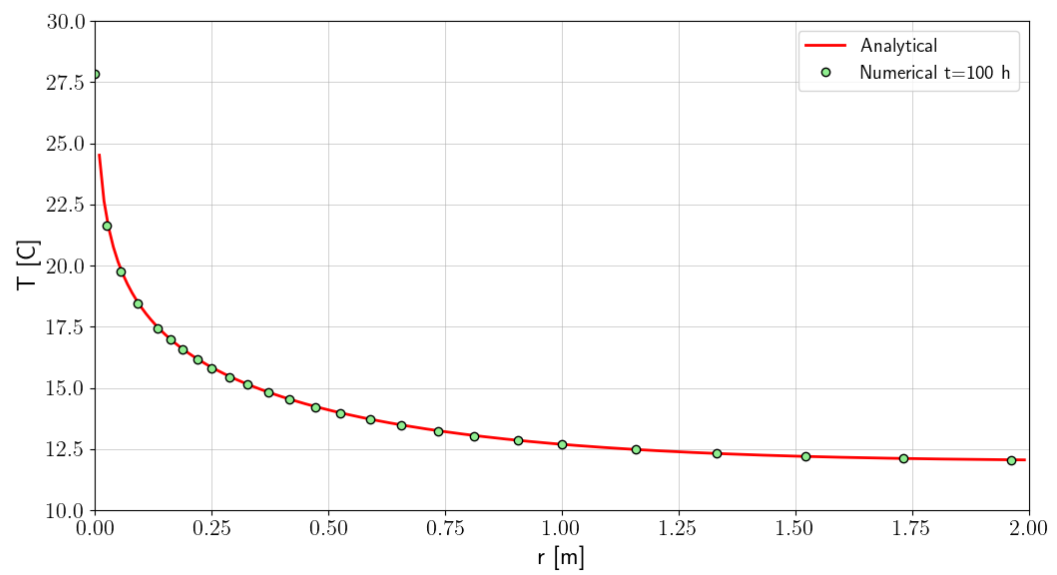


Figure 6.11: Comparison of computed and analytical temperature profiles at $t = 100\text{h}$ for the case of very small refrigerant volumetric discharge

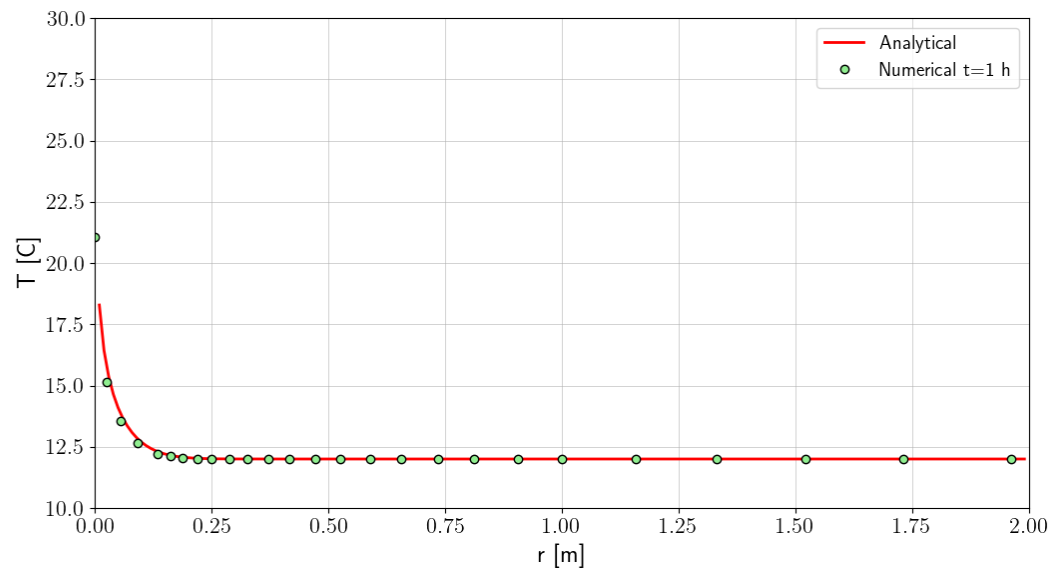


Figure 6.12: Comparizon of computed and analytical temperature profiles at $t = 1h$ for the case of very large refrigerant volumetric discharge

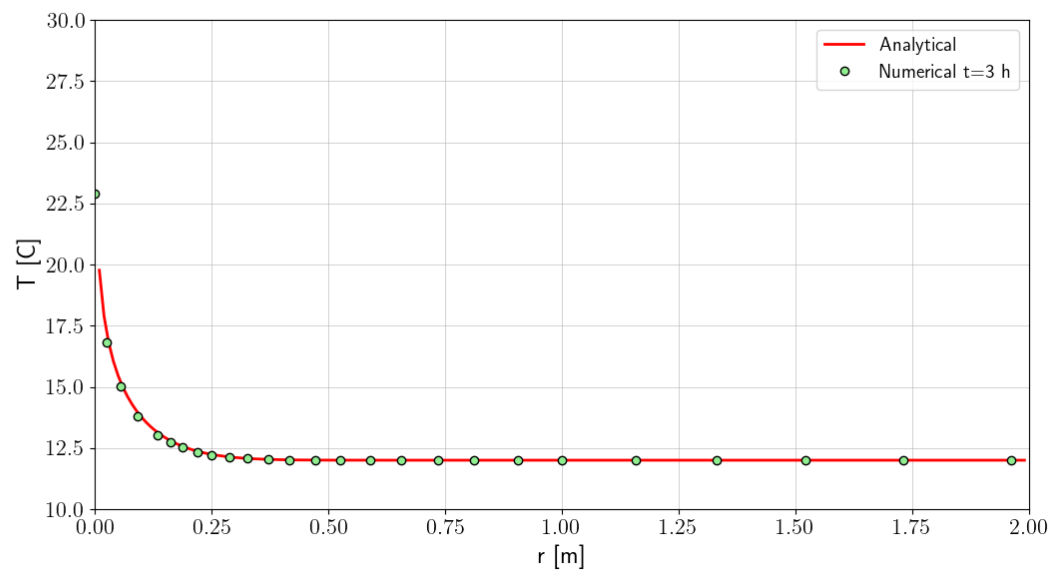


Figure 6.13: Comparizon of computed and analytical temperature profiles at $t = 3h$ for the case of very large refrigerant volumetric discharge

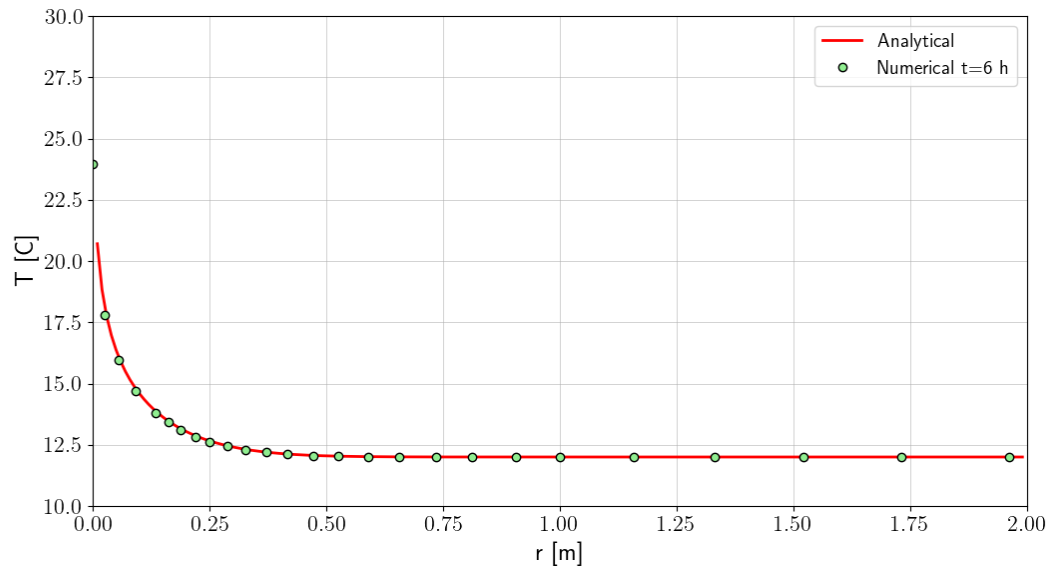


Figure 6.14: Comparison of computed and analytical temperature profiles at $t = 6$ h for the case of very large refrigerant volumetric discharge

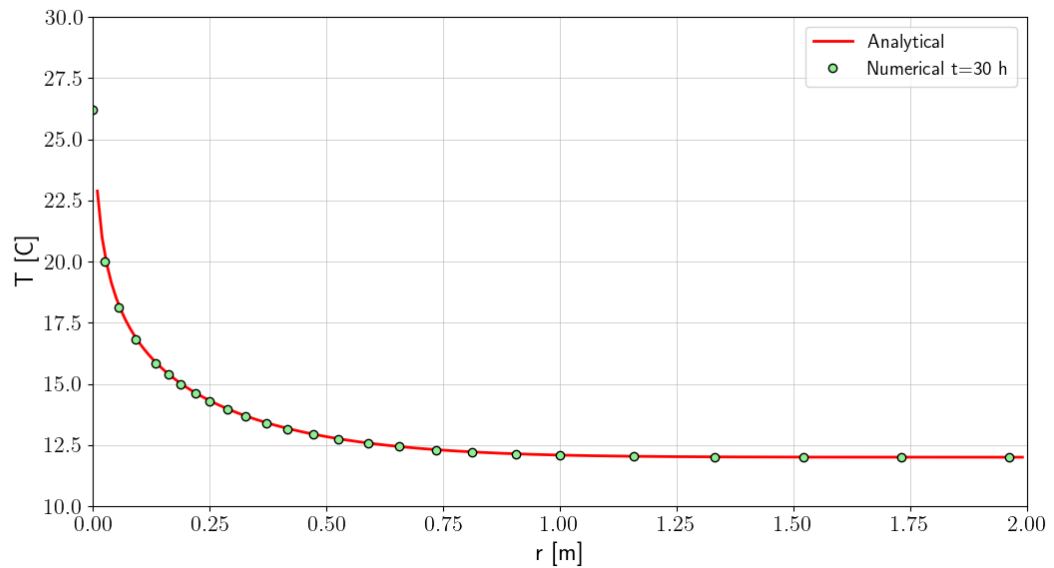


Figure 6.15: Comparison of computed and analytical temperature profiles at $t = 30$ h for the case of very large refrigerant volumetric discharge

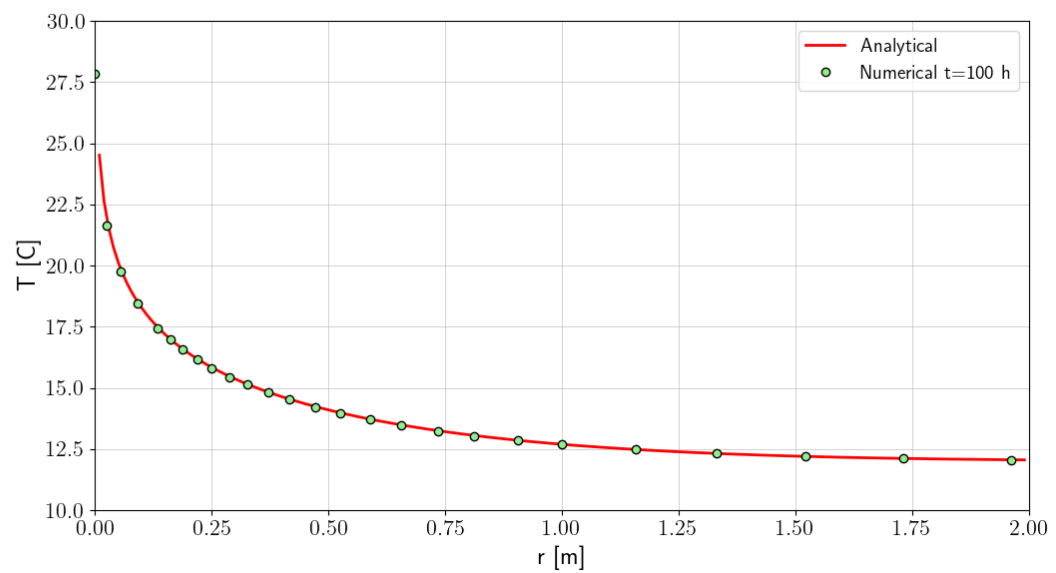


Figure 6.16: Comparizon of computed and analytical temperature profiles at $t = 100\text{h}$ for the case of very large refrigerant volumetric discharge

6.2 Heat exchange problem under steady state conditions and constant borehole wall temperature

This specific problem can be solved analytically using the method elaborated by Eskilson and Claesson [4]. Summary of this solution [1] is given below.

$$T_{ri}(z, t) = T_{ri}(z = 0, t) f_1(z) + T_{ro}(z = 0, t) f_2(z) + \int_0^z T_s(\xi, t) f_4(z - \xi) d\xi \quad (6.5)$$

$$T_{ro}(z, t) = -T_{ri}(z = 0, t) f_2(z) + T_{ro}(z = 0, t) f_3(z) - \int_0^z T_s(\xi, t) f_5(z - \xi) d\xi \quad (6.6)$$

where

$$f_1(z) = e^{\beta z} (\cosh(\gamma z) - \delta \sinh(\gamma z)) \quad (6.7)$$

$$f_2(z) = e^{\beta z} \frac{\beta_{12}}{\gamma} \sinh(\gamma z) \quad (6.8)$$

$$f_3(z) = e^{\beta z} (\cosh(\gamma z) + \delta \sinh(\gamma z)) \quad (6.9)$$

$$f_4(z) = e^{\beta z} \left(\beta_1 \cosh(\gamma z) - \left(\delta \beta_1 + \frac{\beta_2 \beta_{12}}{\gamma} \right) \sinh(\gamma z) \right) \quad (6.10)$$

$$f_5(z) = e^{\beta z} \left(\beta_2 \cosh(\gamma z) + \left(\delta \beta_2 + \frac{\beta_1 \beta_{12}}{\gamma} \right) \sinh(\gamma z) \right) \quad (6.11)$$

and

$$\beta_1 = \frac{1}{R_1^\Delta \rho^r c^r Q^r} \quad (6.12)$$

$$\beta_2 = \frac{1}{R_2^\Delta \rho^r c^r Q^r} \quad (6.13)$$

$$\beta_{12} = \frac{1}{R_{12}^\Delta \rho^r c^r Q^r} \quad (6.14)$$

$$\beta = \frac{\beta_2 - \beta_1}{2} \quad (6.15)$$

$$\gamma = \sqrt{\frac{(\beta_1 + \beta_2)^2}{4} + \beta_{12}(\beta_1 + \beta_2)} \quad (6.16)$$

$$\delta = \frac{1}{\gamma} \left(\beta_{12} + \frac{\beta_1 + \beta_2}{2} \right) \quad (6.17)$$

At $z = L$ temperatures $T_{ri}(L, t) = T_{ro}(L, t)$. This yields the following formula for the $T_{ro}(z = 0, t)$

$$T_{ro}(z = 0, t) = T_{ri}(z = 0, t) \frac{f_1(L) + f_2(L)}{f_3(L) - f_2(L)} + \frac{1}{f_3(L) - f_2(L)} \int_0^L T_s(\xi, t) (f_4(L - \xi) + f_5(L - \xi)) d\xi \quad (6.18)$$

Dedicated formulas for resistances R_1^Δ , R_2^Δ and R_{12}^Δ , as well as the analytical expressions for the grout temperature, for each specific exchanger type, are given in the following subsections. All these formulas can be found in paper [1].

6.2.1 CXA exchanger

Files: **BHE-CXA-bench-steady-Ts-const.inp**

For the CXA exchanger resistances R_1^Δ , R_2^Δ and R_{12}^Δ are expressed as follows[1]

$$R_1^\Delta = R_{fig} + R_{gs} \quad (6.19)$$

$$R_2^\Delta = \infty \quad (6.20)$$

$$R_{12}^\Delta = R_{ff} \quad (6.21)$$

The grout temperature profile is defined by the formula [1]

$$T_g(z, t) = \frac{R_{fig}}{R_{fig} + R_{gs}} (T_s(z, t) - T_{ri}(z, t)) + T_{ri}(z, t) \quad (6.22)$$

To verify the CXA implementation a 100m long CXA heat exchanger is analyzed assuming steady state conditions and fixed temperature $T = 10^\circ\text{C}$ at the borehole wall. The finite element mesh (grid size in the vertical direction is $h^e = 1\text{m}$) used in this benchmark is shown in fig.6.17. Material properties for the CXA exchanger, following the paper [2], are given in table 6.7, while the corresponding heat resistances and heat transfer coefficients are given in table 6.8. As in all soil nodes temperatures are fixed at $T = 10^\circ\text{C}$ hence soil thermal properties do not play here any role. The refrigerant temperature at the top of the inlet pipe varies in time according to the following load time function.

Table 6.6: Load time function for the temperature at the top point of the CXA exchanger

Time [s]	$T_{ri}(z = 0, t) [^\circ\text{C}]$
0	10
1	80
2	80

Comparizon of the analytical and numerical temperature distributions in the inlet/outlet pipes and in the grout is shown in fig.6.18. It is well visible that that the numerical solution matches very well the analytical one.

6.2. HEAT EXCHANGE PROBLEM UNDER STEADY STATE CONDITIONS AND CONSTANT BOREHOLE WALL TEMPERATURE

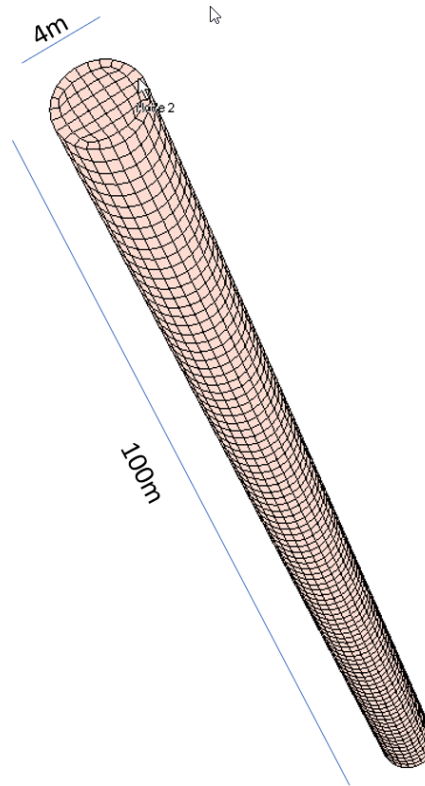


Figure 6.17: FE mesh and geometry of the problem

Table 6.7: Material properties for the CXA heat exchanger

Parameter	Symbol	Unit	Value
BHE type			CXA
Borehole diameter	D	[m]	0.1
Pipe distance	w	[m]	unused
Pipe (IN) outer diameter	d_i^{ext}	[m]	0.05
Pipe (IN) wall thickness	h_i	[m]	0.004
Pipe (IN) thermal conductivity	λ_i^p	[W/m/K]	0.38
Pipe (OUT) outer diameter	d_o^{ext}	[m]	0.024
Pipe (OUT) wall thickness	h_o	[m]	0.003
Pipe (OUT) thermal conductivity	λ_o^p	[W/m/K]	0.38
Refrigerant vol. flow discharge	Q^r	[m ³ /s]	$2.530093 \cdot 10^{-4}$
Refrigerant vol. flow discharge type			unused
Refrigerant thermal conductivity	λ^r	[W/m/K]	0.6405
Refrigerant dynamic viscosity	μ^r	[kPa s]	$5.4741 \cdot 10^{-7}$
Refrigerant vol. heat capacity	$\rho^r c^r$	[kJ/m ³ /K]	4131.2
Refrigerant density	ρ^r	[kg/m ³]	988.1
Grout thermal conductivity	λ^g	[W/m/K]	2.30
Grout heat capacity	$\rho^g c^g$	[kJ/m ³ /K]	2190.0

Table 6.8: Computed thermal resistances and heat transfer coefficients for the CXA exchanger

	Symbol	Unit	Value
Thermal resistances			
Pipe (IN) - Grout	R_{fig}	[m K/W]	0.10874
Pipe (IN) - Pipe(OUT)	R_{ff}	[m K/W]	0.13038
Grout - Soil	R_{gs}	[m K/W]	0.01626
Heat transfer coefficients			
Pipe (IN) - Grout	Φ_{fig}	[W/m/K]	69.697
Pipe (IN) - Pipe(OUT)	Φ_{ff}	[W/m/K]	135.64
Grout - Soil	Φ_{gs}	[W/m/K]	195.74

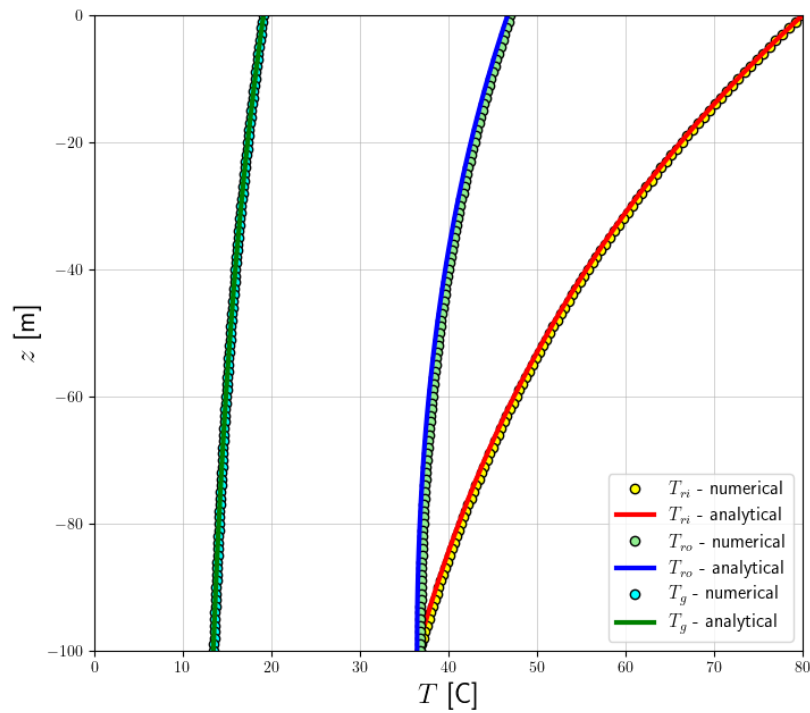


Figure 6.18: Comparizon of the analytical and numerical temperature distributions for CXA exchanger

6.2.2 CXC heat exchanger

Files: BHE-CXC-bench-steady-Ts-const.inp

For the CXC exchanger resistances R_1^Δ , R_2^Δ and R_{12}^Δ are expressed as follows[1]

$$R_2^\Delta = R_{fig} + R_{gs} \quad (6.23)$$

$$R_1^\Delta = \infty \quad (6.24)$$

$$R_{12}^\Delta = R_{ff} \quad (6.25)$$

while the grout temperature profile is defined by the formula [1]

$$T_g(z, t) = \frac{R_{fig}}{R_{fig} + R_{gs}} (T_s(z, t) - T_{ro}(z, t)) + T_{ro}(z, t) \quad (6.26)$$

To verify the implementation a 100m long CXC heat exchanger is analyzed assuming steady state conditions and fixed temperature $T = 10^\circ\text{C}$ at the borehole wall. The finite element mesh is exactly the same as in the benchmark for the CXA exchanger (see fig.6.17). Material properties for the CXC exchanger, following the paper [2], are given in table 6.10, while the corresponding heat resistances and heat transfer coefficients are given in table 6.11. As in all soil nodes temperatures are fixed at $T = 10^\circ\text{C}$ hence soil thermal properties do not play here any role. The refrigerant temperature at the top of the inlet pipe varies in time according to the following load time function.

Table 6.9: Load time function for the temperature at the top point of the CXC exchanger

Time [s]	$T_{ri}(z = 0, t) [^\circ\text{C}]$
0	10
1	80
2	80

Comparizon of the analytical and numerical temperature distributions in the inlet/outlet pipes and in the grout is shown in fig.6.19. It is well visible that that the numerical solution matches very well the analytical one.

Table 6.10: Material properties for the CXC heat exchanger

Parameter	Symbol	Unit	Value
BHE type			CXC
Borehole diameter	D	[m]	0.1
Pipe distance	w	[m]	unused
Pipe (IN) outer diameter	d_i^{ext}	[m]	0.024
Pipe (IN) wall thickness	h_i	[m]	0.003
Pipe (IN) thermal conductivity	λ_i^p	[W/m/K]	0.38
Pipe (OUT) outer diameter	d_o^{ext}	[m]	0.05
Pipe (OUT) wall thickness	h_o	[m]	0.004
Pipe (OUT) thermal conductivity	λ_o^p	[W/m/K]	0.38
Refrigerant vol. flow discharge	Q^r	[m ³ /s]	$2.530093 \cdot 10^{-4}$
Refrigerant vol. flow discharge type			unused
Refrigerant thermal conductivity	λ^r	[W/m/K]	0.6405
Refrigerant dynamic viscosity	μ^r	[kPa s]	$5.4741 \cdot 10^{-7}$
Refrigerant vol. heat capacity	$\rho^r c^r$	[kJ/m ³ /K]	4131.2
Refrigerant density	ρ^r	[kg/m ³]	988.1
Grout thermal conductivity	λ^g	[W/m/K]	2.30
Grout heat capacity	$\rho^g c^g$	[kJ/m ³ /K]	2190.0

Table 6.11: Computed thermal resistances and heat transfer coefficients for the CXC exchanger

	Symbol	Unit	Value
Thermal resistances			
Pipe (OUT) - Grout	R_{fog}	[m K/W]	0.10874
Pipe (IN) - Pipe(OUT)	R_{ff}	[m K/W]	0.13038
Grout - Soil	R_{gs}	[m K/W]	0.01626
Heat transfer coefficients			
Pipe (OUT) - Grout	Φ_{fog}	[W/m/K]	69.697
Pipe (IN) - Pipe(OUT)	Φ_{ff}	[W/m/K]	135.64
Grout - Soil	Φ_{gs}	[W/m/K]	195.74

6.2. HEAT EXCHANGE PROBLEM UNDER STEADY STATE CONDITIONS AND CONSTANT BOREHOLE WALL TEMPERATURE

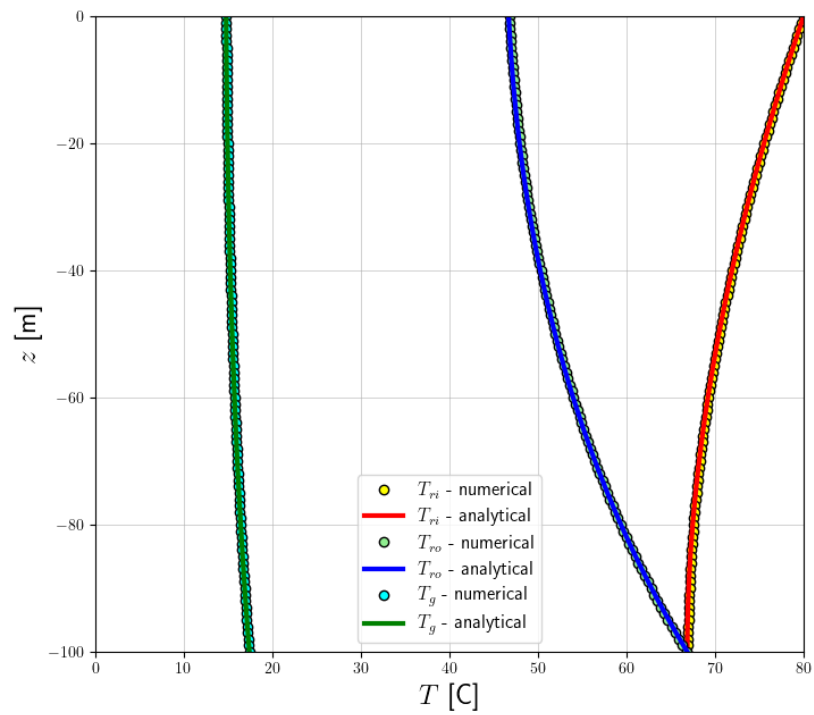


Figure 6.19: Comparizon of the analytical and numerical temperature distributions for CXC exchanger

6.2.3 1U heat exchanger

Files: BHE-1U-bench-steady-Ts-const.inp

For the 1U exchanger, assuming that $R_{fig} = R_{fog}$, resistances R_1^Δ , R_2^Δ and R_{12}^Δ are expressed as follows[1]

$$R_1^\Delta = R_{fig} + R_{gs} \quad (6.27)$$

$$R_2^\Delta = R_{fig} + R_{gs} \quad (6.28)$$

$$R_{12}^\Delta = \frac{(u_1 R_{fig} R_{gg})^2 - R_{fig}^2}{R_{gg}} \quad (6.29)$$

The grout temperature profiles are defined by formulas [1]

$$T_{gi}(z, t) = \frac{\left(\frac{T_s(z, t)}{R_{gs}} + \frac{T_o(z, t)}{R_{fog}} + \left(\frac{T_s(z, t)}{R_{gs}} + \frac{T_i(z, t)}{R_{fig}} \right) u_1 R_{gg} \right) R_{gg}}{R_{gg}^2 u_1^2 - 1} \quad (6.30)$$

$$T_{go}(z, t) = \left(\frac{T_{gi}(z, t)}{R_{gg}} + \frac{T_{go}(z, t)}{R_{fog}} + \frac{T_s(z, t)}{R_{gs}} \right) \frac{1}{u_1} \quad (6.31)$$

where

$$u_1 = \frac{1}{R_{fig}} + \frac{1}{R_{gs}} + \frac{1}{R_{gg}} \quad (6.32)$$

To verify the implementation a 100m long 1U heat exchanger is analyzed assuming steady state conditions and fixed temperature $T = 10^\circ\text{C}$ at the borehole wall. The finite element mesh is exactly the same as in the benchmark for the CXA exchanger (see fig.6.17). Material properties for the CXC exchanger, following the paper [2], are given in table 6.13, while the corresponding heat resistances and heat transfer coefficients are given in table 6.14. As in all soil nodes temperatures are fixed at $T = 10^\circ\text{C}$ hence soil thermal properties do not play here any role. The refrigerant temperature at the top of the inlet pipe varies in time according to the following load time function.

Table 6.12: Load time function for the temperature at the top point of the 1U exchanger

Time [s]	$T_{ri}(z = 0, t) [^\circ\text{C}]$
0	10
1	80
2	80

Comparizon of the analytical and numerical temperature distributions in the inlet/outlet pipes and in the grout is shown in fig.6.20. It is well visible that that the numerical solution matches very well the analytical one.

6.2. HEAT EXCHANGE PROBLEM UNDER STEADY STATE CONDITIONS AND CONSTANT BOREHOLE WALL TEMPERATURE

Table 6.13: Material properties for the 1U heat exchanger

Parameter	Symbol	Unit	Value
BHE type			1U
Borehole diameter	D	[m]	0.13
Pipe distance	w	[m]	0.06
Pipe (IN) outer diameter	d_i^{ext}	[m]	0.032
Pipe (IN) wall thickness	h_i	[m]	0.0029
Pipe (IN) thermal conductivity	λ_i^p	[W/m/K]	0.38
Pipe (OUT) outer diameter	d_o^{ext}	[m]	0.032
Pipe (OUT) wall thickness	h_o	[m]	0.0029
Pipe (OUT) thermal conductivity	λ_o^p	[W/m/K]	0.38
Refrigerant vol. flow discharge	Q^r	[m ³ /s]	$2.530093 \cdot 10^{-4}$
Refrigerant vol. flow discharge type			unused
Refrigerant thermal conductivity	λ^r	[W/m/K]	0.6405
Refrigerant dynamic viscosity	μ^r	[kPa s]	$5.4741 \cdot 10^{-7}$
Refrigerant vol. heat capacity	$\rho^r c^r$	[kJ/m ³ /K]	4131.2
Refrigerant density	ρ^r	[kg/m ³]	988.1
Grout thermal conductivity	λ^g	[W/m/K]	2.30
Grout heat capacity	$\rho^g c^g$	[kJ/m ³ /K]	2190.0

Table 6.14: Computed thermal resistances and heat transfer coefficients for the 1U exchanger

	Symbol	Unit	Value
Thermal resistances			
Pipe (IN)-Grout	R_{fig}	[m K/W]	0.15577
Pipe (OUT)-Grout	R_{fog}	[m K/W]	0.15577
Grout-Grout	R_{gg}	[m K/W]	0.11516
Grout-Soil	R_{gs}	[m K/W]	0.02574
Heat transfer coefficients			
Pipe (IN)-Grout	Φ_{fig}	[W/m/K]	77.993
Pipe (OUT)-Grout	Φ_{fog}	[W/m/K]	77.993
Grout-Grout	Φ_{gg}	[W/m/K]	66.796
Grout-Soil	Φ_{gs}	[W/m/K]	190.238

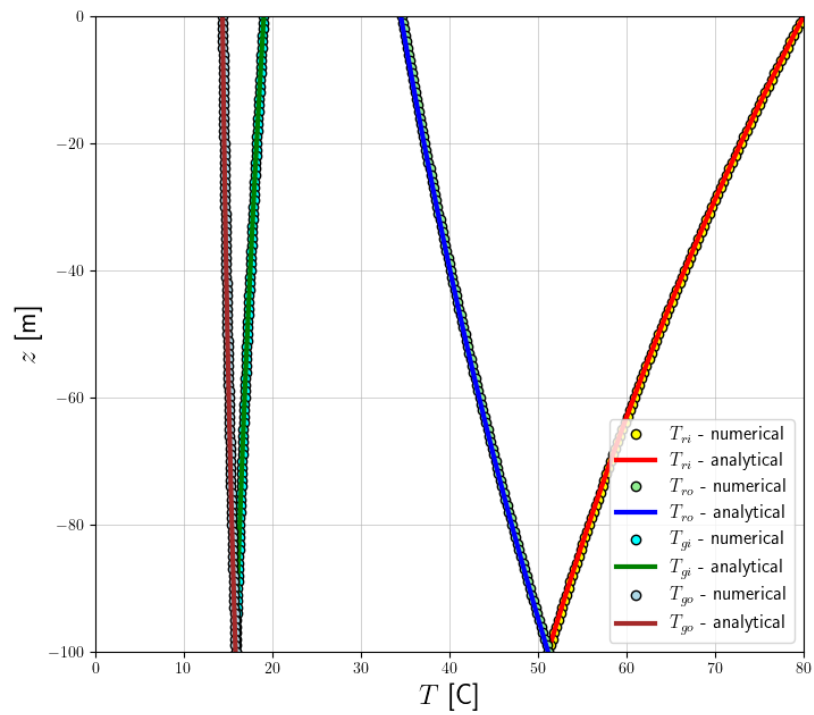


Figure 6.20: Comparizon of the analytical and numerical temperature distributions for 1U exchanger

6.2.4 2U heat exchanger

Files: BHE-2U-bench-steady-Ts-const.inp

For the 2U exchanger, assuming that $R_{fig} = R_{fog}$, resistances R_1^Δ , R_2^Δ and R_{12}^Δ are expressed as follows[1]

$$R_1^\Delta = \frac{R_{fig} + R_{gs}}{2} \quad (6.33)$$

$$R_2^\Delta = \frac{R_{fig} + R_{gs}}{2} \quad (6.34)$$

$$R_{12}^\Delta = \frac{R_{fig}^2}{4} \left(u_2^2 \nu - \frac{1}{\nu} \right) \quad (6.35)$$

where

$$u_2 = \frac{2}{R_{fig}} + \frac{2}{R_{gs}} + \frac{1}{\nu} \quad (6.36)$$

$$\nu = \frac{R_{gg1} R_{gg2}}{2(R_{gg1} + R_{gg2})} \quad (6.37)$$

The grout temperature profiles are defined by formulas [1]

$$T_{gi}(z, t) = \left(\frac{2T_s(z, t)}{R_{gs}} + \frac{2T_o(z, t)}{R_{fog}} + \left(\frac{2T_s(z, t)}{R_{gs}} + \frac{2T_i(z, t)}{R_{fig}} \right) u_2 \nu \right) \left(\frac{\nu}{\nu^2 u_2^2 - 1} \right) \quad (6.38)$$

$$T_{go}(z, t) = \left(\frac{T_{gi}(z, t)}{\nu} + \frac{2T_{go}(z, t)}{R_{fog}} + \frac{2T_s(z, t)}{R_{gs}} \right) \frac{1}{u_2} \quad (6.39)$$

To verify the implementation a 100m long 2U heat exchanger is analyzed assuming steady state conditions and fixed temperature $T = 10^\circ\text{C}$ at the borehole wall. The finite element mesh is exactly the same as in the benchmark for the CXA exchanger (see fig.6.17). Material properties for the CXC exchanger, following the paper [2], are given in table 6.16, while the corresponding heat resistances and heat transfer coefficients are given in table 6.17. As in all soil nodes temperatures are fixed at $T = 10^\circ\text{C}$ hence soil thermal properties do not play here any role. The refrigerant temperature at the top of the inlet pipe varies in time according to the following load time function.

Table 6.15: Load time function for the temperature at the top point of the 1U exchanger

Time [s]	$T_{ri}(z = 0, t) [^\circ\text{C}]$
0	10
1	80
2	80

It has to be underlined that certain differences between given values and the ones reported in the FEFLOW white paper are visible, especially for the R_{gg1} and Φ_{gg1} . This may be caused by the fact that in the standard

Table 6.16: Material properties for the 2U heat exchanger

Parameter	Symbol	Unit	Value
BHE type			2U
Borehole diameter	D	[m]	0.13
Pipe distance	w	[m]	0.04242
Pipe (IN) outer diameter	d_i^{ext}	[m]	0.032
Pipe (IN) wall thickness	h_i	[m]	0.0029
Pipe (IN) thermal conductivity	λ_i^p	[W/m/K]	0.38
Pipe (OUT) outer diameter	d_o^{ext}	[m]	0.032
Pipe (OUT) wall thickness	h_o	[m]	0.0029
Pipe (OUT) thermal conductivity	λ_o^p	[W/m/K]	0.38
Refrigerant vol. flow discharge	Q^r	[m ³ /s]	$2.530093 \cdot 10^{-4}$
Refrigerant vol. flow discharge type			Parallel
Refrigerant thermal conductivity	λ^r	[W/m/K]	0.6405
Refrigerant dynamic viscosity	μ^r	[kPa s]	$5.4741 \cdot 10^{-7}$
Refrigerant vol. heat capacity	$\rho^r c^r$	[kJ/m ³ /K]	4131.2
Refrigerant density	ρ^r	[kg/m ³]	988.1
Grout thermal conductivity	λ^g	[W/m/K]	2.30
Grout heat capacity	$\rho^g c^g$	[kJ/m ³ /K]	2190.0

Table 6.17: Computed thermal resistances and heat transfer coefficients for the 2U exchanger

	Symbol	Unit	Value
Thermal resistances			
Pipe (IN)-Grout (IN)	R_{fig}	[m K/W]	0.14486
Pipe (OUT)-Grout(OUT)	R_{fog}	[m K/W]	0.14486
Grout (IN)-Grout(IN)	R_{gg1}	[m K/W]	0.000268
Grout (IN)-Grout(OUT)	R_{gg2}	[m K/W]	0.11759
Grout-Soil	R_{gs}	[m K/W]	0.06835
Heat transfer coefficients			
Pipe (IN)-Grout (IN)	Φ_{fig}	[W/m/K]	83.872
Pipe (OUT)-Grout(OUT)	Φ_{fog}	[W/m/K]	83.872
Grout(IN)-Grout(IN)	Φ_{gg1}	[W/m/K]	57495
Grout(IN)-Grout(OUT)	Φ_{gg2}	[W/m/K]	65.41
Grout-Soil	Φ_{gs}	[W/m/K]	143.30

approach some resistances become negative and therefore an iterative correction has to be applied to get them positive. The iterative scheme proposed in the FEFLOW white paper is implemented here but slight differences are visible.

Comparizon of the analytical and numerical temperature distributions in the inlet/outlet pipes and in the grout are shown in fig.6.21 and in fig.6.22. It is well visible that that the numerical solution matches very well the analytical one.

6.2. HEAT EXCHANGE PROBLEM UNDER STEADY STATE CONDITIONS AND CONSTANT BOREHOLE WALL TEMPERATURE

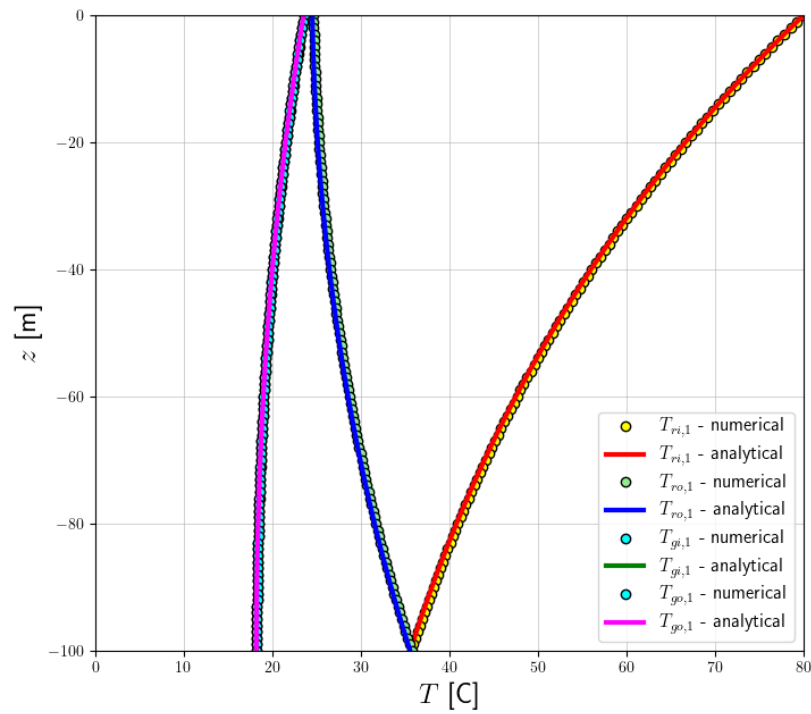


Figure 6.21: Comparizon of the analytical and numerical temperature distributions for the 2U exchanger (inlet pipe $i, 1$, outlet pipe $o, 1$ and their adjacent grout zones $gi, 1$ and $go, 1$ are analyzed here)

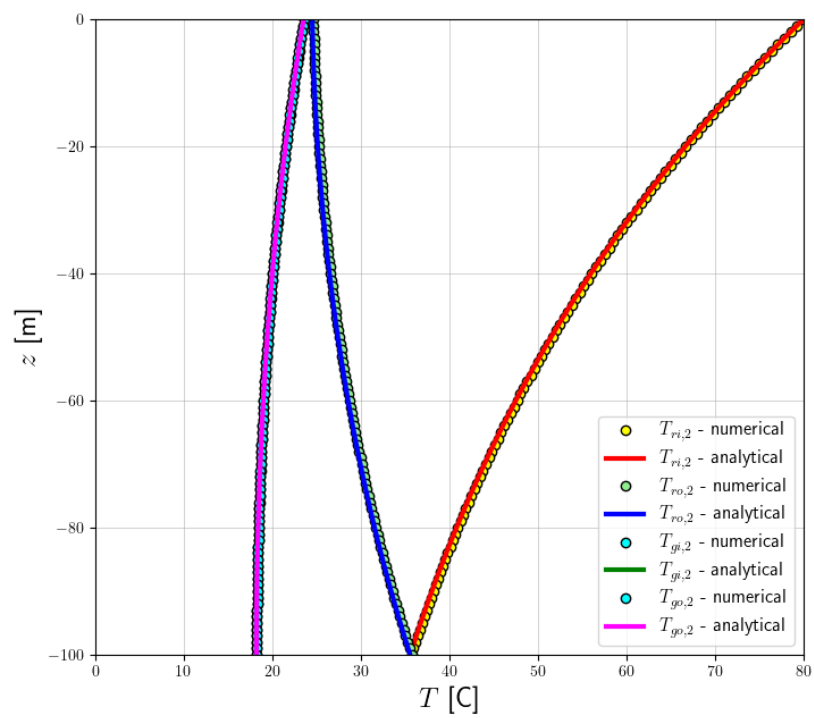


Figure 6.22: Comparizon of the analytical and numerical temperature distributions for the 2U exchanger (inlet pipe $i, 2$, outlet pipe $o, 2$ and their adjacent grout zones $gi, 2$ and $go, 2$ are analyzed here here)

6.3 Heat exchange between single pipe and soil under transient conditions and constant soil temperature

The transient response of the analyzed system can be computed using the following analytical formula [2]

$$T_{ri}(z, t) = T_s + \frac{T_i - T_s}{2} \left[\exp\left(\frac{(v_i^r - \nu)z}{2D}\right) \operatorname{erfc}\left(\frac{z - \nu t}{2\sqrt{Dt}}\right) + \exp\left(\frac{(v_i^r + \nu)z}{2D}\right) \operatorname{erfc}\left(\frac{z + \nu t}{2\sqrt{Dt}}\right) \right] \quad (6.40)$$

where

$$\nu = v_i^r \sqrt{1 + \frac{4\phi D}{(v_i^r)^2}} \quad (6.41)$$

$$D = \frac{\tilde{\lambda}_i^r}{\rho^r c^r} \quad (6.42)$$

$$v_i^r = \frac{Q^r}{A_i^{\text{int}}} \quad (6.43)$$

$$\phi = \frac{\pi d_i^{\text{int}} \Phi_{\text{fig}}}{A_i^{\text{int}} \rho^r c^r} \quad (6.44)$$

In this solution soil temperature is treated as a reference one, therefore, it has to be kept constant ($T_s=10^\circ\text{C}$). At the top of the exchanger the imposed temperature varies in time as follows

Table 6.18: Load time function for the temperature at the top point of the exchanger

Time [s]	$T_{ri}(z = 0, t) [^\circ\text{C}]$
0	10
1	50
2	50

Finite element mesh, used in this benchmark, is shown in fig. 6.23. It is worth to mention that the mesh density in soil is unimportant in fact. To capture the strong temperature gradients along the pipe the vertical grid size is 1cm.

6.3.1 Pipe type heat exchanger

File: BHE-pipe-transient-Ts-const.inp, BHE-pipe-transient-Ts-const-dense.inp

In this benchmark a standard pipe type heat exchanger element is used. Two vertical discretizations (1cm and 2.5mm) are used to prove h —convergence property of the method. One should note that for the benchmarking purposes the heat transfer coefficient Φ_{fig} is not derived from the properties summarized in table 6.19 but it is fixed to a given value (see table 6.20).

Comparizon of the analytical and numerical solutions at $t = 1728$ s, obtained for the two vertical grid sizes are shown in fig.6.24 and fig.6.25.

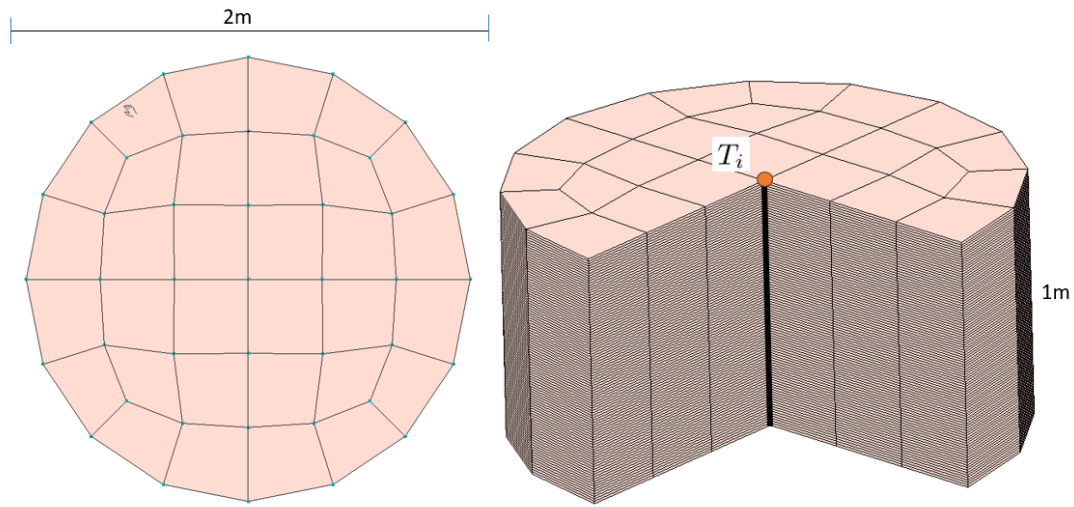


Figure 6.23: FE mesh and geometry of the problem

Table 6.19: Material properties for the pipe heat exchanger

Parameter	Symbol	Unit	Value
BHE type			Pipe
Borehole diameter	D	[m]	0.13 (unimportant)
Pipe distance	w	[m]	unused
Pipe (IN) outer diameter	d_i^{ext}	[m]	0.0262
Pipe (IN) wall thickness	h_i	[m]	0.0029
Pipe (IN) thermal conductivity	λ_i^p	[W/m/K]	0.38
Pipe (OUT) outer diameter	d_o^{ext}	[m]	unused
Pipe (OUT) wall thickness	h_o	[m]	unused
Pipe (OUT) thermal conductivity	λ_o^p	[W/m/K]	unused
Refrigerant vol. flow discharge	Q^r	[m ³ /s]	$2.02546 \cdot 10^{-7}$
Refrigerant vol. flow discharge type			unused
Refrigerant thermal conductivity	λ^r	[W/m/K]	0.65
Refrigerant dynamic viscosity	μ^r	[kPa s]	$5.4741 \cdot 10^{-7}$
Refrigerant vol. heat capacity	$\rho^r c^r$	[kJ/m ³ /K]	4129.8
Refrigerant density	ρ^r	[kg/m ³]	988.1
Grout thermal conductivity	λ^g	[W/m/K]	unused
Grout heat capacity	$\rho^g c^g$	[kJ/m ³ /K]	unused
User given transfer coefficients flag			ON

Table 6.20: Imposed heat transfer coefficients for the pipe exchanger

	Symbol	Unit	Value
Heat transfer coefficients			
Pipe-Grout	Φ_{fig}	[W/m/K]	12.0

6.3. HEAT EXCHANGE BETWEEN SINGLE PIPE AND SOIL UNDER TRANSIENT CONDITIONS AND CONSTANT SOIL TEMPERATURE

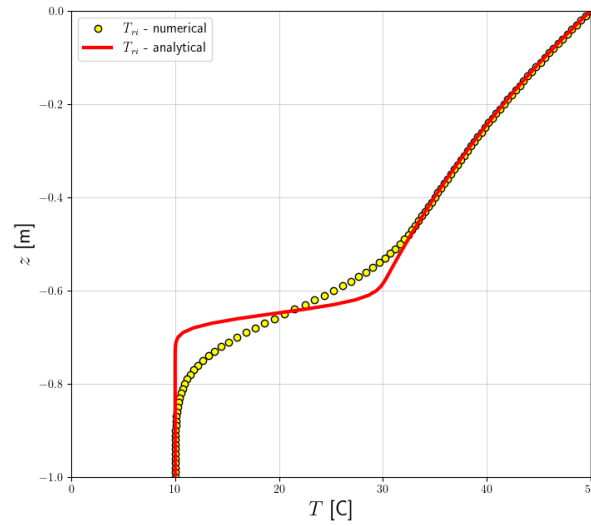


Figure 6.24: Comparizon of the analytical and numerical temperature distributions at t=1728 s for the vertical grid size 1cm

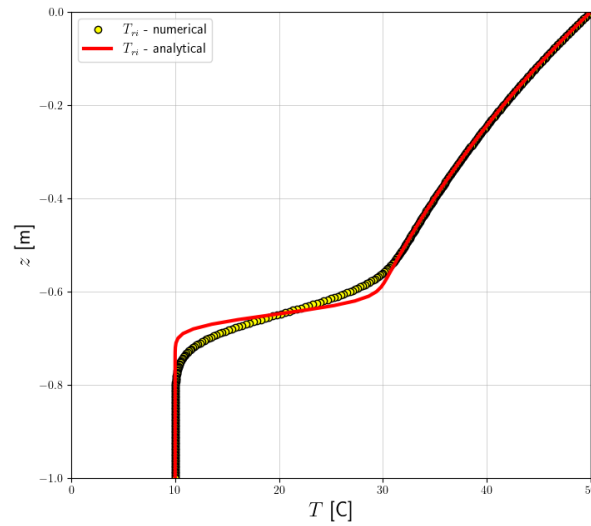


Figure 6.25: Comparizon of the analytical and numerical temperature distributions at t=1728 s for the vertical grid size 2.5mm

6.3.2 1U type heat exchanger

File: BHE-1U-transient-Ts-const.inp

This benchmark is equivalent to the one in which the standard pipe exchanger is used (see section 6.3.1). In order to cancel heat exchange between the outflow pipe and soil and to neglect grout resistance, the heat transfer coefficients must satisfy the following conditions $\Phi_{\text{fog}} = 0.0$, Φ_{gs} is much larger than Φ_{fig} and Φ_{gg} is large. Material data and enforced heat transfer coefficients are summarized in table 6.22.

Comparizon of the analytical and numerical solutions at $t = 1728$ s, obtained for the two vertical grid sizes are shown in fig.6.26 and fig.6.27.

Table 6.21: Material properties for the 1U heat exchanger

Parameter	Symbol	Unit	Value
BHE type			1U
Borehole diameter	D	[m]	0.13 (unimportant)
Pipe distance	w	[m]	0.05 (unimportant)
Pipe (IN) outer diameter	d_i^{ext}	[m]	0.0262
Pipe (IN) wall thickness	h_i	[m]	0.0029
Pipe (IN) thermal conductivity	λ_i^r	[W/m/K]	0.38
Pipe (OUT) outer diameter	d_o^{ext}	[m]	0.0262
Pipe (OUT) wall thickness	h_o	[m]	0.0029
Pipe (OUT) thermal conductivity	λ_o^p	[W/m/K]	0.38
Refrigerant vol. flow discharge	Q^r	[m ³ /s]	$2.02546 \cdot 10^{-7}$
Refrigerant vol. flow discharge type			unused
Refrigerant thermal conductivity	λ^r	[W/m/K]	0.65
Refrigerant dynamic viscosity	μ^r	[kPa s]	$5.4741 \cdot 10^{-7}$
Refrigerant vol. heat capacity	$\rho^r c^r$	[kJ/m ³ /K]	4129.8
Refrigerant density	ρ^r	[kg/m ³]	988.1
Grout thermal conductivity	λ^g	[W/m/K]	2.3 (unimportant)
Grout heat capacity	$\rho^g c^g$	[kJ/m ³ /K]	2190.0 (unimportant)
User given transfer coefficients flag			ON

Table 6.22: Imposed heat transfer coefficients for the 1U exchanger

	Symbol	Unit	Value
Heat transfer coefficients			
Pipe (IN) - Grout (IN)	Φ_{fig}	[W/m/K]	12.0
Pipe (OUT)- Grout(OUT)	Φ_{fog}	[W/m/K]	0.0
Grout(IN)-Grout(IN)	Φ_{gg}	[W/m/K]	1200.0
Grout-Soil	Φ_{gs}	[W/m/K]	1200.0

6.3. HEAT EXCHANGE BETWEEN SINGLE PIPE AND SOIL UNDER TRANSIENT CONDITIONS AND CONSTANT SOIL TEMPERATURE

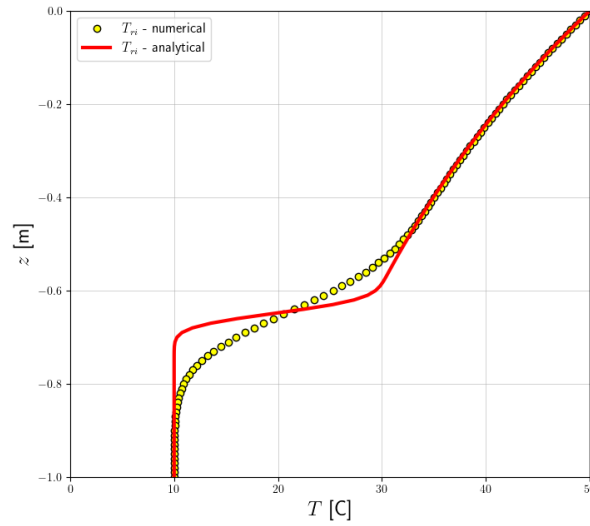


Figure 6.26: Comparizon of the analytical and numerical temperature distributions at t=1728 s for the vertical grid size 1cm

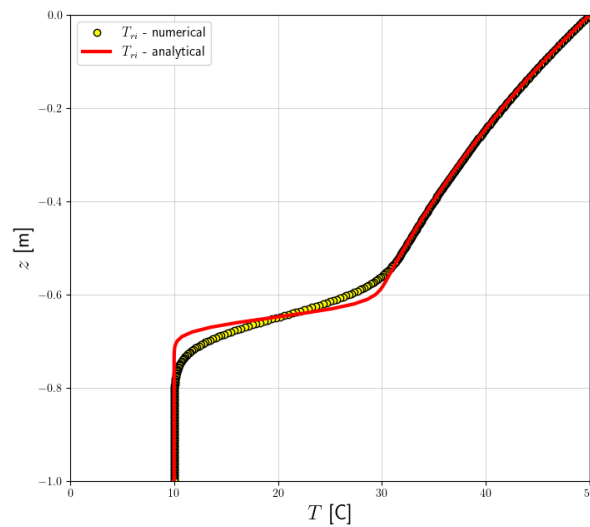


Figure 6.27: Comparizon of the analytical and numerical temperature distributions at t=1728 s for the vertical grid size 2.5mm

6.4 Mesh sensitivity study

6.4.1 Transient BHE solution for the CXA system

In this section a transient heat transfer problem for the CXA heat exchanger (100m long) is analyzed. The main focus is put on the mesh sensitivity issue as the heat exchanger is reduced to a single line within the 3D FE model. This simplified approach must yield results that are mesh dependent. In papers [1] and [3] the optimal mesh size, with respect to the grout radius, was established assuming that linear 3D elements are of wedge shape (triangular bases in the horizontal plane). In case of all hexa meshes, used in the ZSoil implementation, this relation must be reestablished. Another methods of plugging in the heat exchanger elements within the 3D soil mesh in an arbitrary manner are analyzed too. The reference solution for this benchmark is taken from papers [1] and [3]. It is worth to mention that this benchmark data differs between the FEFLOW white paper and paper by Diersch [1] (namely the outflow pipe wall thickness 4mm in [1] and 3mm in FEFLOW). Another problem is such that the refrigerant dynamic viscosity and refrigerant density are not given. These values were taken as in previous benchmarks. With these assumptions the resulting heat transfer coefficients are slightly different from those given in the FEFLOW white paper. Bigger differences appear for the laminar case.

The initial fully conforming coarse mesh (100 × 100 × 100 m) is shown in the fig.6.29. Vertical grid size is uniform and equal to 1m. Further mesh refinements in the horizontal plane are made only in the soil zone nearby the CXA heat exchanger. Dissimilar soil meshes are connected using the highly accurate method called mesh tying implemented in ZSoil. All refined meshes are shown in the fig.6.30 and fig.6.31.

The initial temperature of the system is $T_0=10^{\circ}\text{C}$. Then the temperature at the top point of the heat exchanger varies in time with the following load time function

Table 6.23: Load time function for the temperature at the top point of the heat exchanger

Time [s]	$T_s(t)$ [$^{\circ}\text{C}$]
0	10
0.01	80
90	80
90.01	10
180.0	10

The list of drivers is shown in fig.6.28. Here we use variable time steps with the amplification factor 1.1.

Material properties for the CXA exchanger and soil are summarized in the two following tables (the refrigerant volumetric flow discharge as well as the resulting heat transfer coefficients are given for the both laminar and turbulent flow cases).

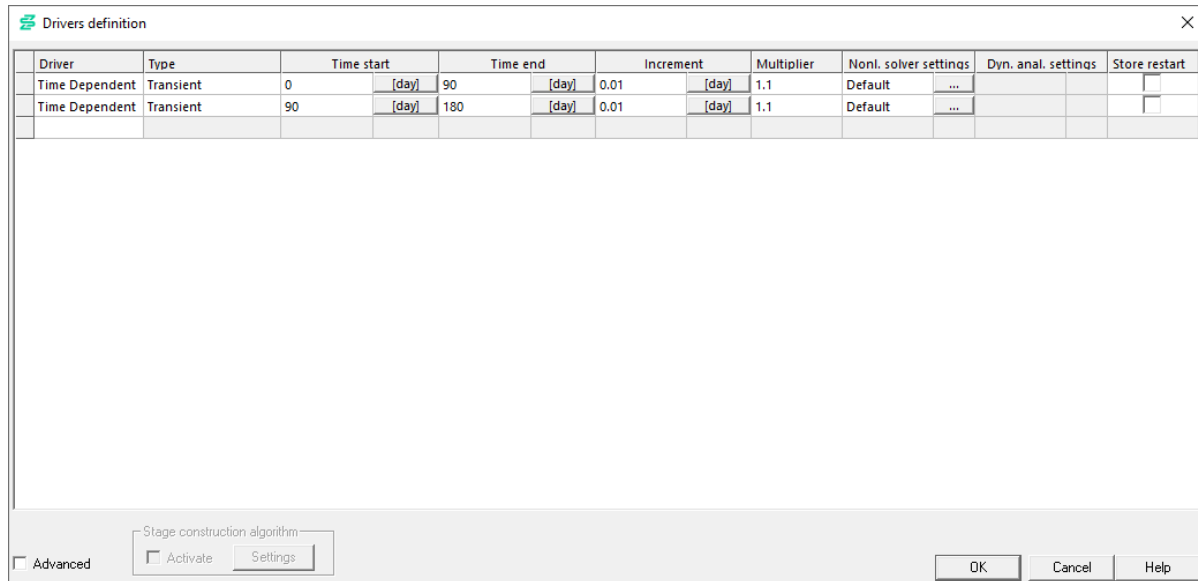


Figure 6.28: List of driers and assumed time stepping

Table 6.24: Material properties for the heat exchanger

Parameter	Symbol	Unit	Value
BHE type			CXA
Borehole diameter	D	[m]	0.1
Pipe distance	w	[m]	unused
Pipe (IN) outer diameter	d_i^{ext}	[m]	0.05
Pipe (IN) wall thickness	h_i	[m]	0.004
Pipe (IN) thermal conductivity	λ_i^p	[W/m/K]	0.38
Pipe (OUT) outer diameter	d_o^{ext}	[m]	0.024
Pipe (OUT) wall thickness	h_o	[m]	0.003
Pipe (OUT) thermal conductivity	λ_o^p	[W/m/K]	0.38
Refrigerant vol. flow discharge	Q^r	[m ³ /d]	1.0931/21.8624
Refrigerant vol. flow discharge type			unused
Refrigerant thermal conductivity	λ^r	[W/m/K]	0.65
Refrigerant dynamic viscosity	μ^r	[kPa s]	5.414e-7
Refrigerant vol. heat capacity	$\rho^r c^r$	[kJ/m ³ /K]	4129.84
Refrigerant density	ρ^r	[kg/m ³]	988.1
Grout thermal conductivity	λ^g	[W/m/K]	2.3
Grout heat capacity	$\rho^g c^g$	[kJ/m ³ /K]	2190.0
Heat transfer coefficient	Φ_{fig}	[W/m ² /K]	56.95031 / 69.71989
Heat transfer coefficient	Φ_{ff}	[W/m ² /K]	62.63806 / 135.72392
Heat transfer coefficient	Φ_{gs}	[W/m ² /K]	195.74317 / 195.74317

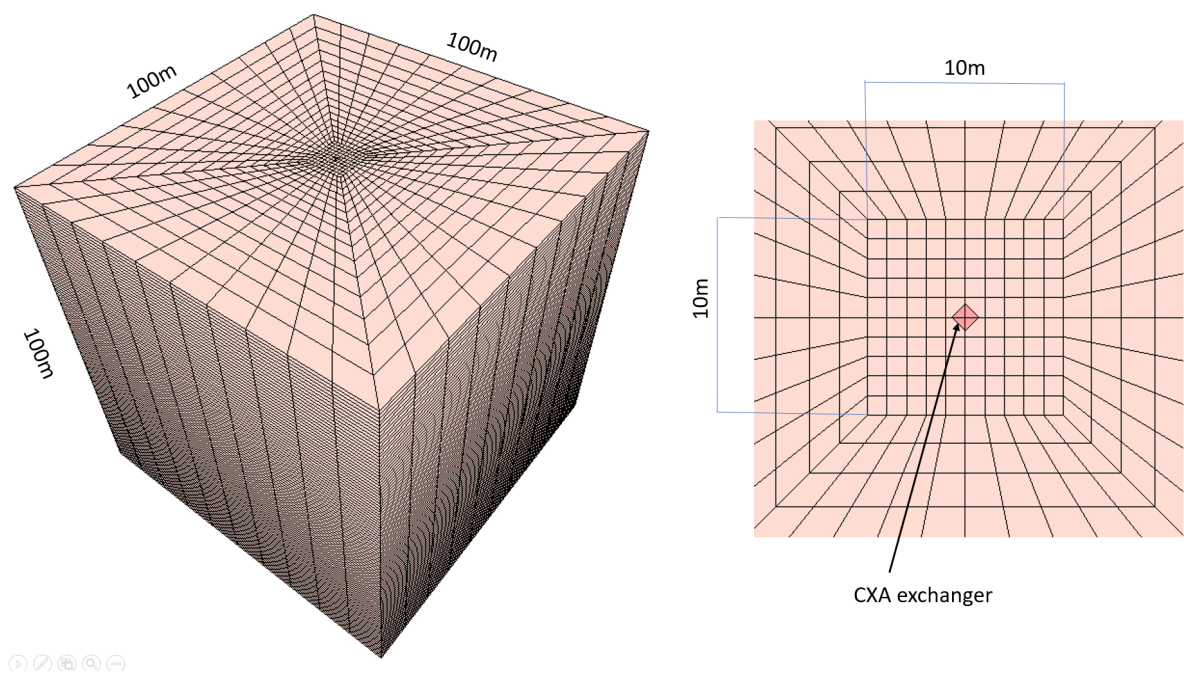


Figure 6.29: Uniform mesh with grid size $h^e = 1\text{m}$ in $10\times 10\text{m}$ central zone

Table 6.25: Material properties for soil

Parameter	Symbol	Unit	Value
Soil thermal conductivity	λ^s	[W/m/K]	2.2
Soil heat capacity	$\rho^s c^s$	[kJ/m ³ /K]	2210

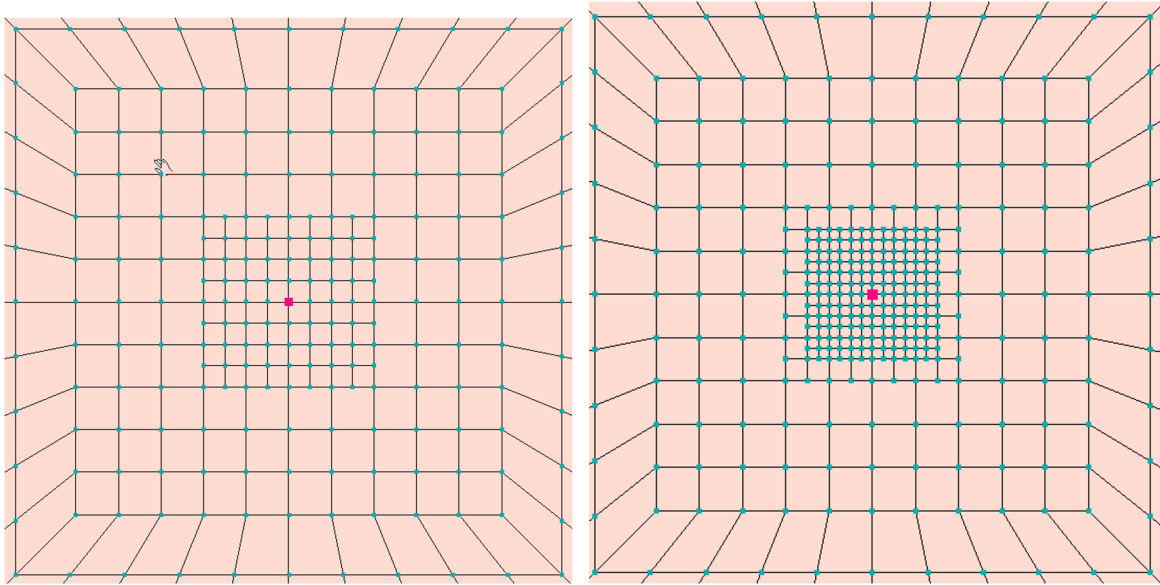


Figure 6.30: Mesh refinement with $h^e = 0.5\text{m}$ (left figure) and $h^e = 0.25\text{m}$ (right figure)

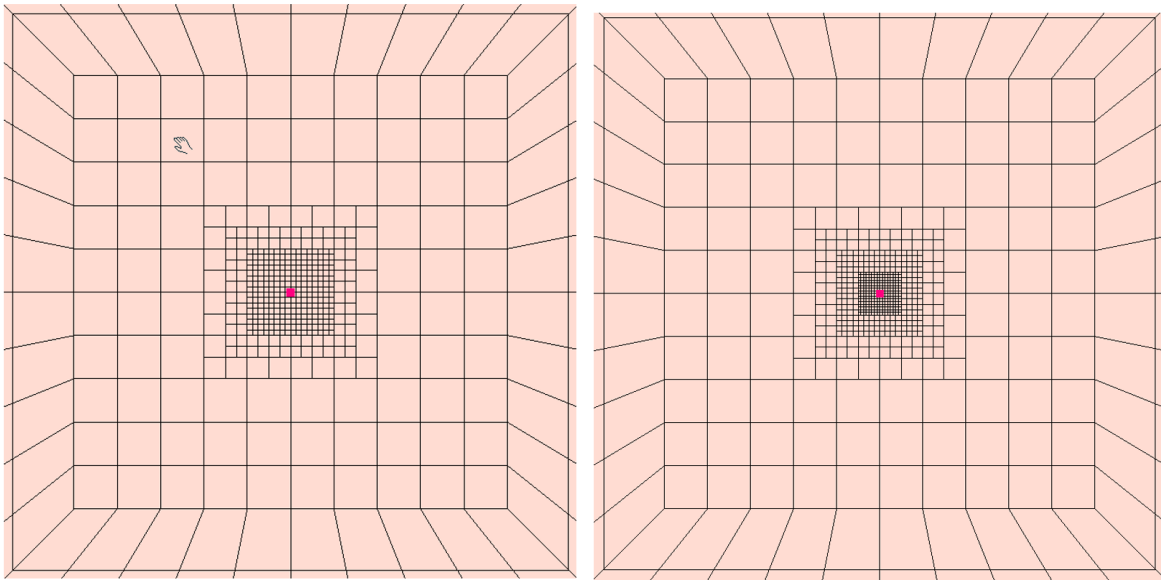


Figure 6.31: Mesh refinement with $h^e = 0.125\text{m}$ (left figure) and $h^e = 0.0625\text{m}$ (right figure)

6.4.1.1 Results for the case of laminar flow with exchanger located at the center of the mesh

Files:

BHE-CXA-Heidemann-laminar-he-1m.inp,
BHE-CXA-Heidemann-laminar-he-1m-link-nnl.inp,
BHE-CXA-Heidemann-laminar-he-0.5m-ex.inp,
BHE-CXA-Heidemann-laminar-he-0.5m-ex-link-nnl.inp,
BHE-CXA-Heidemann-laminar-he-0.25m-ex.inp,
BHE-CXA-Heidemann-laminar-he-0.25m-ex-link-nnl.inp,
BHE-CXA-Heidemann-laminar-he-0.125m-ex.inp,
BHE-CXA-Heidemann-laminar-he-0.125m-ex-link-nnl,
BHE-CXA-Heidemann-laminar-he-0.0625m-ex.inp,
BHE-CXA-Heidemann-laminar-he-0.0625m-ex-link-nnl.inp

In the following figures time history of the refrigerant temperature at the outlet pipe is presented for the laminar flow case. The two methods of connecting exchanger mesh to the soil mesh are used. First the standard approach is used in which soil nodes of the exchanger coincide with soil mesh nodes, then the second method is tested in which soil nodes of the exchanger element are linked using nonlocal constraints to the soil mesh. It is well visible that the mesh size $h^e = 0.5\text{m}$ is optimal for the first method but it is also well visible that it does not exhibit h convergence property required in the FE method. The second method is definitely more consistent as with the further mesh refinements the resulting time history tends to the asymptote. It is worth to mention that exchanger nodes are aligned along soil mesh nodes.

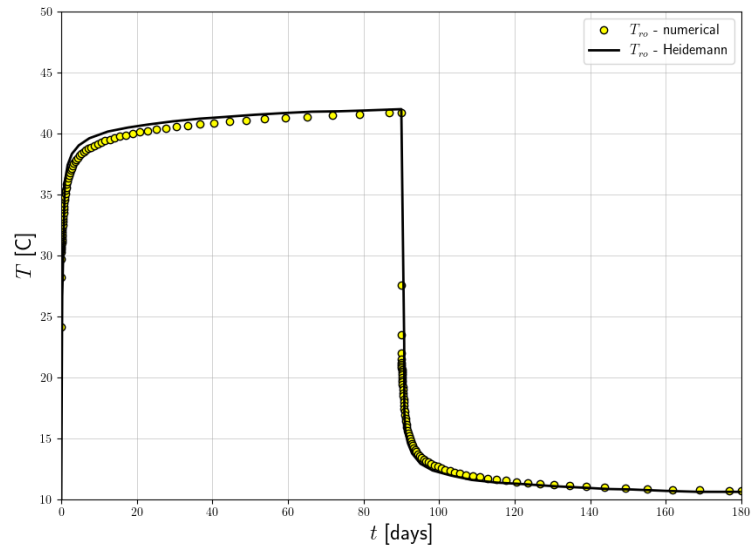


Figure 6.32: Refrigerant temperature time history at the outlet obtained for the laminar flow case, conforming soil mesh, with the inner zone grid size $h^e = 1\text{m}$ (exchanger soil nodes coincide with the soil mesh nodes)

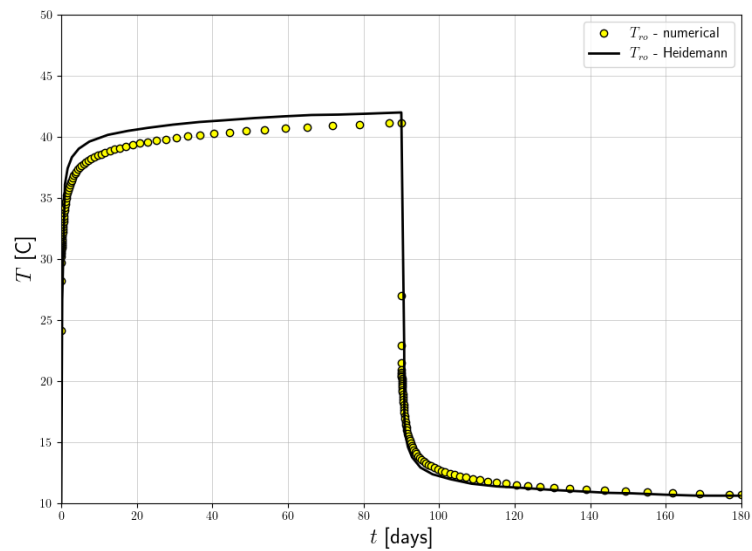


Figure 6.33: Refrigerant temperature time history at the outlet obtained for the laminar flow case, conforming soil mesh, with the inner zone grid size $h^e = 1\text{m}$ (exchanger soil nodes are linked to the soil mesh using nonlocal constraints)

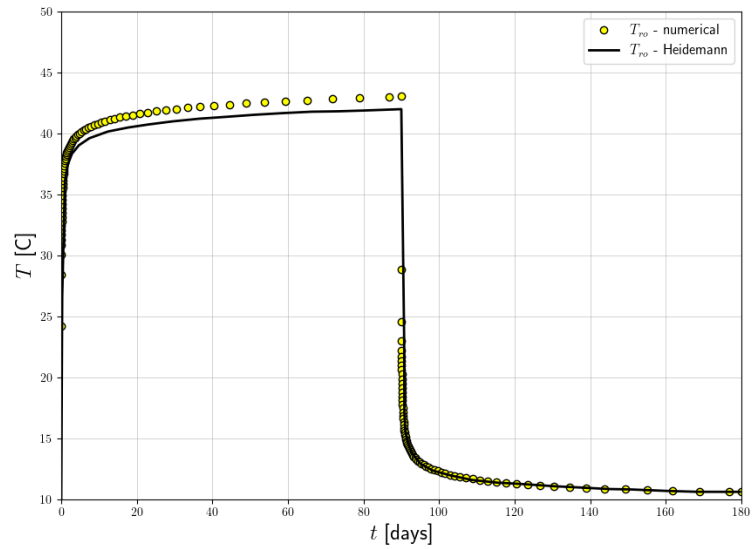


Figure 6.34: Refrigerant temperature time history at the outlet obtained for the laminar flow case, locally refined soil mesh, with the inner zone grid size $h^e = 0.5\text{m}$ (exchanger soil nodes coincide with the soil mesh nodes)

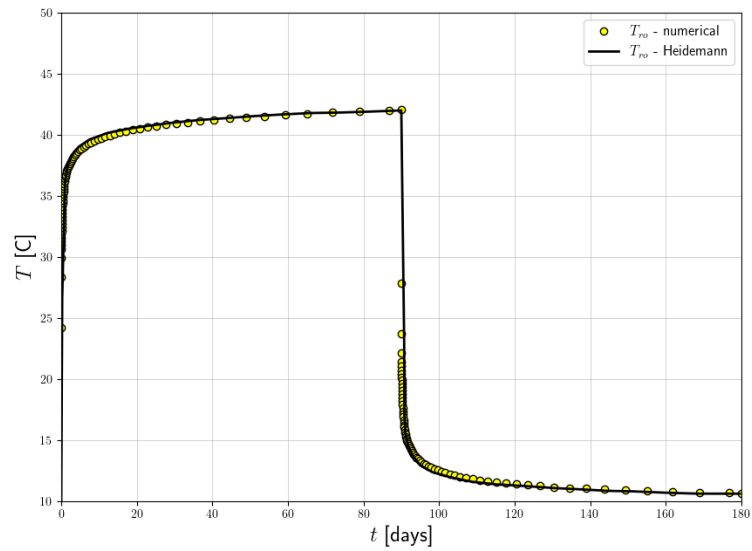


Figure 6.35: Refrigerant temperature time history at the outlet obtained for the laminar flow case, locally refined soil mesh, with the inner zone grid size $h^e = 0.5\text{m}$ (exchanger soil nodes linked using nonlocal constraints to the soil mesh) and laminar flow

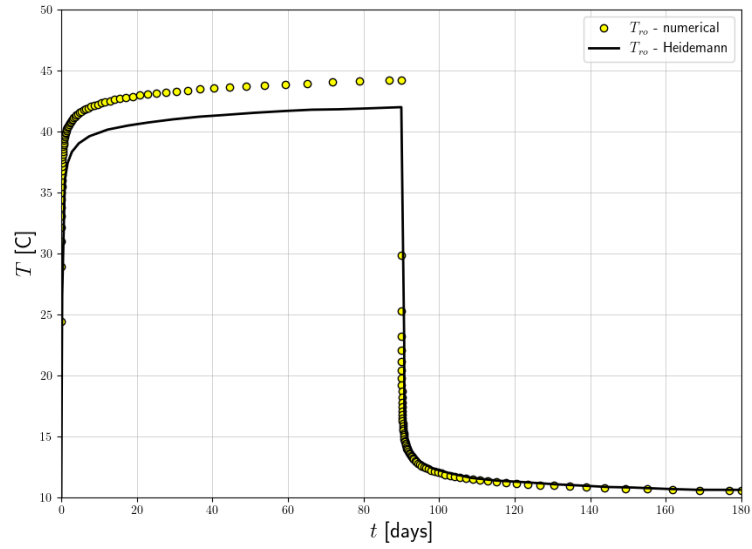


Figure 6.36: Refrigerant temperature time history at the outlet obtained for the laminar flow case, locally refined soil mesh, with the inner zone grid size $h^e = 0.25\text{m}$ (exchanger soil nodes coincide with the soil mesh nodes)

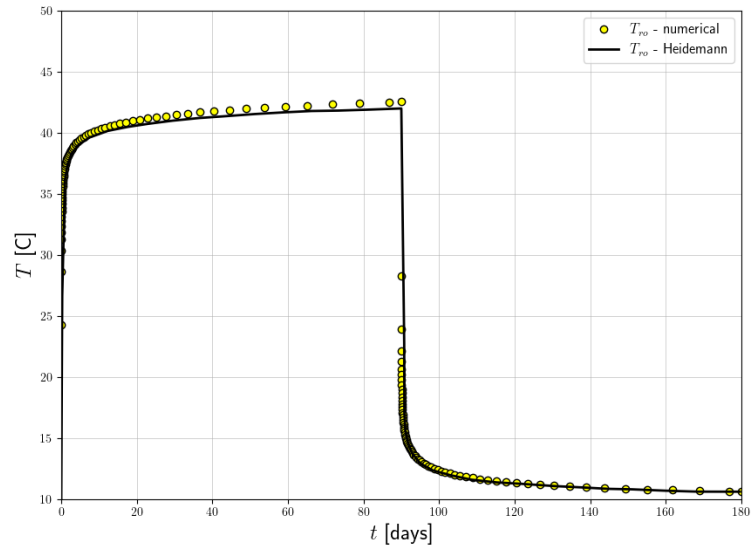


Figure 6.37: Refrigerant temperature time history at the outlet obtained for the laminar flow case, locally refined soil mesh, with the inner zone grid size $h^e = 0.25\text{m}$ (exchanger soil nodes linked using nonlocal constraints to the soil mesh) and laminar flow ZSoil® 220430 report

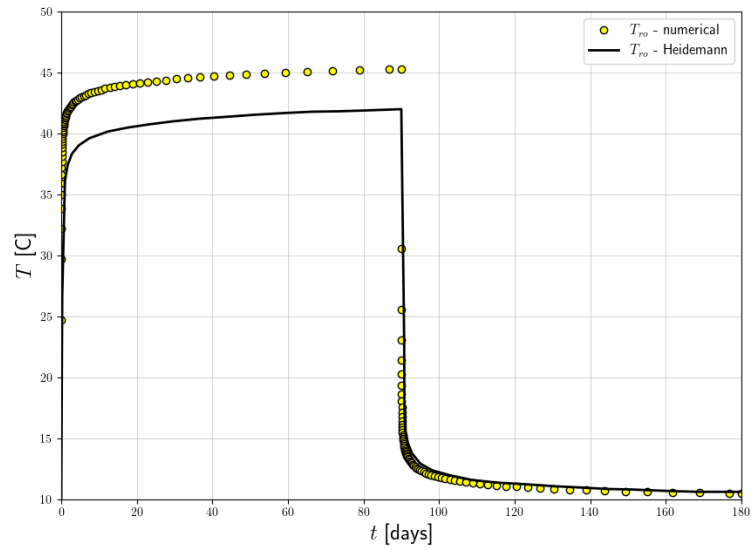


Figure 6.38: Refrigerant temperature time history at the outlet obtained for the laminar flow case, locally refined soil mesh, with the inner zone grid size $h^e = 0.125\text{m}$ (exchanger soil nodes coincide with the soil mesh nodes)

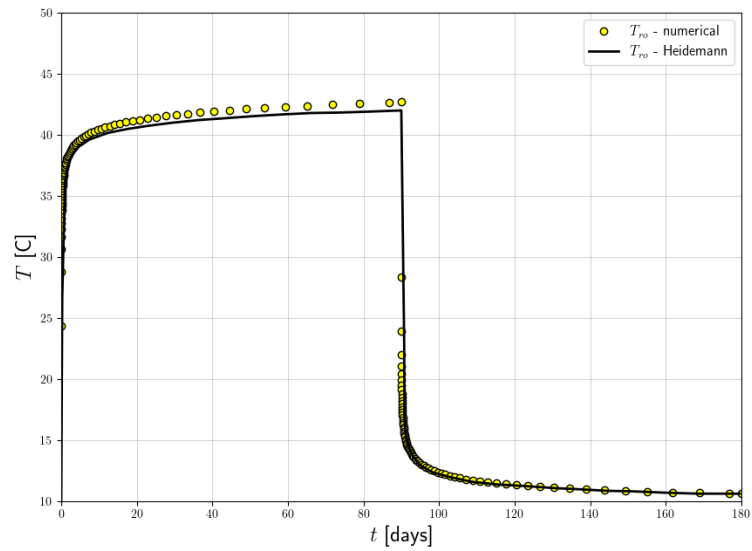


Figure 6.39: Refrigerant temperature time history at the outlet obtained for the laminar flow case, locally refined soil mesh, with the inner zone grid size $h^e = 0.125\text{m}$ (exchanger soil nodes linked using nonlocal constraints to the soil mesh) and laminar flow

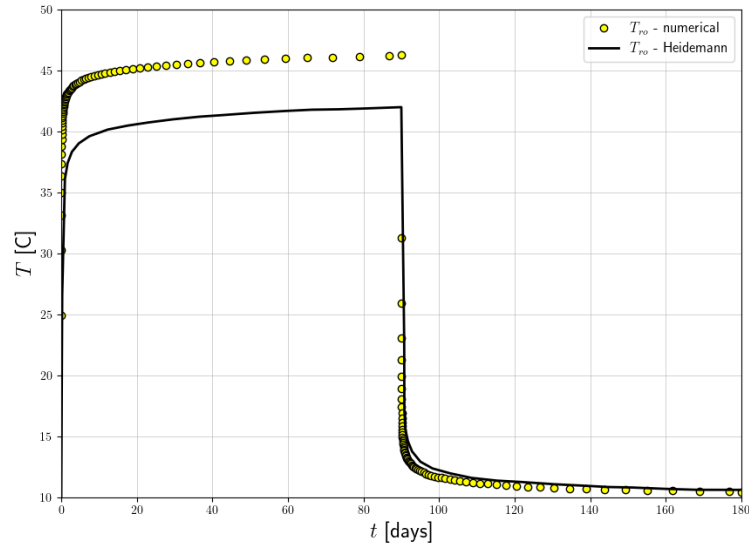


Figure 6.40: Refrigerant temperature time history at the outlet obtained for the laminar flow case, locally refined soil mesh, with the inner zone grid size $h^e = 0.0625\text{m}$ (exchanger soil nodes coincide with the soil mesh nodes)

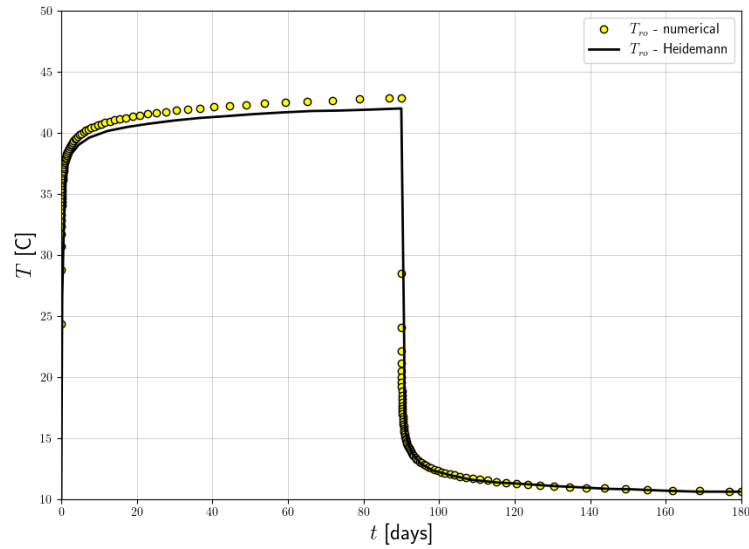


Figure 6.41: Refrigerant temperature time history at the outlet obtained for the laminar flow case, locally refined soil mesh, with the inner zone grid size $h^e = 0.0625\text{m}$ (exchanger soil nodes linked using nonlocal constraints to the soil mesh) and laminar flow ZSoil® 220430 report

6.4.1.2 Results for the case of laminar flow with exchanger shifted from the center of the mesh

Files:

BHE-CXA-Heidemann-laminar-he-1m-shift-link-loc.inp,
BHE-CXA-Heidemann-laminar-he-1m-shift-link-nnl.inp,
BHE-CXA-Heidemann-laminar-he-0.5m-ex-shift-link-loc.inp,
BHE-CXA-Heidemann-laminar-he-0.5m-ex-shift-link-nnl.inp,
BHE-CXA-Heidemann-laminar-he-0.25m-ex-shift-link-loc.inp,
BHE-CXA-Heidemann-laminar-he-0.25m-ex-shift-link-nnl.inp,
BHE-CXA-Heidemann-laminar-he-0.125m-ex-shift-link-loc.inp,
BHE-CXA-Heidemann-laminar-he-0.125m-ex-shift-link-nnl.inp,
BHE-CXA-Heidemann-laminar-he-0.0625m-ex-shift-link-loc.inp,
BHE-CXA-Heidemann-laminar-he-0.0625m-ex-shift-link-nnl.inp

In this set of simulations the heat exchanger is shifted by a distance 0.03125m in the X and Z directions. Hence in the case of the grid size $h^e = 0.0625\text{m}$ it is located at the element center which is the worst case. Both local and nonlocal constraints methods are tested here as the soils nodes of the heat exchanger must be linked to the soil mesh using local or nonlocal constraints.

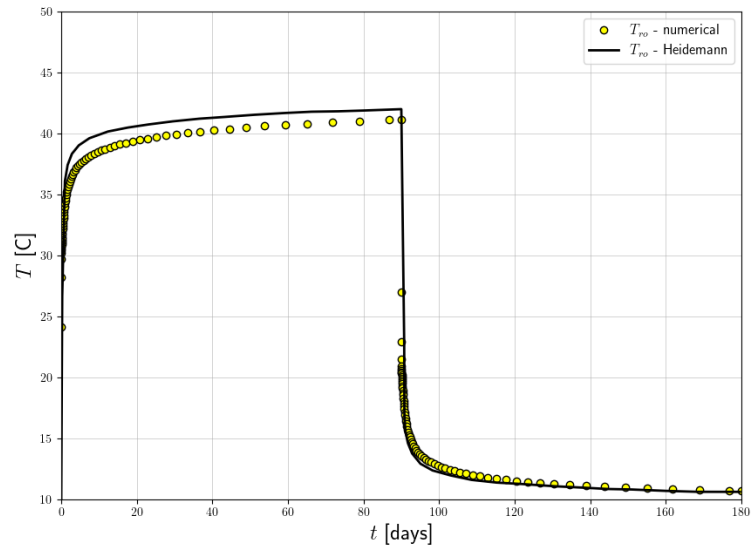


Figure 6.42: Refrigerant temperature time history at the outlet obtained for the laminar flow case, conforming soil mesh, with the inner zone grid size $h^e = 1\text{m}$ (local constraints are used to connect exchanger soil nodes with the soil mesh)

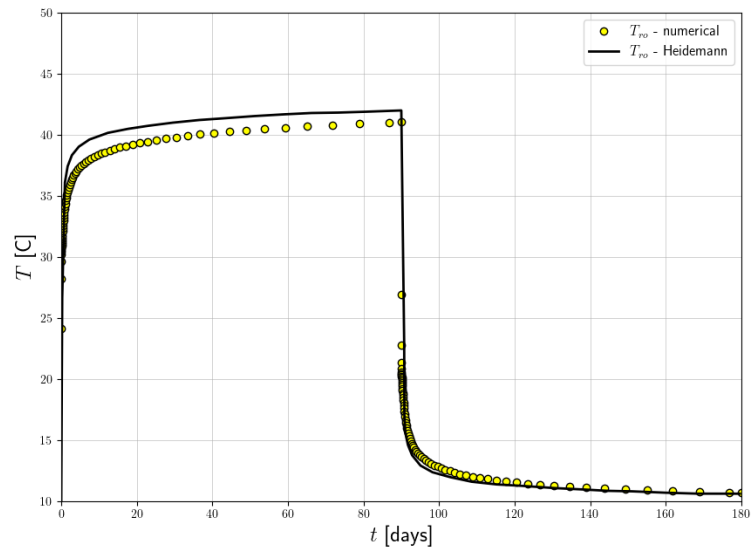


Figure 6.43: Refrigerant temperature time history at the outlet obtained for the laminar flow case, conforming soil mesh, with the inner zone grid size $h^e = 1\text{m}$ (nonlocal constraints are used to connect exchanger soil nodes with the soil mesh)
ZSoil® 220430 report

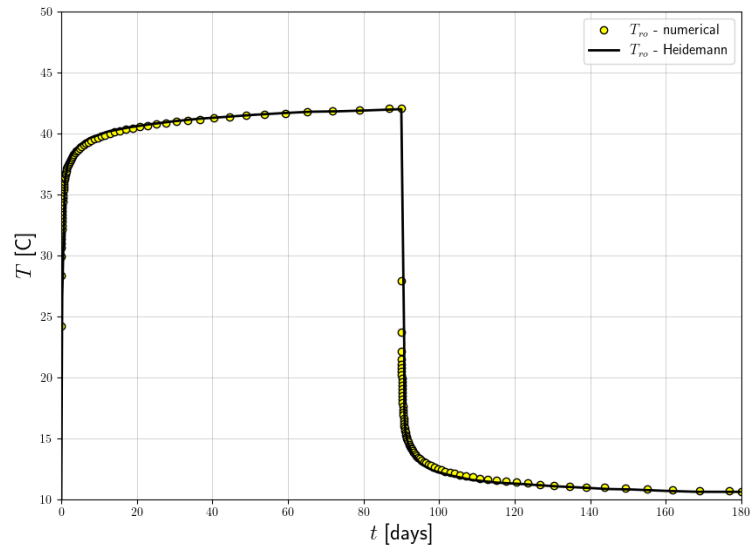


Figure 6.44: Refrigerant temperature time history at the outlet obtained for the laminar flow case, locally refined soil mesh, with the inner zone grid size $h^e = 0.5\text{m}$ (local constraints are used to connect exchanger soil nodes with the soil mesh)

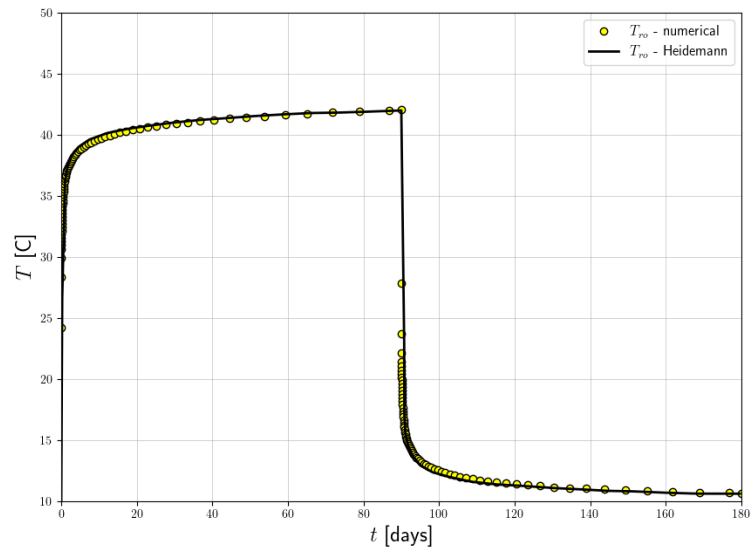


Figure 6.45: Refrigerant temperature time history at the outlet obtained for the laminar flow case, locally refined soil mesh, with the inner zone grid size $h^e = 0.5\text{m}$ (nonlocal constraints are used to connect exchanger soil nodes with the soil mesh)

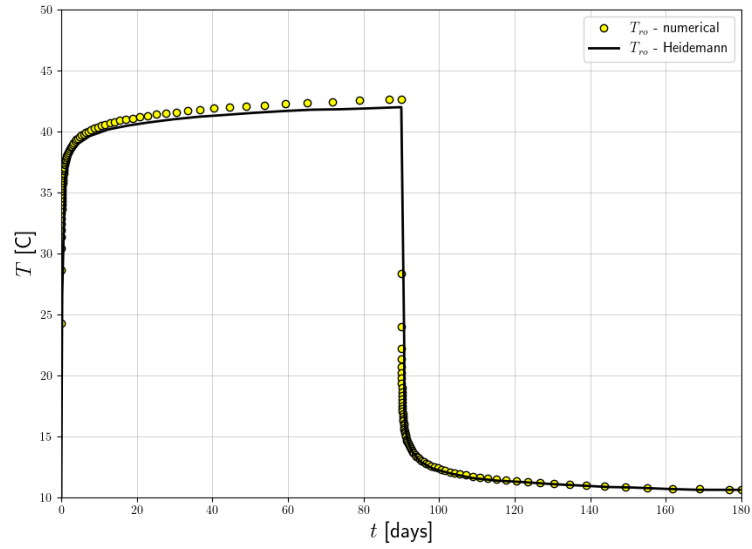


Figure 6.46: Refrigerant temperature time history at the outlet obtained for the laminar flow case, locally refined soil mesh, with the inner zone grid size $h^e = 0.25\text{m}$ (local constraints are used to connect exchanger soil nodes with the soil mesh)

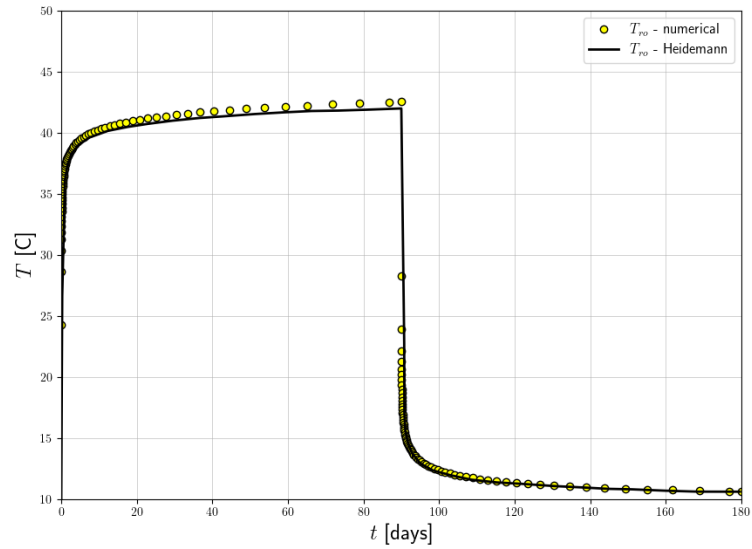


Figure 6.47: Refrigerant temperature time history at the outlet obtained for the laminar flow case, locally refined soil mesh, with the inner zone grid size $h^e = 0.25\text{m}$ (nonlocal constraints are used to connect exchanger soil nodes with the soil mesh)
ZSoil® 220430 report

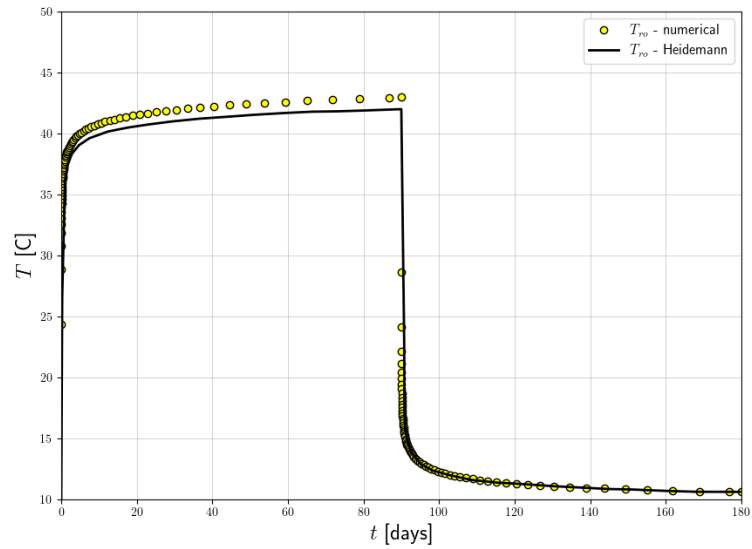


Figure 6.48: Refrigerant temperature time history at the outlet obtained for the laminar flow case, locally refined soil mesh, with the inner zone grid size $h^e = 0.125\text{m}$ (local constraints are used to connect exchanger soil nodes with the soil mesh)

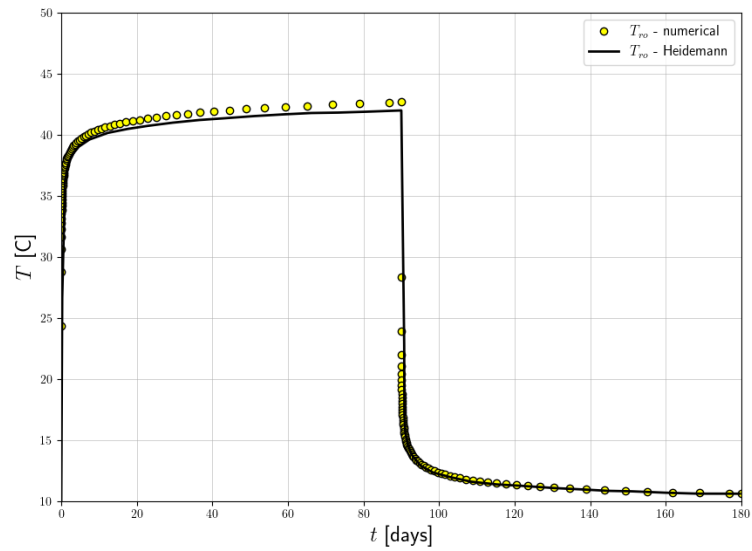


Figure 6.49: Refrigerant temperature time history at the outlet obtained for the laminar flow case, locally refined soil mesh, with the inner zone grid size $h^e = 0.125\text{m}$ (nonlocal constraints are used to connect exchanger soil nodes with the soil mesh)

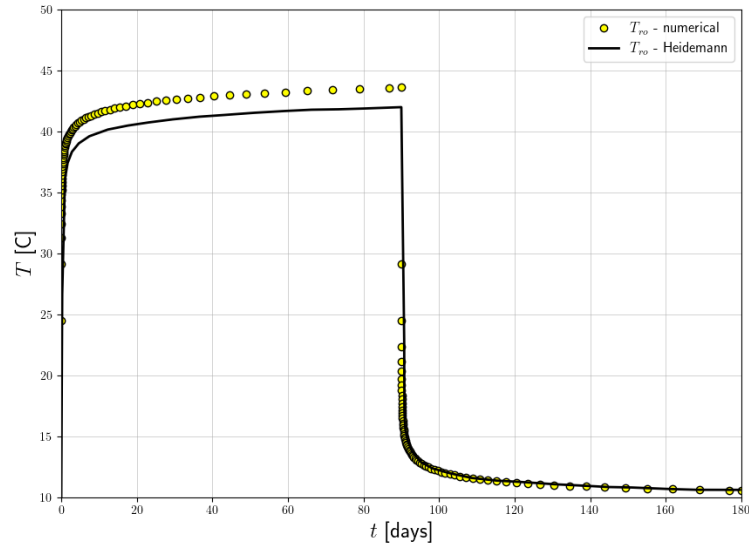


Figure 6.50: Refrigerant temperature time history at the outlet obtained for the laminar flow case, locally refined soil mesh, with the inner zone grid size $h^e = 0.0625\text{m}$ (local constraints are used to connect exchanger soil nodes with the soil mesh)

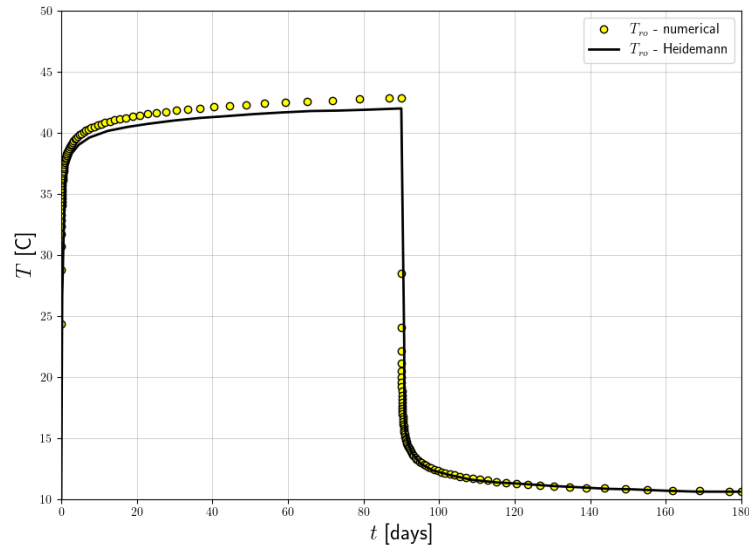


Figure 6.51: Refrigerant temperature time history at the outlet obtained for the laminar flow case, locally refined soil mesh, with the inner zone grid size $h^e = 0.0625\text{m}$ (nonlocal constraints are used to connect exchanger soil nodes with the soil mesh)
ZSoil® 220430 report

6.4.1.3 Results for the case of turbulent flow and exchanger located at the center of the mesh

Files:

BHE-CXA-Heidemann-turbulent-he-1m.inp,
BHE-CXA-Heidemann-turbulent-he-1m-link-nnl.inp,
BHE-CXA-Heidemann-turbulent-he-0.5m-ex.inp,
BHE-CXA-Heidemann-turbulent-he-0.5m-ex-link-nnl.inp,
BHE-CXA-Heidemann-turbulent-he-0.25m-ex.inp,
BHE-CXA-Heidemann-turbulent-he-0.25m-ex-link-nnl.inp,
BHE-CXA-Heidemann-turbulent-he-0.125m-ex.inp,
BHE-CXA-Heidemann-turbulent-he-0.125m-ex-link-nnl,
BHE-CXA-Heidemann-turbulent-he-0.0625m-ex.inp,
BHE-CXA-Heidemann-turbulent-he-0.0625m-ex-link-nnl.inp

In the following figures time history of the refrigerant temperature at the outlet pipe is presented for the turbulent flow case. The two methods of connecting exchanger mesh to the soil mesh are used. First the standard approach is used in which soil nodes of the exchanger coincide with soil mesh nodes, then the second method is tested in which soil nodes of the exchanger element are linked via nonlocal constraints to the soil mesh. It is well visible that the mesh size $h^e = 0.5\text{m}$ is optimal for the first method but it is also well visible that it does not exhibit h convergence property required in the FE method. The second method is definitely more consistent as with the further mesh refinements the resulting time history tends to the asymptote. It is worth to mention that exchanger nodes are aligned along soil mesh nodes.

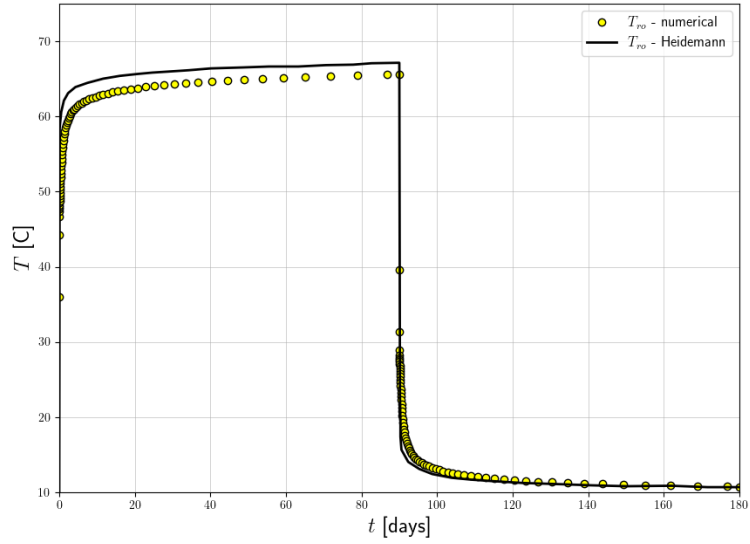


Figure 6.52: Refrigerant temperature time history at the outlet obtained for the turbulent flow case, conforming soil mesh, with the inner zone grid size $h^e = 1\text{m}$ (exchanger soil nodes coincide with the soil mesh nodes)

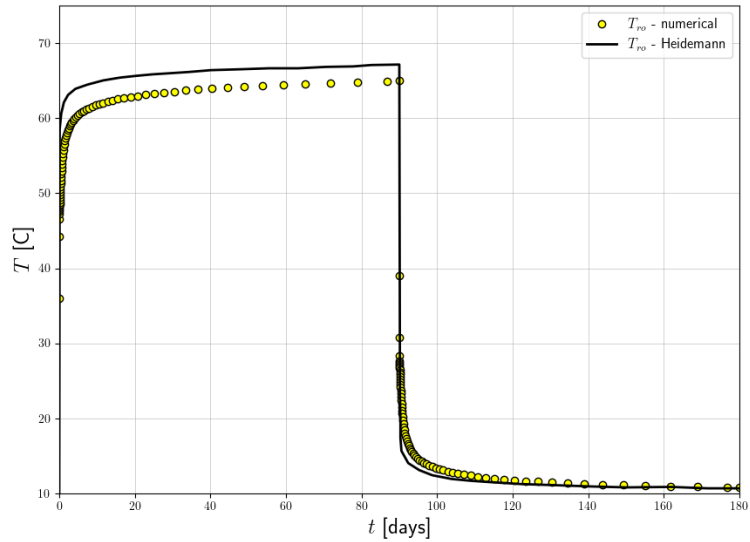


Figure 6.53: Refrigerant temperature time history at the outlet obtained for the turbulent flow case, conforming soil mesh, with the grid size $h^e = 1\text{m}$ (exchanger soil nodes linked via nonlocal constraints to the soil mesh)

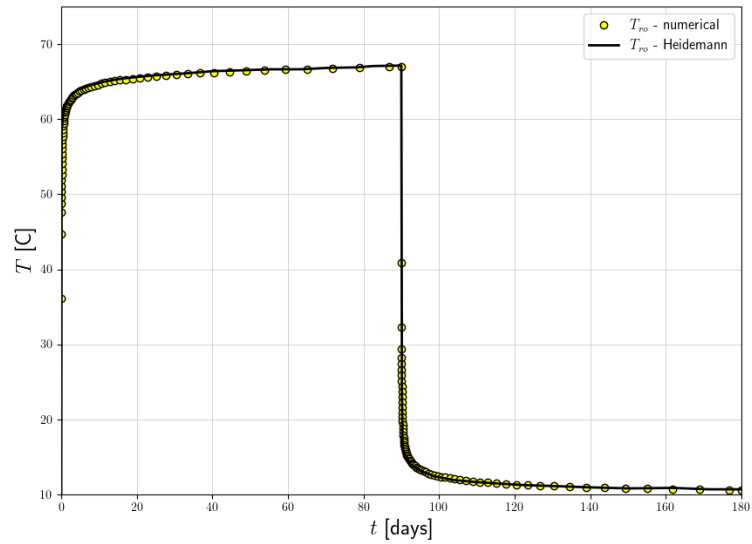


Figure 6.54: Refrigerant temperature time history at the outlet obtained for the turbulent flow case, locally refined soil mesh, with the inner zone grid size $h^e = 0.5\text{m}$ (exchanger soil nodes coincide with the soil mesh nodes)

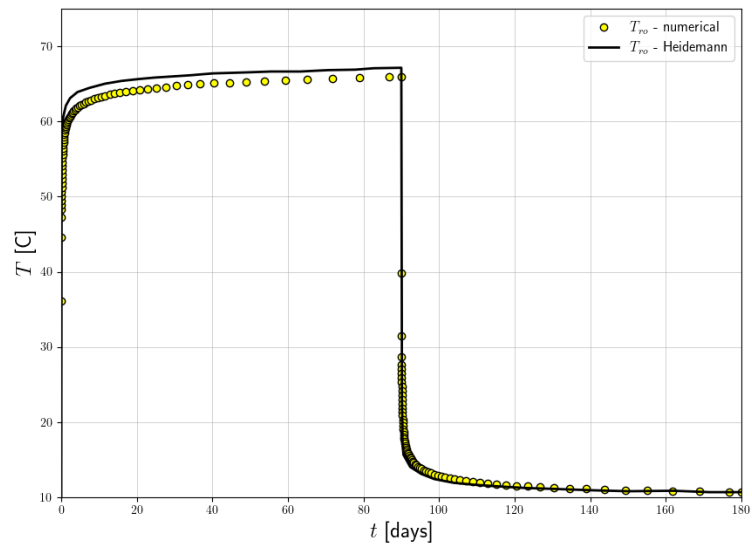


Figure 6.55: Refrigerant temperature time history at the outlet obtained for the turbulent flow case, locally refined soil mesh, with the inner zone grid size $h^e = 0.5\text{m}$ (exchanger soil nodes linked via nonlocal constraints to the soil mesh)

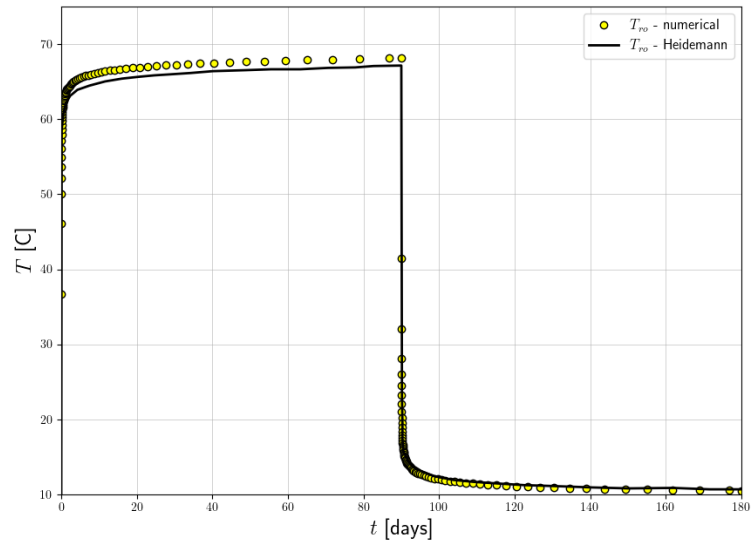


Figure 6.56: Refrigerant temperature time history at the outlet obtained for the turbulent flow case, locally refined soil mesh, with the inner zone grid size $h^e = 0.25\text{m}$ (exchanger soil nodes coincide with the soil mesh nodes)

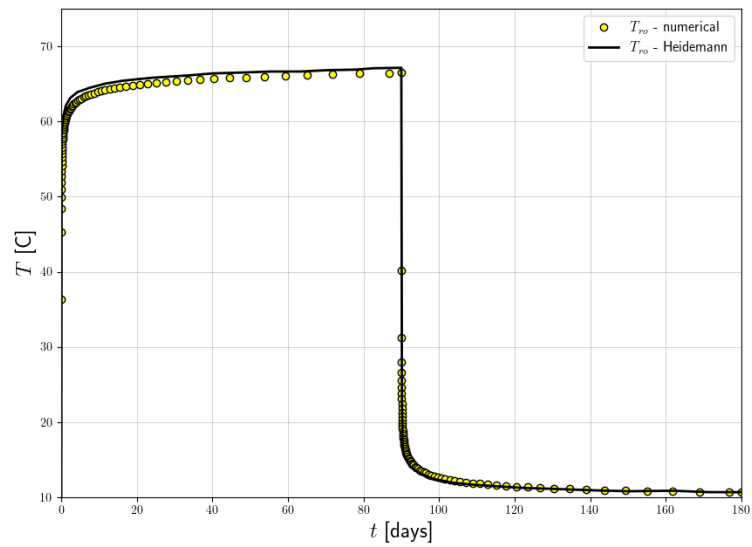


Figure 6.57: Refrigerant temperature time history at the outlet obtained for the turbulent flow case, locally refined soil mesh, with the inner zone grid size $h^e = 0.25\text{m}$ (exchanger soil nodes linked via nonlocal constraints to the soil mesh)
ZSoil® 220430 report

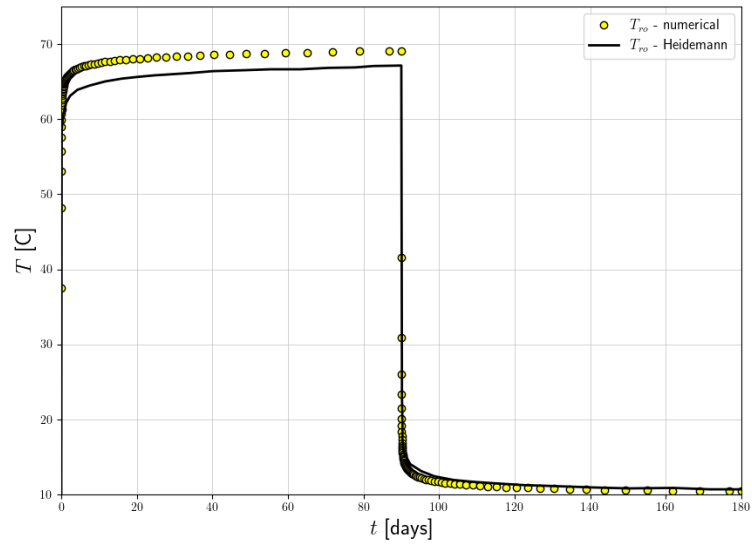


Figure 6.58: Refrigerant temperature time history at the outlet obtained for the turbulent flow case, locally refined soil mesh, with the inner zone grid size $h^e = 0.125\text{m}$ (exchanger soil nodes coincide with the soil mesh nodes)

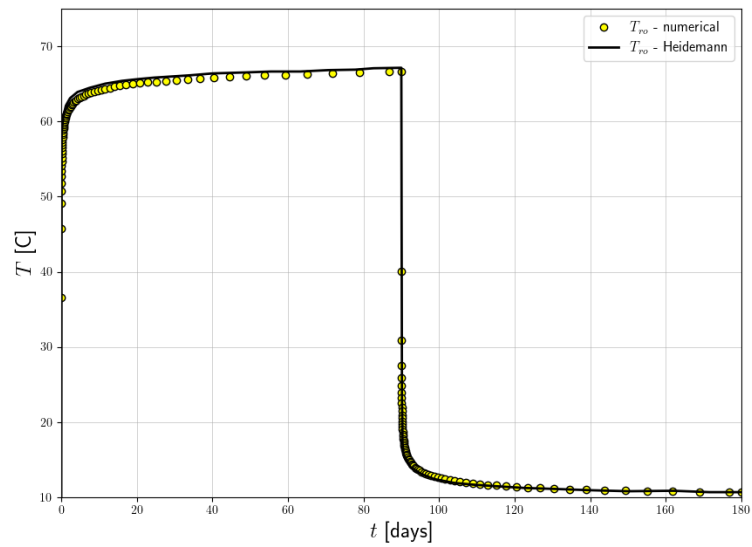


Figure 6.59: Refrigerant temperature time history at the outlet obtained for the turbulent flow case, locally refined soil mesh, with the inner zone grid size $h^e = 0.125\text{m}$ (exchanger soil nodes linked via nonlocal constraints to the soil mesh)

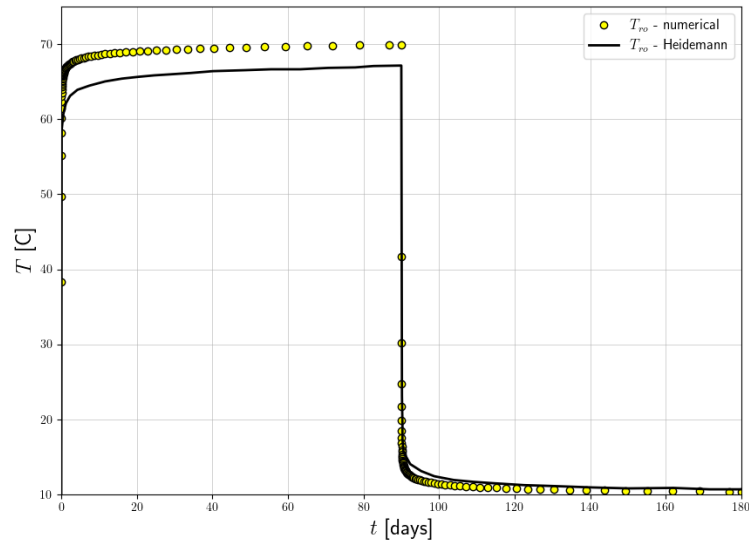


Figure 6.60: Refrigerant temperature time history at the outlet obtained for the turbulent flow case, locally refined soil mesh, with the inner zone grid size $h^e = 0.0625\text{m}$ (exchanger soil nodes coincide with the soil mesh nodes)

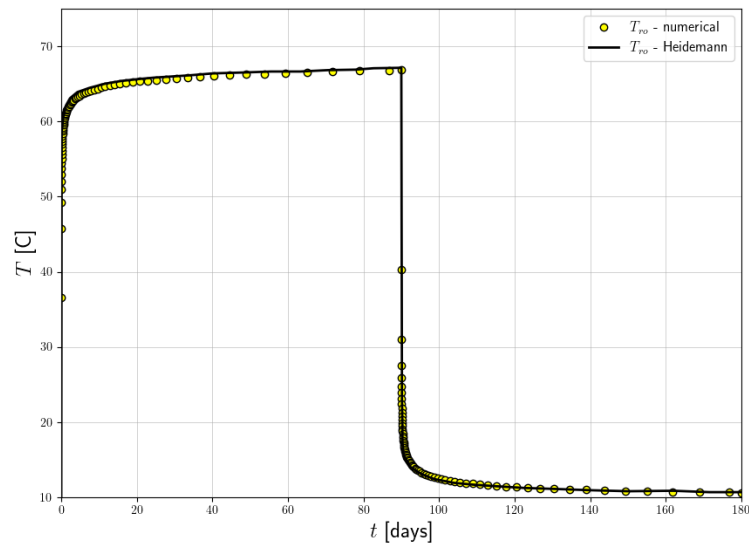


Figure 6.61: Refrigerant temperature time history at the outlet obtained for the turbulent flow case, locally refined soil mesh, with the inner zone grid size $h^e = 0.0625\text{m}$ (exchanger soil nodes linked via nonlocal constraints to the soil mesh)
ZSoil® 220430 report

6.4.1.4 Results for the case of turbulent flow with exchanger shifted from the center of the mesh

Files:

BHE-CXA-Heidemann-turbulent-he-1m-shift-link-loc.inp,
BHE-CXA-Heidemann-turbulent-he-1m-shift-link-nnl.inp,
BHE-CXA-Heidemann-turbulent-he-0.5m-ex-shift-link-loc.inp,
BHE-CXA-Heidemann-turbulent-he-0.5m-ex-shift-link-nnl.inp,
BHE-CXA-Heidemann-turbulent-he-0.25m-ex-shift-link-loc.inp,
BHE-CXA-Heidemann-turbulent-he-0.25m-ex-shift-link-nnl.inp,
BHE-CXA-Heidemann-turbulent-he-0.125m-ex-shift-link-loc.inp,
BHE-CXA-Heidemann-turbulent-he-0.125m-ex-shift-link-nnl.inp,
BHE-CXA-Heidemann-turbulent-he-0.0625m-ex-shift-link-loc.inp,
BHE-CXA-Heidemann-turbulent-he-0.0625m-ex-shift-link-nnl.inp

In this set of simulations the heat exchanger is shifted by a distance 0.03125m in the X and Z directions. Hence in the case of the grid size $h^e = 0.0625\text{m}$ it is located at the element center which is the worst case. Both local and nonlocal constraints methods are tested here as the soils nodes of the heat exchanger must be linked to the soil mesh using local or nonlocal constraints.

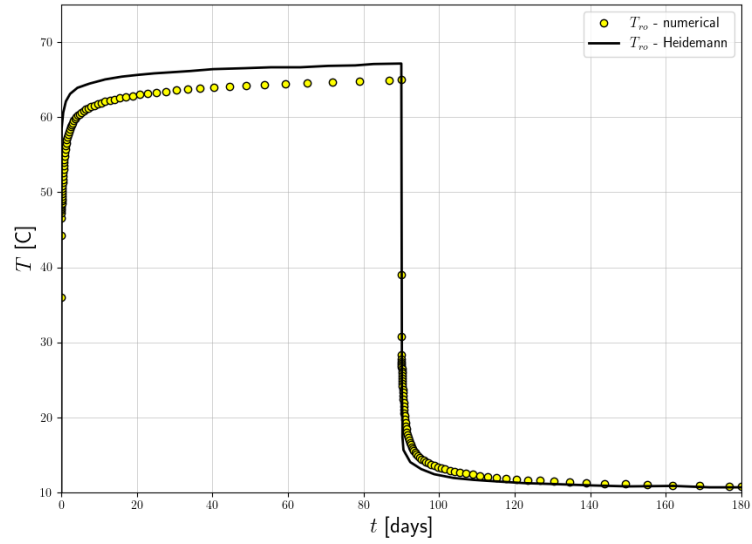


Figure 6.62: Refrigerant temperature time history at the outlet obtained for the turbulent flow case, conforming soil mesh, with the inner zone grid size $h^e = 1\text{m}$ (local constraints are used to connect exchanger soil nodes with the soil mesh)

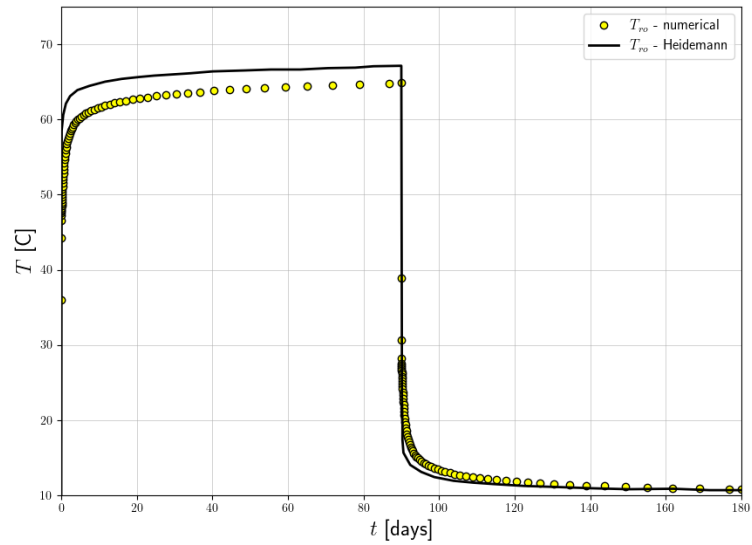


Figure 6.63: Refrigerant temperature time history at the outlet obtained for the turbulent flow case, conforming soil mesh, with the inner zone grid size $h^e = 1\text{m}$ (nonlocal constraints are used to connect exchanger soil nodes with the soil mesh)
ZSoil® 220430 report

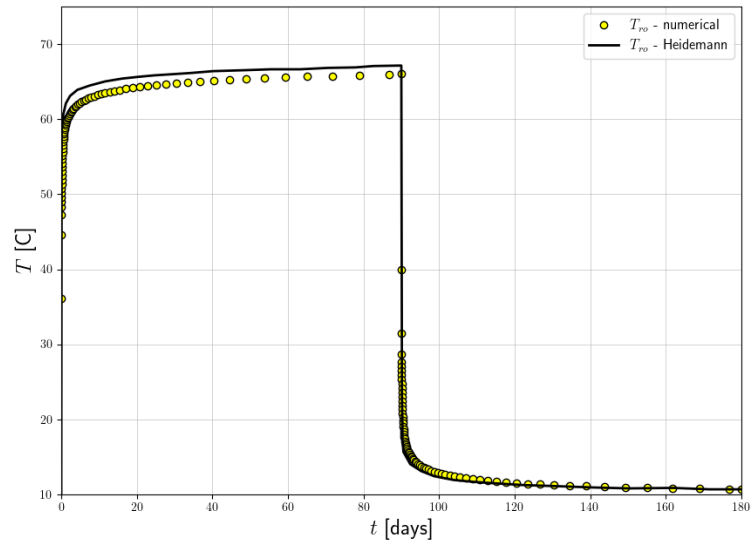


Figure 6.64: Refrigerant temperature time history at the outlet obtained for the turbulent flow case, locally refined soil mesh, with the inner zone grid size $h^e = 0.5\text{m}$ (local constraints are used to connect exchanger soil nodes with the soil mesh)

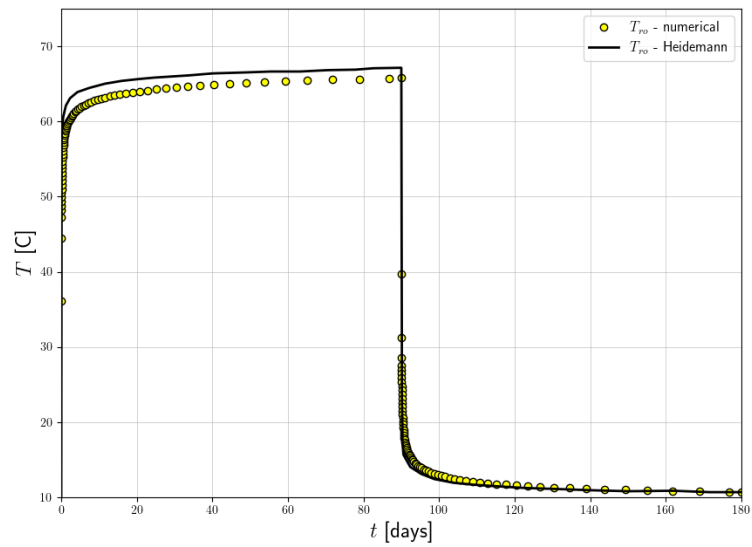


Figure 6.65: Refrigerant temperature time history at the outlet obtained for the turbulent flow case, locally refined soil mesh, with the inner zone grid size $h^e = 0.5\text{m}$ (nonlocal constraints are used to connect exchanger soil nodes with the soil mesh)

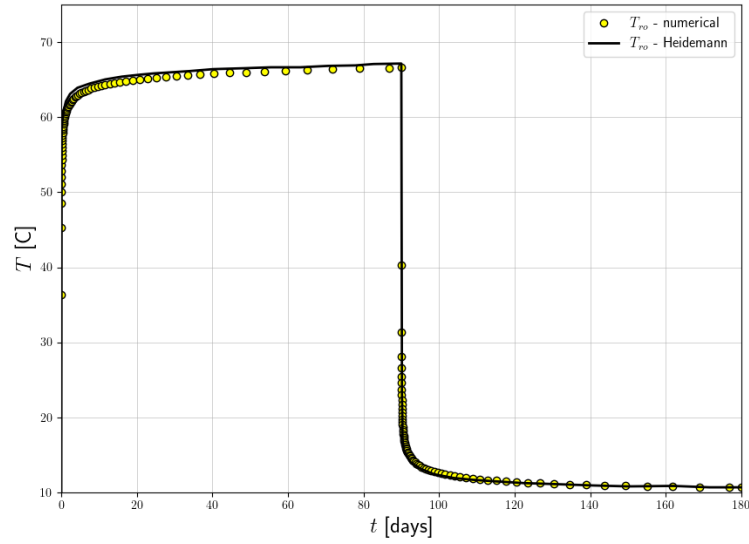


Figure 6.66: Refrigerant temperature time history at the outlet obtained for the turbulent flow case, locally refined soil mesh, with the inner zone grid size $h^e = 0.25\text{m}$ (local constraints are used to connect exchanger soil nodes with the soil mesh)

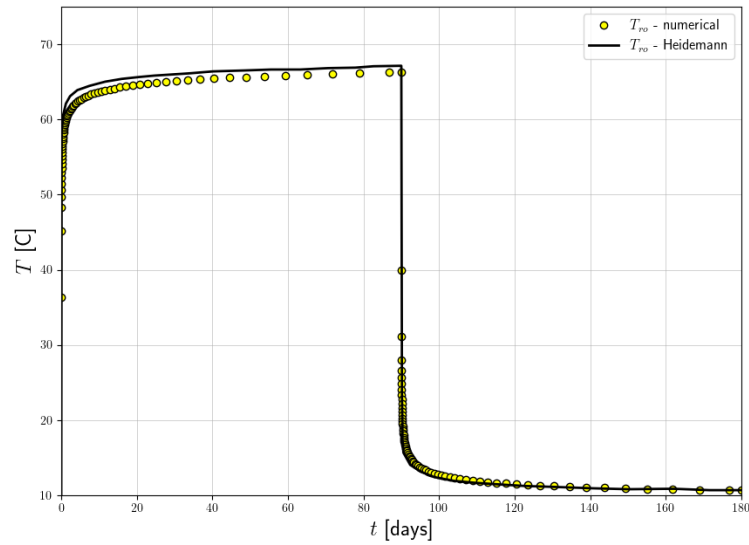


Figure 6.67: Refrigerant temperature time history at the outlet obtained for the turbulent flow case, locally refined soil mesh, with the inner zone grid size $h^e = 0.25\text{m}$ (nonlocal constraints are used to connect exchanger soil nodes with the soil mesh)
ZSoil® 220430 report

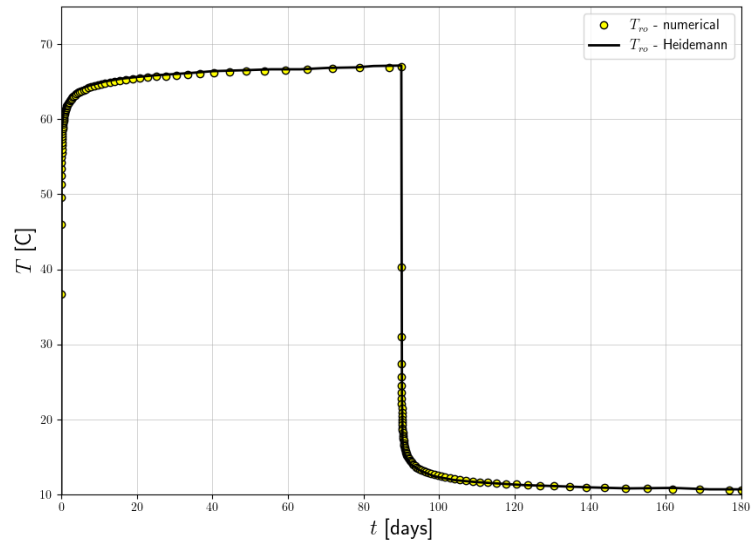


Figure 6.68: Refrigerant temperature time history at the outlet obtained for the turbulent flow case, locally refined soil mesh, with the inner zone grid size $h^e = 0.125\text{m}$ (local constraints are used to connect exchanger soil nodes with the soil mesh)

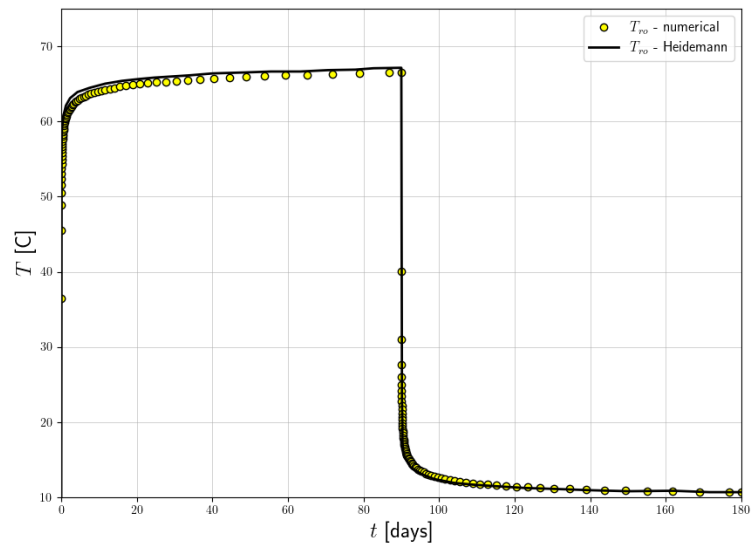


Figure 6.69: Refrigerant temperature time history at the outlet obtained for the turbulent flow case, locally refined soil mesh, with the inner zone grid size $h^e = 0.125\text{m}$ (nonlocal constraints are used to connect exchanger soil nodes with the soil mesh)

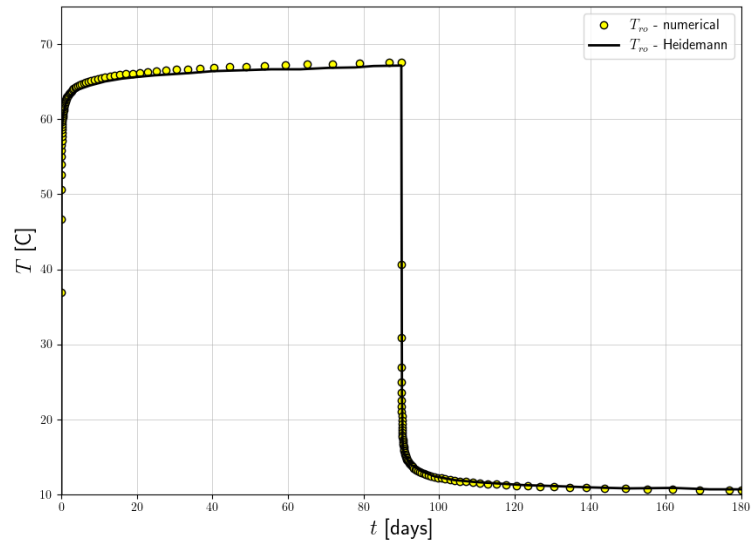


Figure 6.70: Refrigerant temperature time history at the outlet obtained for the turbulent flow case, locally refined soil mesh, with the inner zone grid size $h^e = 0.0625\text{m}$ (local constraints are used to connect exchanger soil nodes with the soil mesh)

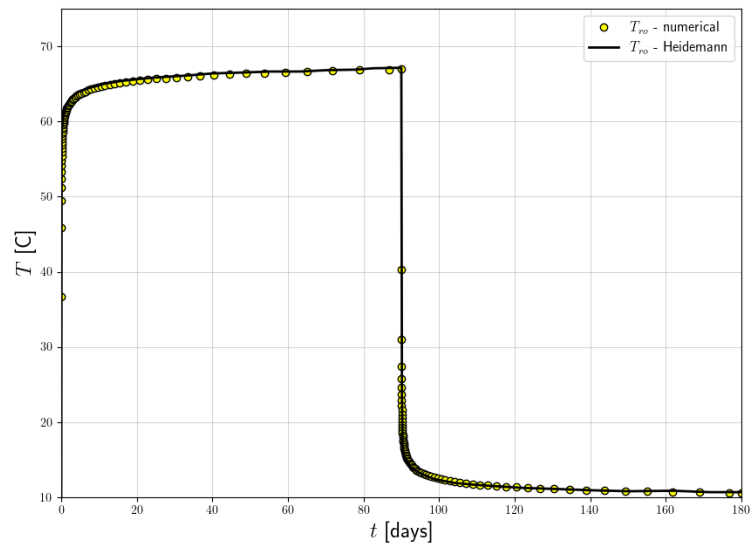


Figure 6.71: Refrigerant temperature time history at the outlet obtained for the turbulent flow case, locally refined soil mesh, with the inner zone grid size $h^e = 0.0625\text{m}$ (nonlocal constraints are used to connect exchanger soil nodes with the soil mesh)
ZSoil® 220430 report

6.4.2 Conclusions concerning meshing

Based on the results for the transient analysis of CXA heat exchanger the following conclusions can be drawn

1. When heat exchanger mesh is compatible with the soil mesh then the standard approach may yield a strong mesh dependency, therefore, it is recommended to refine locally the mesh and apply nonlocal constraints
2. Nonlocal constraints as the only method exhibit h convergence property. Standard approach as well as local constraints do not posses it
3. In the general case when using all hexa meshing nonlocal constraints, including very limited local mesh refinement near the exchanger, is the most reliable method
4. If one wants to use the standard approach (exchanger and soil meshes are compatible) the optimal grid size for the regular hexa meshing should be of order $h_{\text{in plane}}^e \approx 5D$

Chapter 7

Benchmarks for soil-structure interaction problems

7.1 Energy pile problem using 1U exchanger with the explicit grout zone

In this section energy pile-subsoil interaction problem is analyzed based on the data and problem statement given in article [5]. The subsoil stratigraphy and 1U exchanger are shown in fig.7.1. In this benchmark an energy pile is modeled using 1U heat exchanger with the explicit grout zone. Therefore the grout zone which is equivalent to the concrete material has to be explicitly discretized using standard brick continuum elements. Pile length is 28m and its diameter is 90cm. In the first step thermal problem is solved for the period of 15 days of the permanent heating applied as an imposed temperature $T_{in} = 5^{\circ}\text{C}$. In the second step computed temperature field is used in weakly coupled thermo-mechanical analysis of a pile interacting with subsoil due to temperature changes. In both steps same continuum mesh is used.

Material data used in this benchmark is taken from the aforementioned article. It is summarized in the following table. Due to lack of the complete set of the data for the heat exchanger the user defined heat transfer coefficient $\Phi_{fig} = 104.664\text{ W}/(\text{m}^2\text{K})$ is used.

Material	E [MPa]	ν [-]	n [-]	ρ_s [kg/m ³]	c [J/(kg K)]	λ [W/(m K)]	α [1/K]
Soil A1	190	0.22	0.1	2769	880	1.8	$0.33 \cdot 10^{-5}$
Soil A2	190	0.22	0.1	2769	880	1.8	$0.33 \cdot 10^{-5}$
h! Soil B	84	0.40	0.35	2735	890	1.8	$0.33 \cdot 10^{-5}$
Soil C	90	0.40	0.3	2740	890	1.8	$0.33 \cdot 10^{-5}$
Soil D	3000	0.20	0.1	2167	923	1.11	$0.33 \cdot 10^{-5}$
Concrete	28000	0.25	0.1	2500	837	1.628	$1.0 \cdot 10^{-5}$
Pipe	-	-	-	-	-	0.42	-

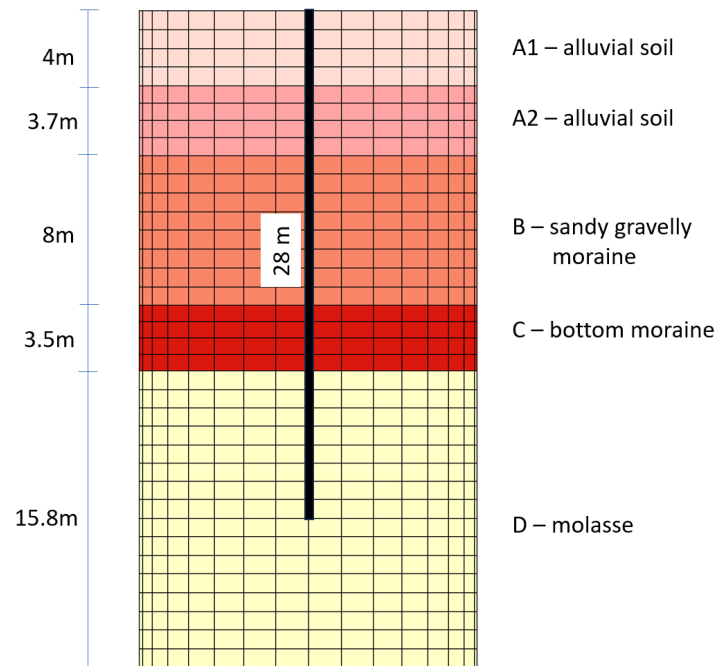


Figure 7.1: Subsoil stratigraphy at Swiss Tech Convention Center energy foundation

7.1.1 Thermal problem

File: energy-pile-thermal-1.inp

Thermal problem is solved using the two drivers. First the initial condition is generated using *Initial state* driver which is equivalent to the steady state analysis run at time $t = 0$. At all nodes on the vertical and bottom boundaries temperature is fixed to $T = 13.2^\circ \text{C}$. Top surface is assumed as isolated. Then transient driver is activated and temperature at the inlet pipe varies from 13.2°C to 5°C during period of 10s, to avoid sharp temperature variation. Location of the 1U exchanger is shown in fig.7.3. It is well visible that the exchanger mesh does not conform the subsoil one therefore nonlocal constraints method is used here to connect dissimilar meshes. Temperature field, at time $t = 15$ days is shown in fig.7.4. Temperature color contours in pile, in the molasse zone, drops down to 9.3°C which is in agreement with the result obtained in article [5]. It is also well visible that in the insulation zone at shallow depth temperature is close to the initial one.

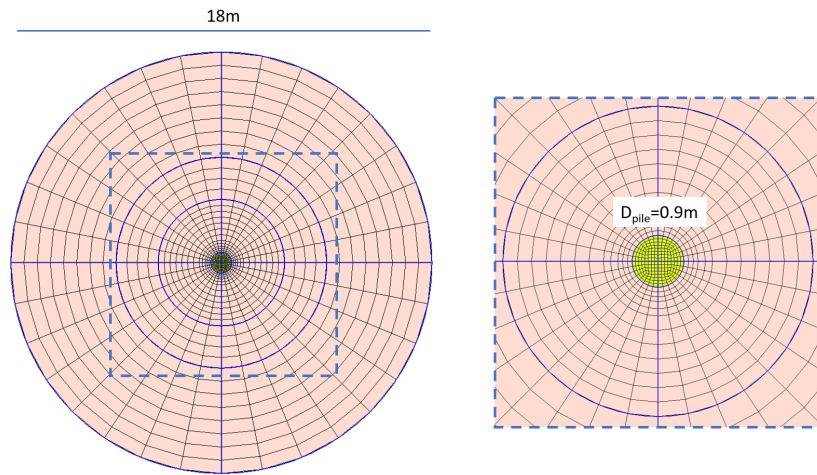


Figure 7.2: Top view of the subsoil mesh with focus put on pile zone

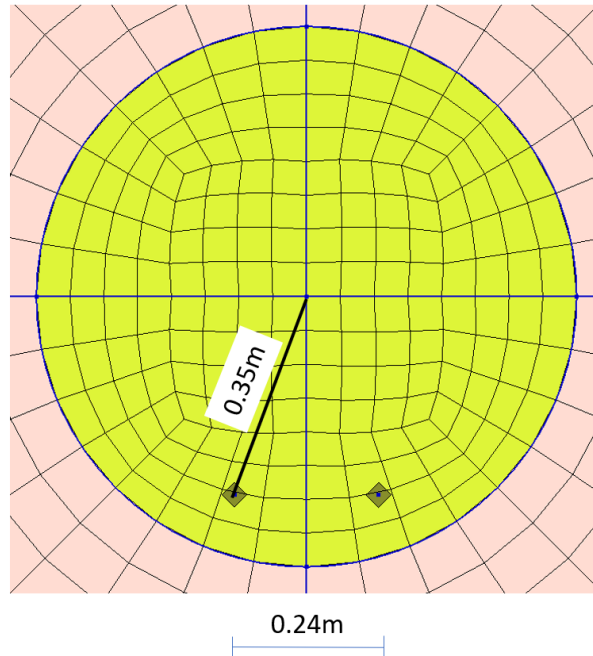


Figure 7.3: Location of the inlet and outlet pipes with respect to the subsoil mesh

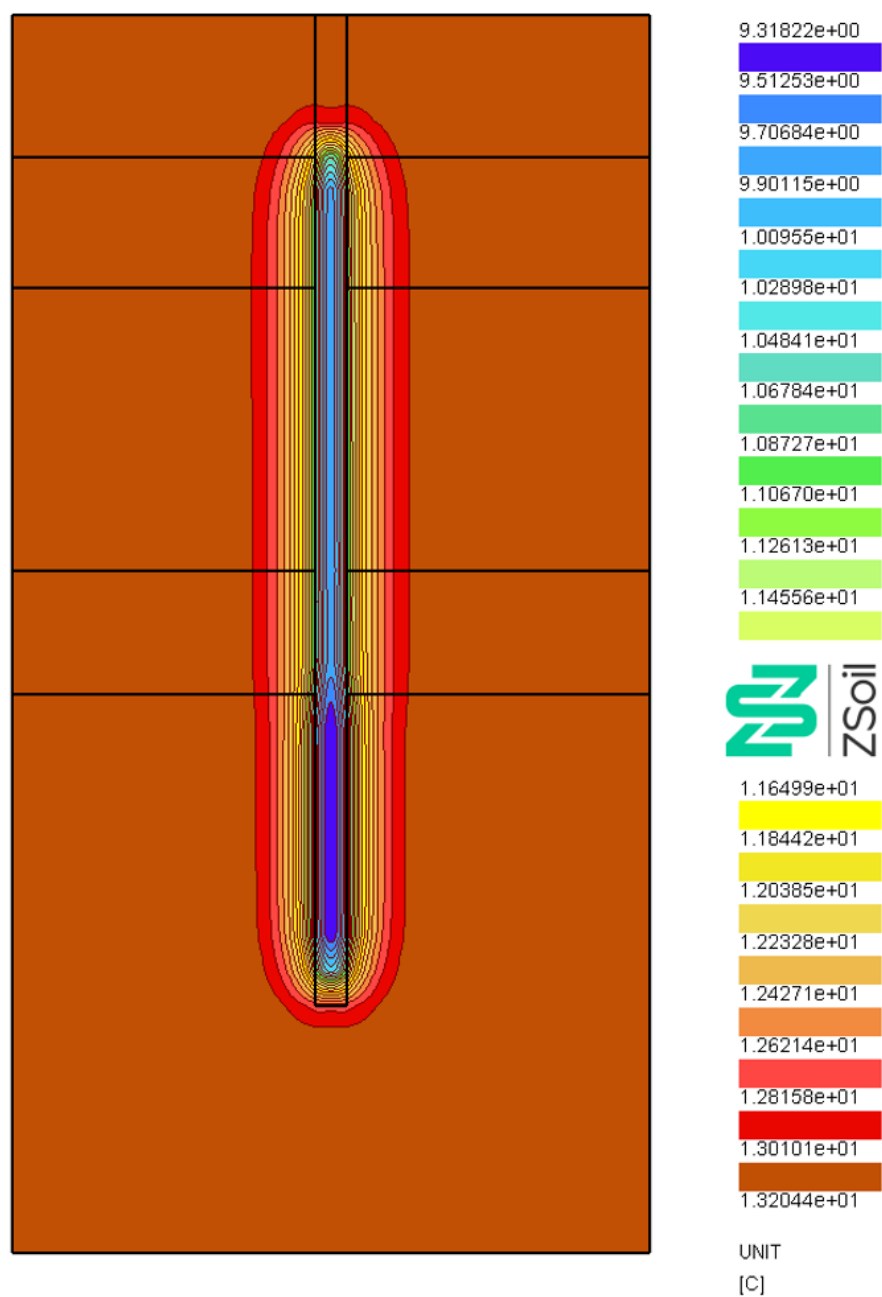


Figure 7.4: Temperature field in the pile and subsoil at time $t = 15$ days

7.1.2 Thermo-mechanical problem

File: energy-pile-mechanical-1.inp

In the second step mechanical analysis is carried out in order to assess thermal stresses in the pile induced by the temperature variation. In this analysis pile is discretized using continuum elements without shaft/tip interfaces. Computation consists of the two stages. First the initial state is generated for the subsoil and pile (existing from the very beginning) and then driven load driver is activated with the same time stepping as the one applied for the thermal analysis. Here major focus is put on stress evolution in the pile and its settlements due to temperature variation. The normal thermal stress distribution is shown in fig.7.5. It is well visible that the distribution is not uniform in the cross section due to eccentric exchanger position. The integral of this stress distribution, at time $t = 15$ days is equal to 568.2 kN which yields an averaged normal stress $\sigma_n = 893$ kPa. In the article authors claim that the maximum axial stress they get (not clearly defined what it means in fact) is of order 800 kPa. However, Fig.4 in this article clearly shows that the achieved maximum axial stress is larger than 800 kPa. Reported in the article maximum settlement of order 0.3mm, at time 15 days, is well reproduced in this benchmark (see fig.7.6).

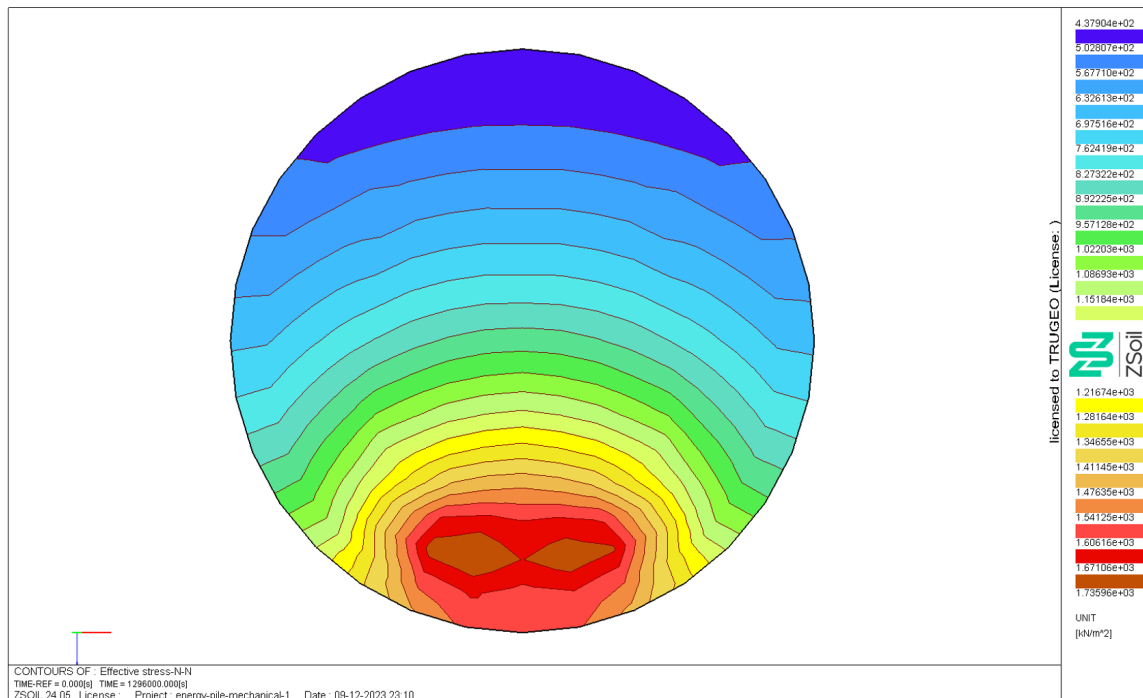


Figure 7.5: Differential (with respect to the initial state) normal stress in the pile cross section at depth 23m ($t = 15$ days)

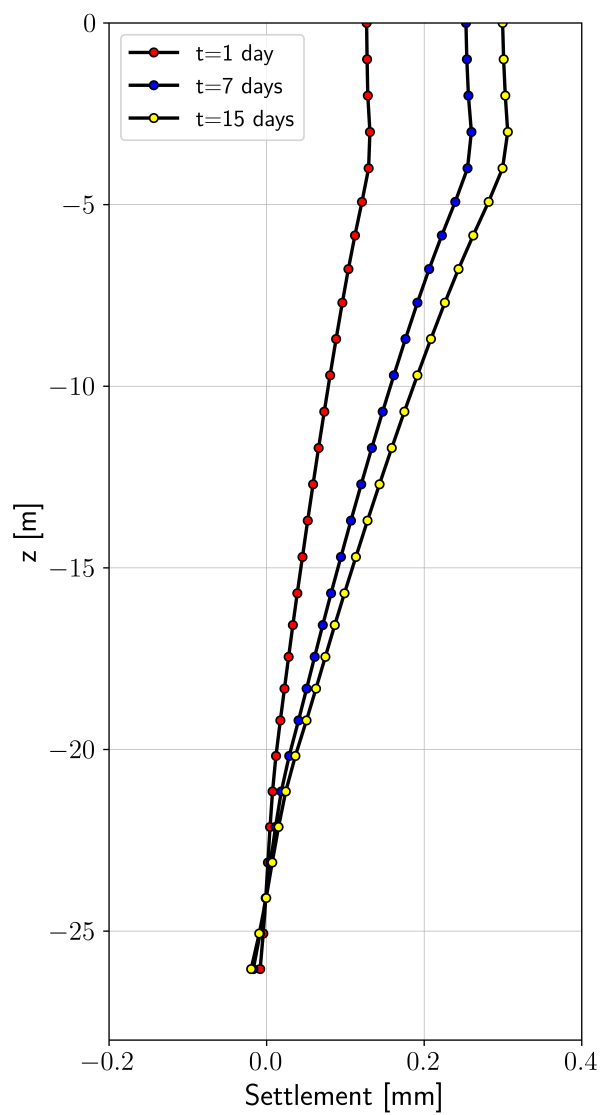


Figure 7.6: Profiles of pile settlements at $t = 1$ day, 7 days and 15 days

7.2 Energy pile problem using 1U exchanger with the implicit grout zone

In this section energy pile-subsoil interaction problem is analyzed based on the data and problem statement, given in section 7.1. Here 1U heat exchanger with the implicit grout zone is used in thermal step and non-local 1D pile formulation in the mechanical one. The exchanger is located at the pile center.

Detailed material data used for the 1U heat exchanger is summarized in the following table.

Table 7.1: Material properties for the 1U heat exchanger

Parameter	Symbol	Unit	Value
BHE type			1U
Borehole diameter	D	[m]	0.90
Pipe distance	w	[m]	0.24
Pipe (IN) outer diameter	d_i^{ext}	[m]	0.04
Pipe (IN) wall thickness	h_i	[m]	0.004
Pipe (IN) thermal conductivity	λ_i^p	[W/m/K]	0.42
Pipe (OUT) outer diameter	d_o^{ext}	[m]	0.04
Pipe (OUT) wall thickness	h_o	[m]	0.004
Pipe (OUT) thermal conductivity	λ_o^p	[W/m/K]	0.42
Refrigerant vol. flow discharge	Q^r	[m ³ /s]	$1.6088 \cdot 10^{-4}$
Refrigerant vol. flow discharge type			unused
Refrigerant thermal conductivity	λ^r	[W/m/K]	0.64
Refrigerant dynamic viscosity	μ^r	[kPa s]	$5.5 \cdot 10^{-7}$
Refrigerant vol. heat capacity	$\rho^r c^r$	[kJ/m ³ /K]	4130
Refrigerant density	ρ^r	[kg/m ³]	1000
Grout thermal conductivity	λ^g	[W/m/K]	1.628
Grout heat capacity	$\rho^g c^g$	[kJ/m ³ /K]	2092

7.2.1 Thermal problem

File: BHE-energy-pile-thermal-1.inp

Thermal problem is solved using the two drivers. First the initial condition is generated using *Initial state* driver which is equivalent to the steady state analysis run at time $t = 0$. At all nodes on the vertical and bottom boundaries temperature is fixed to $T = 13.2^\circ \text{C}$. Top surface is assumed as isolated. Then transient driver is activated and temperature at the inlet pipe varies from 13.2°C to 5°C during period of 10s, to avoid sharp temperature variation. Heat exchanger mesh is linked to the background continuum mesh using non-local constraints. This is very important as the pile diameter is relatively large. Temperature field, at time $t = 15$ days is shown in fig.7.7. Temperature value, at the molasse zone, drops down to 10.15°C . It is also well visible that in the insulation zone temperature is close to the initial one. Non-locality effect is visible as well.

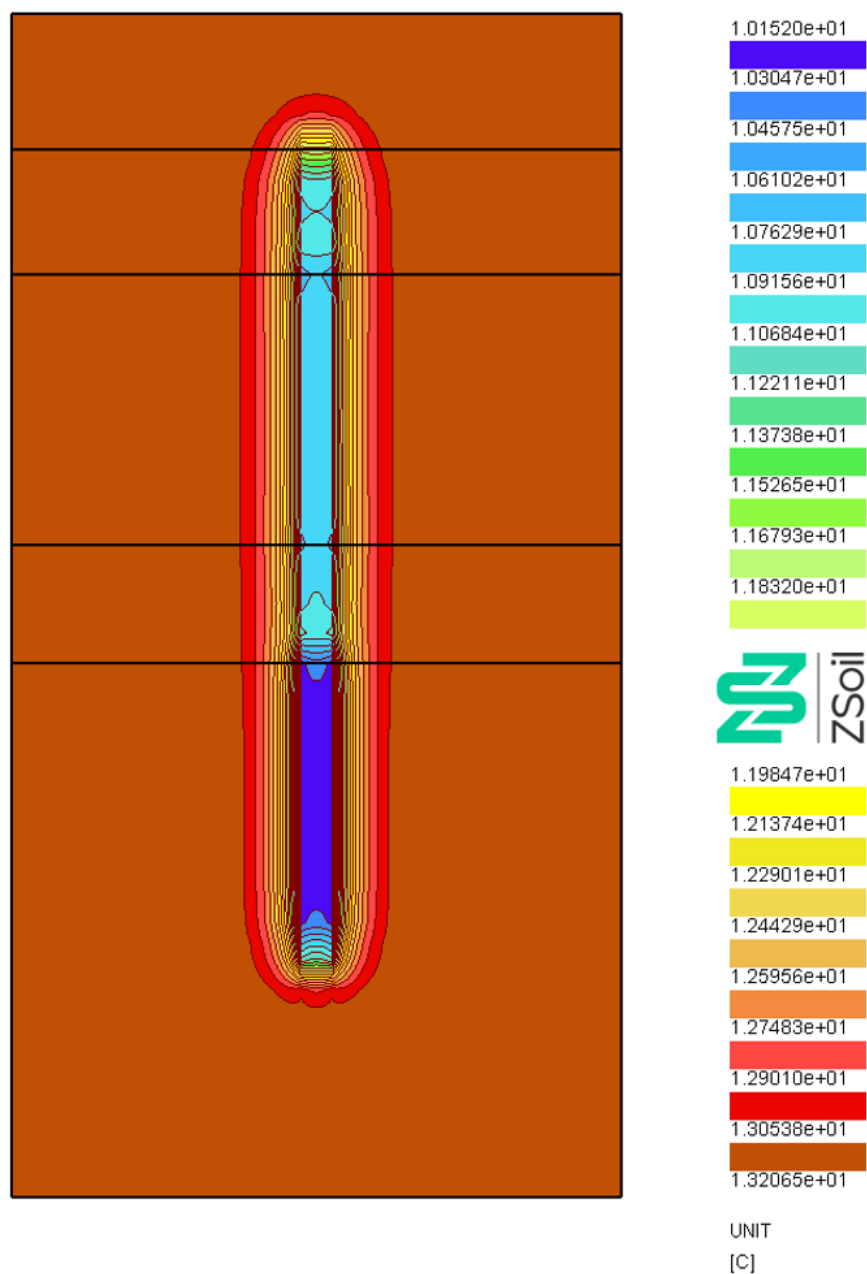


Figure 7.7: Temperature field in the pile and subsoil at time $t = 15$ days

7.2.2 Thermo-mechanical problem

File: BHE-energy-pile-mechanical-1.inp

In the second step mechanical analysis is carried out in order to assess thermal stresses in pile, induced by temperature variation. In this analysis pile is discretized using beam elements embedded in the continuum. Non-local pile formulation is used here to cancel severe mesh dependency. As the pile axis is colinear with the heat exchanger one the averaged temperature from the two grout zones (zone of the pipe-OIN and pipe-OUT) is mapped from the thermal mesh onto mechanical one. The computation consists of the two stages. First the initial state is generated for the subsoil and pile (existing from the very beginning) and then driven load driver is activated using the same time stepping as the one applied for the thermal analysis. Here major focus is put on stress evolution in the pile and its settlements due to temperature variation.

The axial force distribution is shown in fig.7.8 (the initial axial force is subtracted to assess thermally induced force only). The maximum axial force is equal to 658 kN. This yields normal stress of order 1034 kPa. Pile settlements at three selected time instances $t = 1, 7, 15$ days is shown in fig.7.9. It is worth to mention that the local pile formulation is unable to reproduce presented results for the assumed mesh density.

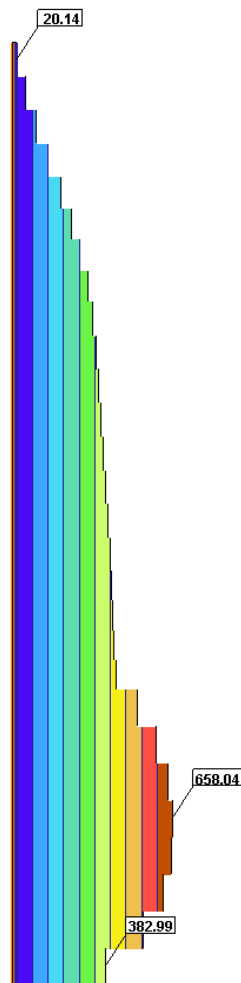


Figure 7.8: Differential (with respect to the initial state) normal force distribution ($t = 15$ days)

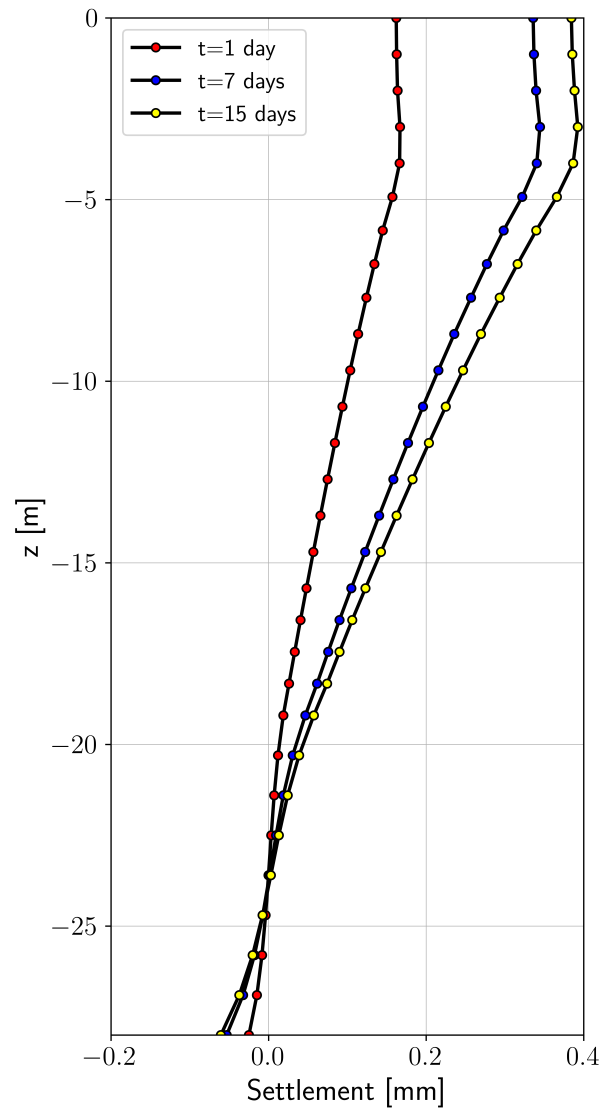


Figure 7.9: Profiles of pile settlements at $t = 1$ day, 7 days and 15 days

Appendix A

Thermal resistances for heat exchangers with the implicit grout zones

A.1 Thermal resistances for the 1U heat exchanger

Thermal resistances for 1U exchanger between inlet/outlet pipes and grout are computed using the following expressions

$$R_{fig} = R_{adv_k} + R_{con_k^a} + R_{con^b} \quad (k = i1) \quad (A.1)$$

$$R_{fog} = R_{adv_k} + R_{con_k^a} + R_{con^b} \quad (k = o1) \quad (A.2)$$

$$(A.3)$$

A.1.1 Thermal resistances caused by the advective flow of refrigerant in inlet/outlet pipes

Thermal resistance R_{adv_k} is defined as follows

$$R_{adv_k} = \frac{1}{Nu_k \lambda^r \pi} \quad (k = i1, o1) \quad (A.4)$$

where Nusselt numbers Nu_k depend on the refrigerant velocity.

In the laminar flow regime ($Re_k < 2300$)

$$Nu_k = Nu_k^{lam} = 4.364 \quad (A.5)$$

In the turbulent flow regime ($Re_k > 10^4$)

$$Nu_k = Nu_k^{trb} = \frac{(\xi_k/8)Re_k Pr}{1 + 12.7\sqrt{\xi_k/8}(Pr^{2/3} - 1)} \left(1 + \left(\frac{d_k^{int}}{L} \right)^{2/3} \right) \quad (A.6)$$

APPENDIX A. THERMAL RESISTANCES FOR HEAT EXCHANGERS WITH THE IMPLICIT GROUT ZONES

In the transition flow regime ($2300 \leq \text{Re}_k < 10^4$ (here Nu_k^{trb} is computed assuming $\text{Re}_k = 10^4$))

$$\text{Nu}_k = (1 - \gamma_k) \text{Nu}_k^{\text{lam}} + \gamma_k \text{Nu}_k^{\text{trb}} (\text{Re}_k = 10^4) \quad (\text{A.7})$$

The refrigerant velocity, Prandtl and Reynolds numbers are defined as follows

$$\text{Pr} = \frac{\mu^r c^r}{\lambda^r} \quad (\text{A.8})$$

$$\text{Re}_k = \frac{|v_k^r| d_k^{\text{int}}}{\mu^r / \rho^r} \quad k = i1, o1 \quad (\text{A.9})$$

$$\xi_k = (1.8 \log_{10} \text{Re}_k - 1.5)^{-2} \quad (\text{A.10})$$

$$\gamma_k = \frac{\text{Re}_k - 2300}{10^4 - 2300} \quad (\text{A.11})$$

$$|v_k^r| = \frac{Q^r}{\frac{\pi (d_k^{\text{int}})^2}{4}} \quad (\text{A.12})$$

A.1.2 Thermal resistances resulting from pipes material and grout transition

This resistance is expressed as follows

$$R_{\text{con}_k^a} = \frac{\ln \left(\frac{d_k^{\text{ext}}}{d_k^{\text{int}}} \right)}{2\pi \lambda_k^p} \quad k = i1, o1 \quad (\text{A.13})$$

$$R_{\text{con}^b} = x R_g \quad (\text{A.14})$$

where

$$x = \frac{\ln \left(\frac{\sqrt{D^2 + 2 d_0^2}}{2 d_0} \right)}{\ln \left(\frac{D}{\sqrt{2} d_0} \right)} \quad (\text{A.15})$$

$$R_g = \frac{\text{arcosh} \left(\frac{D^2 + d_0^2 - w^2}{2 D d_0} \right)}{2\pi \lambda^g} \left(1.601 - 0.888 \frac{w}{D} \right) \quad (\text{A.16})$$

$$d_0 = \frac{1}{2} \sum_k d_k^{\text{ext}} \quad (\text{A.17})$$

A.1.3 Thermal resistances between grout zones

Thermal resistances along Γ_{gg} boundary is expressed as follows

$$R_{gg} = \frac{2R_{gs}(R_{ar} - 2x R_g)}{2R_{gs} - R_{ar} + 2x R_g} \quad (\text{A.18})$$

$$(\text{A.19})$$

where

$$R_{ar} = \frac{\text{arcosh}\left(\frac{2w^2 - d_0^2}{d_0^2}\right)}{2\pi\lambda^g} \quad (\text{A.20})$$

$$(\text{A.21})$$

It has to be mentioned, following the FEFLOW white paper [3], that for some geometries certain resulting resistances may be negative and a correcting procedure is needed. In fact the following constraint must be satisfied

$$\left(\frac{1}{R_{gg}} + \frac{1}{2R_{gs}}\right)^{-1} > 0 \quad (\text{A.22})$$

$$(\text{A.23})$$

In case the above constraint is violated the initial x value is multiplied by factor $2/3$. If constraint is still violated then the initial x value is multiplied by factor $1/3$. In the limit case $x = 0$ is assumed.

A.1.4 Thermal resistance due to grout-soil exchange

This resistance is expressed as follows

$$R_{gs} = (1 - x) R_g \quad (\text{A.24})$$

$$(\text{A.25})$$

A.2 Thermal resistances for the 2U heat exchanger

Thermal resistances for 2U exchanger between inlet/outlet pipes and grout are computed using the following expressions

$$R_{fig} = R_{adv_k} + R_{con_k^a} + R_{con^b} \quad (k = i1..i2) \quad (A.26)$$

$$R_{fog} = R_{adv_k} + R_{con_k^a} + R_{con^b} \quad (k = o1..o2) \quad (A.27)$$

$$(A.28)$$

A.2.1 Thermal resistances caused by the advective flow of refrigerant in inlet/outlet pipes

Thermal resistance R_{adv_k} is defined as follows

$$R_{adv_k} = \frac{1}{Nu_k \lambda^r \pi} \quad (k = i1, i2, o1, o2) \quad (A.29)$$

where Nusselt numbers Nu_k depend on the refrigerant velocity.

In the laminar flow regime ($Re_k < 2300$)

$$Nu_k = Nu_k^{lam} = 4.364 \quad (A.30)$$

In the turbulent flow regime ($Re_k > 10^4$)

$$Nu_k = Nu_k^{trb} = \frac{(\xi_k/8)Re_k Pr}{1 + 12.7\sqrt{\xi_k/8}(Pr^{2/3} - 1)} \left(1 + \left(\frac{d_k^{int}}{L} \right)^{2/3} \right) \quad (A.31)$$

In the transition flow regime ($2300 \leq Re_k < 10^4$ (here Nu_k^{trb} is computed assuming $Re_k = 10^4$))

$$Nu_k = (1 - \gamma_k)Nu_k^{lam} + \gamma_k Nu_k^{trb}(Re_k = 10^4) \quad (A.32)$$

The refrigerant velocity, Prandtl and Reynolds numbers are defined as follows

$$Pr = \frac{\mu^r c^r}{\lambda^r} \quad (A.33)$$

$$Re_k = \frac{|v_k^r| d_k^{int}}{\mu^r / \rho^r} \quad k = i1, i2, o1, o2 \quad (A.34)$$

$$\xi_k = (1.8 \log_{10} Re_k - 1.5)^{-2} \quad (A.35)$$

$$\gamma_k = \frac{Re_k - 2300}{10^4 - 2300} \quad (A.36)$$

$$|v_k^r| = \begin{cases} \frac{Q^r}{2\pi(d_k^{int})^2} & \text{for parallel discharge} \\ \frac{Q^r}{\frac{\pi(d_k^{int})^2}{4}} & \text{for serial discharge} \end{cases} \quad (A.37)$$

A.2.2 Thermal resistances resulting from pipes material and grout transition

This resistance is expressed as follows

$$R_{\text{con}^a_k} = \frac{\ln\left(\frac{d_k^{\text{ext}}}{d_k^{\text{int}}}\right)}{2\pi\lambda_k^p} \quad k = i1, i2, o1, o2 \quad (\text{A.38})$$

$$R_{\text{con}^b} = x R_g \quad (\text{A.39})$$

where

$$x = \frac{\ln\left(\frac{\sqrt{D^2 + 4d_0^2}}{2\sqrt{2}d_0}\right)}{\ln\left(\frac{D}{2d_0}\right)} \quad (\text{A.40})$$

$$R_g = \frac{\text{arcosh}\left(\frac{D^2 + d_0^2 - s^2}{2Dd_0}\right)}{2\pi\lambda^g} \left(3.098 - 4.432\frac{s}{D} + 2.364\frac{s^2}{D^2}\right) \quad (\text{A.41})$$

$$d_0 = \frac{1}{4} \sum_k^4 d_k^{\text{ext}} \quad (\text{A.42})$$

$$s = w\sqrt{2} \quad (\text{A.43})$$

A.2.3 Thermal resistances between grout zones

Thermal resistances along Γ_{gg1} and Γ_{gg2} boundaries are expressed as follows

$$R_{gg1} = \frac{2R_{gs}(R_{ar1} - 2x R_g)}{2R_{gs} - R_{ar1} + 2x R_g} \quad (\text{A.44})$$

$$R_{gg2} = \frac{2R_{gs}(R_{ar2} - 2x R_g)}{2R_{gs} - R_{ar2} + 2x R_g} \quad (\text{A.45})$$

where

$$R_{ar1} = \frac{\text{arcosh}\left(\frac{s^2 - d_0^2}{d_0^2}\right)}{2\pi\lambda^g} \quad (\text{A.46})$$

$$R_{ar1} = \frac{\text{arcosh}\left(\frac{2s^2 - d_0^2}{d_0^2}\right)}{2\pi\lambda^g} \quad (\text{A.47})$$

APPENDIX A. THERMAL RESISTANCES FOR HEAT EXCHANGERS WITH THE IMPLICIT GROUT ZONES

It has to be mentioned, following the FEFLOW white paper [3], that for some geometries certain resulting resistances may be negative and a correcting procedure is needed. In fact the following constraints must be satisfied

$$\left(\frac{1}{R_{gg1}} + \frac{1}{2R_{gs}} \right)^{-1} > 0 \quad (\text{A.48})$$

$$\left(\frac{1}{R_{gg2}} + \frac{1}{2R_{gs}} \right)^{-1} > 0 \quad (\text{A.49})$$

In case the above constraints are violated the initial x value is multiplied by factor $2/3$. If these constraints are still violated then the initial x value is multiplied by factor $1/3$. In the limit case $x = 0$ is assumed.

A.2.4 Thermal resistance due to grout-soil exchange

This resistance is expressed as follows

$$R_{gs} = (1 - x) R_g \quad (\text{A.50})$$

A.3 Thermal resistances for the CXA heat exchanger

Thermal resistances for CXA exchanger between inlet/outlet pipes and grout are computed using the following expressions

$$R_{ff} = R_{adv_o} + R_{adv_i^a} + R_{con_o} \quad (A.51)$$

$$R_{fig} = R_{adv_i^b} + R_{con_i} + R_{con^b} \quad (A.52)$$

A.3.1 Thermal resistances caused by the advective flow of refrigerant in inlet/outlet pipes

$$R_{adv_o} = \frac{1}{Nu_o \lambda^r \pi} \quad (A.53)$$

$$R_{adv_i^a} = \frac{1}{Nu_i \lambda^r \pi} \frac{d_h}{d_o^{ext}} \quad (A.54)$$

$$R_{adv_i^b} = \frac{1}{Nu_i \lambda^r \pi} \frac{d_h}{d_i^{int}} \quad (A.55)$$

where Nusselt numbers Nu_o , Nu_i depend on refrigerant velocities.

In the laminar flow regime ($Re_o < 2300$, $Re_i < 2300$)

$$Nu_o = Nu_o^{lam} = 4.364 \quad (A.56)$$

$$Nu_i = Nu_i^{lam} = 3.66 + \left(4 - \frac{0.102}{\frac{d_o^{ext}}{d_i^{int}} + 0.02} \right) \left(\frac{d_o^{ext}}{d_i^{int}} \right)^{0.04} \quad (A.57)$$

In the turbulent flow regime ($Re_o > 10^4$, $Re_i > 10^4$)

$$Nu_o = Nu_o^{trb} = \frac{(\xi_o/8)Re_oPr}{1 + 12.7\sqrt{\xi_o/8}(Pr^{2/3} - 1)} \left(1 + \left(\frac{d_o^{int}}{L} \right)^{2/3} \right) \quad (A.58)$$

$$Nu_i = Nu_i^{trb} = \frac{(\xi_i/8)Re_iPr}{1 + 12.7\sqrt{\xi_i/8}(Pr^{2/3} - 1)} \left(1 + \left(\frac{d_h}{L} \right)^{2/3} \right) \frac{0.86 \left(\frac{d_o^{ext}}{d_i^{int}} \right)^{0.84} + 1 - 0.14 \left(\frac{d_o^{ext}}{d_i^{int}} \right)^{0.6}}{1 + \frac{d_o^{ext}}{d_i^{int}}} \quad (A.59)$$

In the transition flow regime ($2300 \leq Re_o, Re_i < 10^4$ (here Nu_o^{trb} , Nu_i^{trb} are computed assuming $Re_o = 10^4$, $Re_i = 10^4$)

$$Nu_o = (1 - \gamma_o)Nu_o^{lam} + \gamma_o Nu_o^{trb}(Re_o = 10^4) \quad (A.60)$$

$$Nu_i = (1 - \gamma_i)Nu_i^{lam} + \gamma_i Nu_i^{trb}(Re_i = 10^4) \quad (A.61)$$

APPENDIX A. THERMAL RESISTANCES FOR HEAT EXCHANGERS WITH THE IMPLICIT GROUT ZONES

The refrigerant velocity, Prandtl and Reynolds numbers are defined as follows

$$\text{Pr} = \frac{\mu^r c^r}{\lambda^r} \quad (\text{A.62})$$

$$\text{Re}_o = \frac{|v_o^r| d_o^{\text{int}}}{\mu^r / \rho^r} \quad (\text{A.63})$$

$$\text{Re}_i = \frac{|v_i^r| d_h}{\mu^r / \rho^r} \quad (\text{A.64})$$

$$\xi_o = (1.8 \log_{10} \text{Re}_o - 1.5)^{-2} \quad (\text{A.65})$$

$$\xi_i = (1.8 \log_{10} \text{Re}_i - 1.5)^{-2} \quad (\text{A.66})$$

$$\gamma_o = \frac{\text{Re}_o - 2300}{10^4 - 2300} \quad (\text{A.67})$$

$$\gamma_i = \frac{\text{Re}_i - 2300}{10^4 - 2300} \quad (\text{A.68})$$

$$|v_o^r| = \frac{Q^r}{\frac{\pi (d_o^{\text{int}})^2}{4}} \quad (\text{A.69})$$

$$|v_i^r| = \frac{Q^r}{\pi \left(\frac{(d_i^{\text{int}})^2}{4} - \frac{(d_o^{\text{ext}})^2}{4} \right)} \quad (\text{A.70})$$

$$d_h = d_i^{\text{int}} - d_o^{\text{ext}} \quad (\text{A.71})$$

A.3.2 Thermal resistances resulting from pipes material and grout transition

This resistance is expressed as follows

$$R_{\text{con}_k} = \frac{\ln \left(\frac{d_k^{\text{ext}}}{d_k^{\text{int}}} \right)}{2\pi \lambda_k^p} \quad k = i, o \quad (\text{A.72})$$

$$R_{\text{con}^b} = x R_g \quad (\text{A.73})$$

where

$$x = \frac{\ln \left(\frac{\sqrt{D^2 + (d_i^{\text{ext}})^2}}{\sqrt{2} d_i^{\text{ext}}} \right)}{\ln \left(\frac{D}{d_i^{\text{ext}}} \right)} \quad (\text{A.74})$$

$$R_g = \frac{\ln \left(\frac{D}{d_i^{\text{ext}}} \right)}{2\pi \lambda^g} \quad (\text{A.75})$$

A.3.3 Thermal resistance due to grout-soil exchange

This resistance is expressed as follows

$$R_{gs} = (1 - x) R_g \quad (\text{A.76})$$

(A.77)

A.4 Thermal resistances for the CXC heat exchanger

Thermal resistances for CXC exchanger between inlet/outlet pipes and grout are computed using the following expressions

$$R_{ff} = R_{adv_i} + R_{adv_o^a} + R_{con_i} \quad (A.78)$$

$$R_{fog} = R_{adv_o^b} + R_{con_o} + R_{con^b} \quad (A.79)$$

A.4.1 Thermal resistances caused by the advective flow of refrigerant in inlet/outlet pipes

$$R_{adv_i} = \frac{1}{Nu_i \lambda^r \pi} \quad (A.80)$$

$$R_{adv_o^a} = \frac{1}{Nu_o \lambda^r \pi} \frac{d_h}{d_i^{ext}} \quad (A.81)$$

$$R_{adv_o^b} = \frac{1}{Nu_o \lambda^r \pi} \frac{d_h}{d_o^{int}} \quad (A.82)$$

where Nusselt numbers Nu_i , Nu_o depend on refrigerant velocities.

In the laminar flow regime ($Re_o < 2300$, $Re_i < 2300$)

$$Nu_i = Nu_i^{lam} = 4.364 \quad (A.83)$$

$$Nu_o = Nu_o^{lam} = 3.66 + \left(4 - \frac{0.102}{\frac{d_i^{ext}}{d_o^{int}} + 0.02} \right) \left(\frac{d_i^{ext}}{d_o^{int}} \right)^{0.04} \quad (A.84)$$

In the turbulent flow regime ($Re_i > 10^4$, $Re_o > 10^4$)

$$Nu_i = Nu_i^{trb} = \frac{(\xi_i/8)Re_iPr}{1 + 12.7\sqrt{\xi_i/8}(Pr^{2/3} - 1)} \left(1 + \left(\frac{d_i^{int}}{L} \right)^{2/3} \right) \quad (A.85)$$

$$Nu_o = Nu_o^{trb} = \frac{(\xi_o/8)Re_oPr}{1 + 12.7\sqrt{\xi_o/8}(Pr^{2/3} - 1)} \left(1 + \left(\frac{d_h}{L} \right)^{2/3} \right) \frac{0.86 \left(\frac{d_i^{ext}}{d_o^{int}} \right)^{0.84} + 1 - 0.14 \left(\frac{d_i^{ext}}{d_o^{int}} \right)^{0.6}}{1 + \frac{d_i^{ext}}{d_o^{int}}} \quad (A.86)$$

In the transition flow regime ($2300 \leq Re_o, Re_i < 10^4$ (here Nu_o^{trb} , Nu_i^{trb} are computed assuming $Re_o = 10^4$, $Re_i = 10^4$))

$$Nu_i = (1 - \gamma_o)Nu_i^{lam} + \gamma_i Nu_i^{trb}(Re_i = 10^4) \quad (A.87)$$

$$Nu_o = (1 - \gamma_i)Nu_o^{lam} + \gamma_o Nu_o^{trb}(Re_o = 10^4) \quad (A.88)$$

A.4. THERMAL RESISTANCES FOR THE CXC HEAT EXCHANGER

The refrigerant velocity, Prandtl and Reynolds numbers are defined as follows

$$\text{Pr} = \frac{\mu^r c^r}{\lambda^r} \quad (\text{A.89})$$

$$\text{Re}_i = \frac{|v_i^r| d_i^{\text{int}}}{\mu^r / \rho^r} \quad (\text{A.90})$$

$$\text{Re}_o = \frac{|v_o^r| d_h}{\mu^r / \rho^r} \quad (\text{A.91})$$

$$d_h = d_o^{\text{int}} - d_i^{\text{ext}} \quad (\text{A.92})$$

$$\xi_i = (1.8 \log_{10} \text{Re}_i - 1.5)^{-2} \quad (\text{A.93})$$

$$\xi_o = (1.8 \log_{10} \text{Re}_o - 1.5)^{-2} \quad (\text{A.94})$$

$$\gamma_i = \frac{\text{Re}_i - 2300}{10^4 - 2300} \quad (\text{A.95})$$

$$\gamma_o = \frac{\text{Re}_o - 2300}{10^4 - 2300} \quad (\text{A.96})$$

$$|v_i^r| = \frac{Q^r}{\frac{\pi (d_i^{\text{int}})^2}{4}} \quad (\text{A.97})$$

$$|v_o^r| = \frac{Q^r}{\pi \left(\frac{(d_o^{\text{int}})^2}{4} - \frac{(d_i^{\text{ext}})^2}{4} \right)} \quad (\text{A.98})$$

A.4.2 Thermal resistances resulting from pipes material and grout transition

This resistance is expressed as follows

$$R_{\text{con}_k} = \frac{\ln \left(\frac{d_k^{\text{ext}}}{d_k^{\text{int}}} \right)}{2\pi \lambda_k^p} \quad k = i, o \quad (\text{A.99})$$

$$R_{\text{con}^b} = x R_g \quad (\text{A.100})$$

where

$$x = \frac{\ln \left(\frac{\sqrt{D^2 + (d_o^{\text{ext}})^2}}{\sqrt{2} d_o^{\text{ext}}} \right)}{\ln \left(\frac{D}{d_o^{\text{ext}}} \right)} \quad (\text{A.101})$$

$$R_g = \frac{\ln \left(\frac{D}{d_o^{\text{ext}}} \right)}{2\pi \lambda^g} \quad (\text{A.102})$$

A.4.3 Thermal resistance due to grout-soil exchange

This resistance is expressed as follows

$$R_{gs} = (1 - x) R_g \quad (A.103)$$

(A.104)

References

1. H.J.G. Diersch, D. Bauer, W. Heidemann, W. Rühaak and P. Schätzl. Finite element modeling of borehole heat exchanger system. Part 1. Fundamentals. Computers & Geosciences 37: 1122-1135, 2011.
2. H.J.G. Diersch, D. Bauer, W. Heidemann, W. Rühaak and P. Schätzl. Finite element modeling of borehole heat exchanger system. Part 2. Numerical simulation. Computers & Geosciences 37: 1136-1147, 2011.
3. FEFLOW white papers vol. V.
4. P. Eskilson and J. Claesson. Simulation model for thermally interacting heat extraction boreholes. Numerical Heat Transfer 13:149-165, 1988.
5. N. Batini and A.F. Rotta Loria and P. Conti and D. Test and W. Grassi and L. Laloui. Energy and geotechnical behavior of energy piles for different design solutions. Applied Thermal Engineering 86: 199-213, 2015.